ISTANBUL TECHNICAL UNIVERSITY ★ INSTITUTE OF SCIENCE AND TECHNOLOGY

ANALYSIS OF CFRP RETROFITTED MASONRY INFILLED RC FRAMES SUBJECTED TO LATERAL LOADS

M.Sc. Thesis by
Levent KILIC

Department : Civil Engineering

Programme : Structural Engineering

Thesis Supervisor: Assist. Prof. Dr. Ercan YUKSEL

DECEMBER 2009

ISTANBUL TECHNICAL UNIVERSITY ★ INSTITUTE OF SCIENCE AND TECHNOLOGY

ANALYSIS OF CFRP RETROFITTED MASONRY INFILLED RC FRAMES SUBJECTED TO LATERAL LOADS

M.Sc. Thesis by
Levent KILIC
(501061074)

Date of submission : 25 Dec 2009
Date of defence examination: 28 Jan 2010

Supervisor (Chairman) : Assist.Prof. Dr. Ercan YUKSEL (ITU)
Members of the Examining Committee : Prof. Dr. Zekai CELEP (ITU)
Assoc. Prof. Dr.Oguz Cem CELIK(ITU)

DECEMBER 2009

İSTANBUL TEKNİK ÜNİVERSİTESİ ★ FEN BİLİMLERİ ENSTİTÜSÜ

CFRP İLE GÜÇLENDİRİLMİŞ DOLGU DUVARLI BETONARME ÇERÇEVELERİN YATAY YÜKLER ETKİSİNDE KURAMSAL ANALİZİ

YÜKSEK LİSANS TEZİ

Levent KILIÇ
(501061074)

Tezin Enstitüye Verildiği Tarih : 25 Aralık 2009
Tezin Savunulduğu Tarih : 28 Ocak 2010

Tez Danışmanı : Yrd. Doç.Dr. Ercan YÜKSEL (İTÜ)
Diğer Jüri Üyeleri : Prof. Dr. Zekai CELEP (İTÜ)
Doç. Dr. Oğuz Cem ÇELİK (İTÜ)

ARALIK 2009

FOREWORD

I would like to express my gratitude to Assistant Professor Ercan Yüksel for his invaluable support and attention in completing this study. Research Assistant Melih Sürmeli is gratefully acknowledged, for helping in simulation study. It has been great pleasure to work with him. Hasan Özkaynak is also greatfully acknowledged, for helping in coordination between experimental and simulation studies.
Finally, I am deeply indebted to my family for their endless support troughout my life.

Jan 2010 Levent Kılıç
Civil Engineer

TABLE OF CONTENTS

Page

ABBREVIATIONS

PHM : Polygonal Hysteretic Model
SHM : Smooth Hysteretic Model
CFRP : Carbon-Fiber Reinforced Polymer
CC : Corner-Crushing Mode
DC : Diagonal-Crushing Mode
SF : Shear-Failure Mode
HC : Stiffness Degrading Parameter
HBD : Ductility-Based Strength Degrading Parameter
HBE : Energy-Based Strength Degrading Parameter
HS : Slip or Crack Closing Parameter
PGA : Peak Ground Acceleration
NTH **:** Nonlinear Time History

LIST OF TABLES

Page

LIST OF FIGURES

Page

LIST OF SYMBOLS

$f_c^{'}$	: 28-day concrete cylindrical compressive strength
$f_{cc}^{'}$	: Confined concrete strength
f_c	: Concrete stress
f_{cp}	: Unconfined concrete post spalling strength
f_{cu}	: Stress at ε_{cu}
f_s	: Steel stress
f_y	: Steel yield stress
f_u	: Steel ultimate stress
ε_c	: Concrete strain
ε_t	: Concrete tension strain capacity
ε_{cc}	: Concrete strain at peak stress
ε_{cu}	: Ultimate concrete strain
ε_{sp}	: Spalling strain
ε_y	: Yield strain
ε_s	: Longitudinal reinforcement strain
ε_{sh}	: Strain at strain hardening
ε_{su}	: Failure strain of steel
A_g	: Gross sectional area of column
A_{ck}	: Area of confined concrete
E_s	: Elastic modulus of concrete
E_{sec}	: Secant modulus of concrete
I	: Moment of Inertia
EI	: Initial flexural stiffness
EA	: Axial stiffness
EI3P	: Post yield flexural stiffness
M_{cr}	: Cracking moment
M_y	: Yield moment
M_u	: Ultimate moment
χ_y	: Yield curvature
χ_u	: Ultimate curvature
α	: Stiffness degrading parameter
β_1	: Ductility based strength-deterioration parameter
β_2	: Energy based strength- deterioration parameter
h	: Height of column measured on center of beams
$h^{'}$	: Height of infill
l	: Length of column measured on center of columns
$l^{'}$	: Length of infill
r	: Aspect ratio

θ	: Sloping angle of diagonal infill
$\theta^{'}$	: Sloping angle of masonry diagonal strut at shear failure
μ_f	: Coefficient of friction of frame-infill interface
$f_m^{'}$	: Prism strength of masonry
$\varepsilon_m^{'}$	: Corresponding strain for masonry prism strength
f_m	: Effective [factored] compressive strength of infill
σ_{c0}	: Column-infill nominal [upper bound] uniform contact normal stress
σ_{b0}	: Beam-infill nominal [upper bound] uniform contact normal stress
M_{pc}	: Plastic resisting moment of column
M_{pb}	: Plastic resisting moment of beam
M_{pj}	: Joint plastic resisting moment
t	: Infill thickness
α_c	: Normalized contact length of column-infill interface
α_b	: Normalized contact length of beam-infill interface
A_c	: Column-Infill interface contact stress
A_b	: Beam-Infill interface contact stress
σ_c	: Actual normal stress column-infill interface
σ_b	: Actual normal stress beam-infill interface
τ_c	: Contact shear stress column-infill interface
τ_b	: Contact shear stress beam-infill interface
l_{eff}	: Effective length of the equivalent diagonal struts
f_a	: Permissible stress
A_d	: Area of the equivalent diagonal struts
ν	: Basic shear strength or cohesion of masonry
V_m	: Maximum lateral force
U_m	: Corresponding displacement for V_m
K_0	: Initial stiffness
α	: Post-yield stiffness ratio
V_y	: Lateral yield force
A	: Parameter A in Wen's Model
β	: Parameter β in Wen's Model
γ	: Parameter γ in Wen's Model
η	: Parameter η in Wen's Model
A_s	: Control parameter for slip length
Z_s	: Control parameter for slip sharpness
$\overline{Z}$	: Offset value for slip response
s_k	: Control parameter to vary the rate of stiffness decay
s_{p1}	: Control parameter of the rate of strength deterioration
s_{p2}	: Control parameter of the rate of strength deterioration

ANALYSIS OF CFRP RETROFITTED MASONRY INFILLED RC FRAMES SUBJECTED TO CYCLIC LATERAL LOADS

SUMMARY

An analytical study consisting of the simulation of some experiments related with the retrofitting of infilled RC frames with CFRP sheets tested in Structural and Earthquake Engineering Laboratory of ITU, was conducted in the scope of this thesis. The evaluated experiments in the analytical study include three groups of specimens which are reference bare frame, infilled frame and CFRP retrofitted infilled frame. Each group of specimens was subjected to quasi-static and pseudo-dynamic types of loading. The quasi-static tests were performed by using displacement based cycles which were gradually increased. For two different loading protocol, one and three repetition were applied for each displacement target, respectively. Pseudo-dynamic tests were performed for two different inertia mass conditions.

The simulation study was performed by using IDARC2D computer program. In the program, columns and beam are modeled as frame members. Moment-curvature relations were defined for the end sections of the frame members. These relations were obtained from cross-sectional analysis program of XTRACT. Experimental results of the material tests performed were used in the calculation. The contribution of the infill panel is taken into account as a bilinear shear force-displacement relation whose parameters were defined from 500×500 mm masonry brick tests. Similarly, the contribution of the retrofitted infilled panel was idealized as bi-linear shear spring. The main difference from the infill panel is increased strength and coefficient of friction on the frame-infill interface, and decreased strain capacity.

In the analyses performed by IDARC2D, to characterize the sectional behaviour under the static and dynamic external loads, poligonal hysteretic model (PHM) and smooth hysteretic model were used for beam-columns and infill panels, respectively.

The results obtained from the experiments which were subjected to quasi-staic loads, were used in the calibration of sectional response parameters. There exist some differences between the parameters of strength, stiffness and ductility for one cyclic and three cyclic quasi-static loadings. The analytical responses were compared with the corresponding experimental results.

Nonlinear time history analysis were performed for the selected acceleration records. In the dynamic analysis, the sectional response parameters were used as those obtained in the quasi-static tests. The analytical responses were compared with the existing experimental results.

The infill panel constitutive model defined in IDARC2D were used for the CFRP retrofitted infill panel with the modification of some parameters such as strength, ductility, lateral yield force and friction. The comparison of the analytical and experimental results obtained for the static and dynamic load cases shows that the response of CFRP retrofitted infilled frame can be estimated accurately with the analytical model.

CFRP İLE GÜÇLENDİRİLMİŞ DOLGU DUVARLI BETONARME ÇERÇEVELERİN YATAY YÜKLER ETKİSİNDE KURAMSAL ANALİZİ

ÖZET

İTÜ İnşaat Fakültesi Yapı ve Deprem Mühendisliği Laboratuvarında tamamlanmış olan ve karbon lifli polimerler (CFRP) ile dolgu duvarlı betonarme çerçevelerin güçlendirilmesini konu alan deneysel çalışmada incelenmiş bazı numuneler, bu tez kapsamında kuramsal olarak incelenmiştir.

Yalın, dolgu duvarlı ve güçlendirilmiş dolgu duvarlı betonarme çerçeveler statik ve dinamik etkiler altında incelenmiştir. Doğrusal olmayan statik analizlerde tek ve üç çevrimli tersinir tekrarlı yerdeğiştirme girdileri kullanılmıştır. Dinamik analizlerde ise Deprem Yönetmeliğinde tanımlanmış tasarım ivme spektrumuna göre değiştirilmiş gerçek bir ivme kaydı parçası kullanılmıştır. Tüm numuneler için, dinamik analiz iki farklı atalet kuvveti durumu için gerçekleştirilmiştir.

Analitik çözüm için IDARC2D yazılımı kullanılmıştır. Kolonlar ve kiriş çubuk eleman olarak modellenmiştir. Kesit moment-eğrilik ilişkilerinin belirlenmesinde XTRACT yazılımı kullanılmıştır. Moment-eğrilik ilişkilerinin oluşturulmasında deneysel olarak elde edilen malzeme karekteristikleri kullanılmıştır. Dolgu duvarın yalın çerçeveye katkısı iki doğrulu yatay yük-tepe yerdeğiştirmesi zarf eğrisi ile ifade edilmiştir. Dolgu duvar davranış parametreleri 500×500 mm boyutlarındaki yalın ve güçlendirilmiş dolgu duvar eleman deneylerinden belirlenmiştir. CFRP ile güçlendirilmiş duvarda yalın duvar durumuna göre dayanım, çevre elemanlarla olan sürtünme artmış buna karşılık şekil değiştirme kapasitesi azalmıştır.

IDARC2D yazılımı ile yapılan çözümlerde; statik ve dinamik tersinir yükler etkisinde kesit davranışını ifade etmek üzere kolon ve kiriş türü betonarme elemanlarda çokgen çevrimsel model (PHM) ve yalın ve güçlendirilmiş duvar için de eğrisel çevrimsel model (SHM) kullanılmıştır.

Tersinir tekrarlı statik yükler etkisinde incelenen numunelere ait sonuçlar, kesit davranışını tanımlayan çevrim parametrelerinin uyarlanması için kullanılmıştır. Tek çevrimli statik yüklemeler ile üç çevrimli statik yüklemeler arasında dayanım, riijitlik ve süneklik parametreleri açısından farklılıklar oluşmuştur. Kuramsal olarak belirlenen çevrimsel davranış büyüklükleri mevcut deney sonuçları ile farklı açılardan karşılaştırılmıştır.

Tersinir tekrarlı statik yükler için belirlenen kesit davranış parametreleri sabit tutularak, seçilen ivme kayıtları için zaman tanım alanında doğrusal olmayan analiz gerçekleştirilmiştir. Kuramsal olarak belirlenen davranış büyüklükleri mevcut benzeşik dinamik deney sonuçları ile karşılaştırılmıştır.

IDARC2D yazılımında mevcut olan duvar davranış modeli, CFRP ile güçlendirilmiş dolgu duvarın modellenmesinde kullanılmıştır. Statik ve dinamik yükler için elde edilen kuramsal sonuçlar mevcut deneysel sonuçlar ile karşılaştırılmıştır. CFRP ile güçlendirilmiş duvarda dayanım, süneklik ve çevre betonarme elemanlarla olan sürtünmedeki artış dikkate alındığında genel sistem davranışının başarı ile elde edilebildiği görülmüştür.

1. INTRODUCTION

Although unreinforced masonry infill walls are often treated as non-structural components, they will interact with the bounding frames when subjected to lateral loads. Because of the complexity of the problem and lack of a rational and simple analytical model, the contribution of infill wall is often neglected in the nonlinear analysis of building structures. Such an assumption may lead to substantial inaccuracy in determining the lateral stiffness, strength and ductility of the structure. Determining strength and stiffness inaccurately can lead greater base shear force on buildings subjected to earthquake load and structural members can subject greater loads than their design loads. The retrofitting of infill wall with a rational method yields that the infill wall contribution to the structural response should be taken into account.

1.1 Objective of Study

The main objective of this study is to determine a consistent constitutive model which combines analytical and experimental results for the masonry infill walls retrofitted by CFRP. It has been tried to utilize an existing constitutive model of infill panel in IDARC2D [1] which has capability of performing quasi-static cyclic analysis and non-linear time history analysis, for the case of infilled walls retrofitted by CFRP. In the framework of the study, the behavior of different types of frames including bare frame, infilled frame and infilled frame retrofitted by CFRP are analysed analytically and compared with the existing experimental results.

1.2 Literature Survey

The behavior of masonry infilled frames has been the subject of many studies throughout the world since 1950's in order to develop a rational method for the analysis and design of such frames. The studies in this area can be categorized into two groups which are experimental based and analytical based studies.

Early studies were mainly experimental (Polyakov 1952 [9]) and especially usefull in understanding the behavior of infilled frames under in-plane forces. Klinger and Bertero (1978), Bertero and Brokken (1983) [10], Zarnic (1980), Mander and Nair (1994) [11] focused on evaluating the experimental behavior of masonry infilled frame to obtain limit strength and equivalent stiffness. They have concluded that proper use of masonry infill could result in significant increases in the strength and stiffness of the stuructures [3].

Saatcioglu et al. (2004) [4] completed an experimental study for seismic performance of masonry infill walls retrofitted with CFRP sheets and they concluded that retrofitting with CFRP sheets controls cracking and improves elastic capacity overall structural system.

More reliable analysis of masonry infilled frame structures requires analytical models to obtain force-displacement response. Analytical studies can be classified into two groups which are micromodel and macromodel approaches. In micromodel approach, masonry infill is analyzed by finite element method (FEM) whereas in macromodel approach, masonry infill is considered with equivalent members.

Dhanasekar and Page (1986) [12], Mosalam (1996), Shing et al. (1992) used FEM to predict the response of infilled frame. Although the method is precise, it is time-consuming approach especially for large structures.

Generalized macromodels seem more suitable for representing the global behavior of components in the analysis of such structures. The control parameters of macromodel can be calibrated using experimental data or micromodels to simulate real behaviour. For analysis where the emphasis in on evaluating the overall structural response, macromodels can be substituted for micromodels without substantial loss in accuracy and with significant gains in computational efficiency [3].

Holmes (1961) [13], replaced the infill by an equivalent pin-jointed diagonal strut of the same material with a width of the one-third of the infill's diagonal length.

Stafford Smith (1966) and Stafford Smith & Carter (1969) proposed a theoretical relation for the width of the diagonal strut linked to infill-frame stiffness parameter λh in which λh is a coefficient less than 1.0.

Mainstone (1971) [14] obtained an empirical formulations in terms of λh for the same relation.

Elastic methods could not completely represent the actual behavior of the infilled frame so attention was paid to theories of plasticity. Wood (1978) extended the limit analysis of plasticity with the assumption of perfect plasticity. The method was developed by May (1981) to predict the collapse loads and modes of infilled frames with openings.

Zarnic (1990) also proposed an elastic perfectly plastic equivalent strut model with parameters expressed as function of the dimensions of the infilled frame subassemblies, linked to the mechanical properties of the component materials and additional empirical parameters depending on frame-infill interaction.

Multi-strut model or named as compression-only three strut model investigated Chrysotomou et al. (1992). Mosalam (1996) suggested a simplified model based on the equivalent strut approach which accounts for slip along frame-masonry infill interface. This model uses empirically determined correction factors to obtain effective strut dimensions.

Mander et al. (1993) reported the results of cyclic pseudo-dynamic test performed on masonry infilled frame subassemblies. The report presents the observed strength and deformation limit states as well as the hysteretic characteristics such as strength and stiffness degradation due to cyclic loading. The report also summarized the important in-plane failure modes of masonry infilled frames which include; (1) torsion failure of the columns, (2) flexural or shear failure of the columns, (3) compression failure of the equivalent diagonal strut, (4) diagonal tension failure of the infill, (5) sliding shear failure of the masonry along horizontal mortar beds.

Mander et al. (1995) proposed a computational method of the hysteretic in-plane force deformation behavior of the masonry infilled frame based on tie and strut approach. In this method masonry infill was modelled as a combination of three non-parallel strut in each direction of loading.

Saneinejad and Hobbs (1995) [5] developed a method based on the equivalent diagonal strut approach for the analysis and design of infilled frames subjected in-plane forces. The method takes into account the elastoplastic behavior of infilled frame considering the infill’s limited ductility. Infill aspect ratio, shear stresses at the frame-infill interface, beam and colum strength are accounted in the method.

2. EXPERIMENTAL BACKGROUND

An experimental study related with the current topics was conducted in Structural and Earthquake Engineering Laboratory of Istanbul Technical University. Geometrically identical 12, 1/3 scaled reinforced concrete (RC) frame specimens classified into three groups were produced and tested. First group specimen consisted of bare frames, the second group was hollow brick infilled RC frames and the third group consists of infilled frames retrofitted by CFRP in the form of cross bracing [6].

Four different types of tests were conducted. They are defined as follows: 1-cyclic quasi-static tests, 3-cyclic quasi-static tests, low mass pseudo-dynamic (PSD) tests (8.5 kNs^2/m) and high mass (22.1 kNs^2/m) PSD tests.

Although no axial force were affected to the columns, the beam was under the action 50 kN compression force arose from the fixation of the actuator to the specimen. Therefore the beam of specimen is more stiff and has more strength compared with the columns.

1/3 scaled specimen has 1000 mm height and 1333 mm span length. The foundation has 400 mm height and 1533 mm witdh. The colums and beam have the same cross-sectional dimensions of 200×100 mm and the same longitudinal (4ϕ8) and transversal reinforcements (ϕ6/140). Foundation longitudinal reinforcement is 12ϕ12. Concrete cover is supplied as 15 mm for all RC members. Unfortunatelly for some of the specimens, it is obtained different thickness of the concrete cover. Each specimens have identical reinforcement and concrete quality. The reinforcing details are shown in Figure 2.1

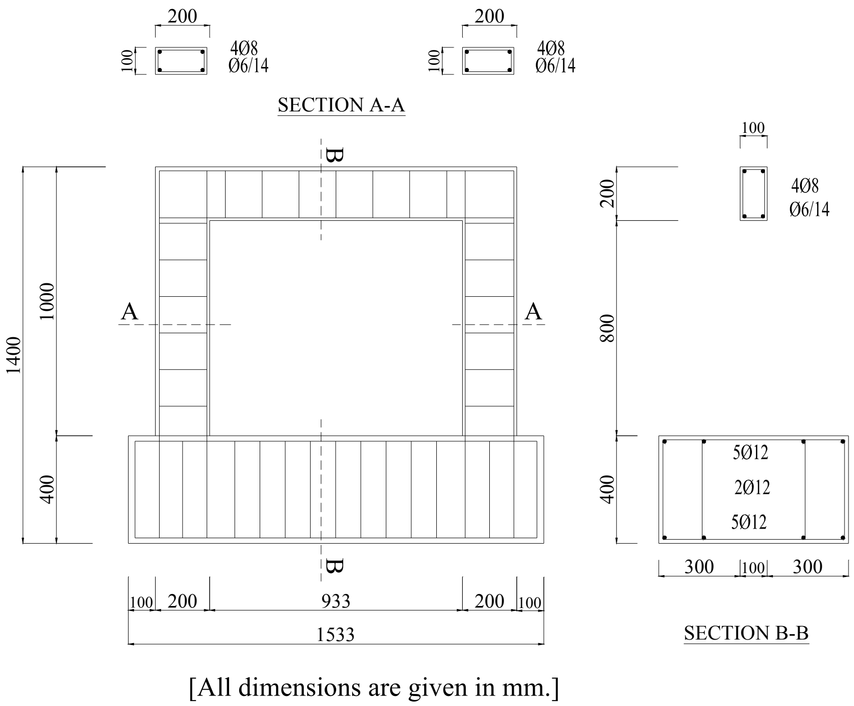

Figure 2.1: Reinforcement details of specimens

2.1 Test Specimen

2.1.1 Bare Frame

The dimensions of one-bay and one-storey test frame is given in Figure 2.2.

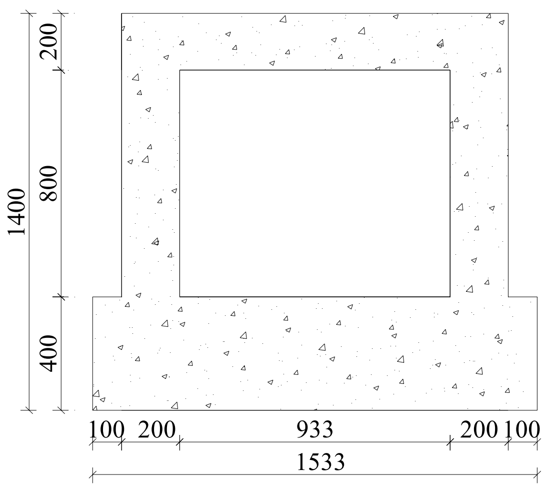

Figure 2.2: Bare Frame

2.1.2 Infilled Frame

Infilled Frame has identical dimensions with the bare frame. 1/3 scaled hollow clay bricks were produced and used in infill wall. Horizontal and vertical joints of infill wall had 10 mm thickness. Both faces of the infill wall were covered with 10 mm thick plaster. Dimensions of Infilled Frame and typical clay hollow brick are illustrated in Figure 2.3.

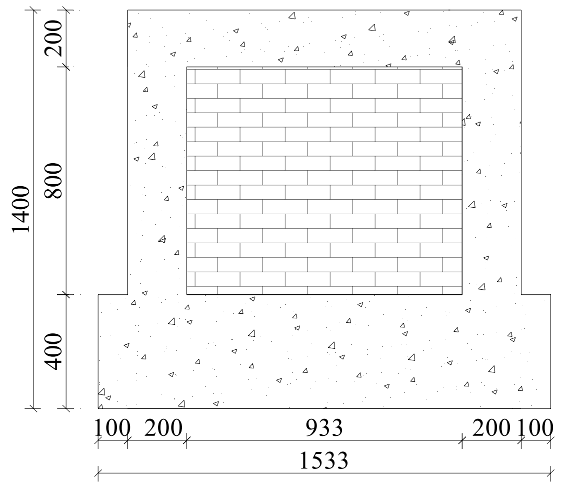

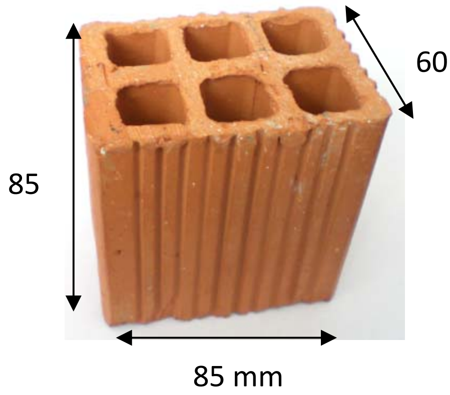

Figure 2.3: Infilled Frame and clay hollow brick dimensions

2.1.3 Retrofitted Infilled Frame

Infilled RC frames are retrofitted by using CFRP sheets. Epoxy resin was applied on the plaster to adhere CFRP sheets in the form of X-bracing at both faces of the infilled RC frame. The diagonal CFRP sheets were fixed at column to beam and column to foundation joints with CFRP struts. The diagonal sheets at both faces of the frame were connected each other by CFRP made anchorage members. Also, some holes having 150 mm depth were used to place CFRP made anchorages. Cross-Braced Frame dimensions are given in Figure 2.4.

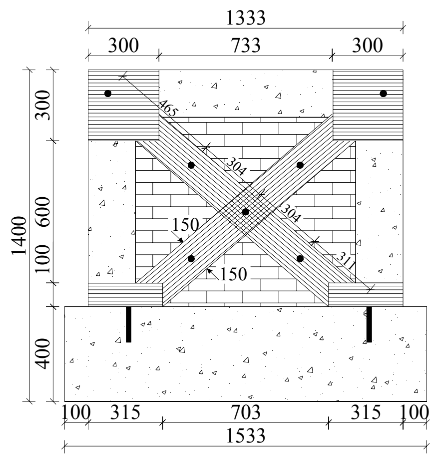

Figure 2.4: Retrofitted Infilled Frame

2.2 Material Tests

A variety of material tests have been conducted in order to use in the analytical model.

2.2.1 Concrete Test

Several cyclindirical concrete samples were taken to be tested in the days of 28 and 90. The concrete standart compresive tests were performed in order to determine the mechanical properties to be used in the analytical model. The stress-strain relationship is demonstrated in Figure 2.5.

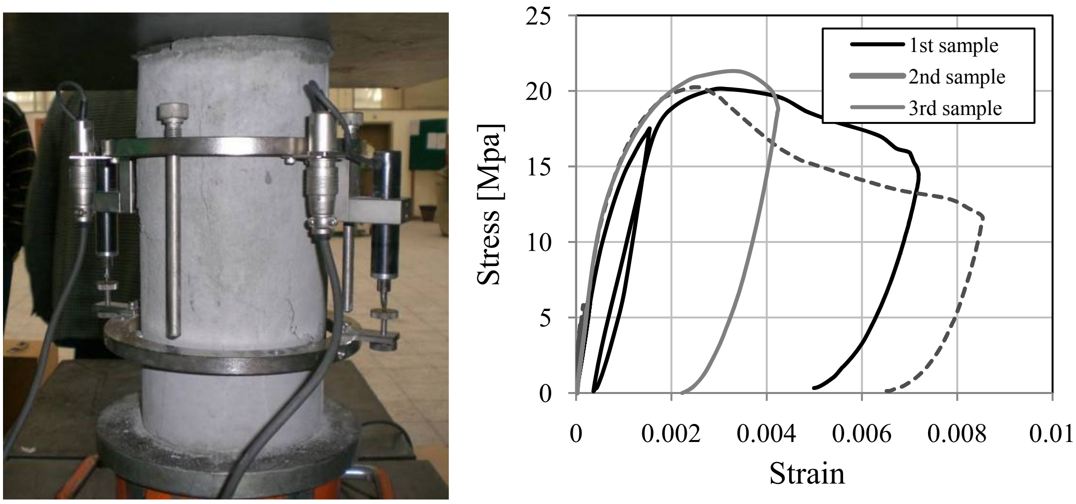

Figure 2.5: Standart unconfined concrete test set-up and stress-strain relationship

2.2.2 Re-bar Tensile Tests

Reinforcement steel tensile tests were conducted in ITU Construction Materials Laboratory as per defined in Turkish Code no. TS 708.

2.2.2.1 Transversal Re-bar tensile tests

3@ϕ6 mm transversal reinforcement samples were tested. Elongations were recorded by using both comparator and straingauges. Test set-up and stress-strain relationship of tensile test are depicted below:

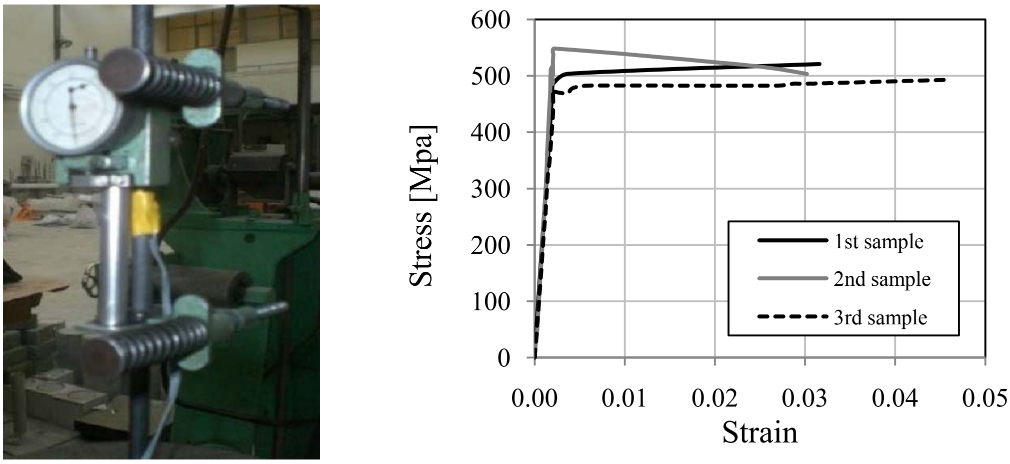

Figure 2.6: Transversal steel tensile test set-up and stress-strain relationship

2.2.2.2 Longitudinal Re-bar tensile tests

3@ϕ8 mm longitudinal reinforcement samples were tested. Elongations were recorded by using both comparator and straingauges. Test set-up and stress-strain relationship of tensile test are depicted below:

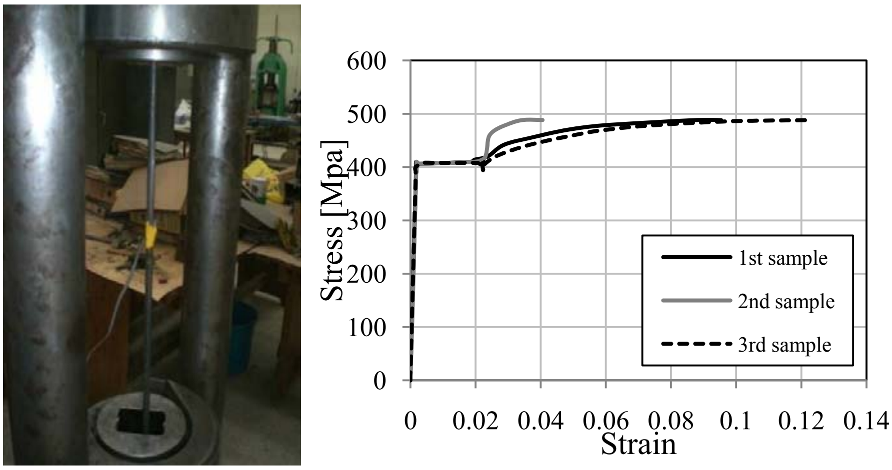

Figure 2.7: Longitudinal steel tensile test set-up and stress-strain relationship

Strength and strain values obtained from the material tests for unconfined concrete, longitudinal and transversal reinforcement steel which used in the analysis are summarized in the Table 2.1. In the table, f_c is concrete compression strength, f_y is steel yield strength, ε_y is corresponding strain for f_y, f_u is steel ultimate strength and ε_u is corresponding strain for f_u.

Table 2.1: Frame members mechanical properties considered in analysis

Material	f_c [MPa]	f_y [MPa]	ε_y [%]	f_u [MPa]	ε_u [%]
Unconfined Concrete	18.3	NA	NA	NA	0.4
Longitudinal Re-bar	-	410	0.2	490	9.5
Transversal Re-bar	-	550	0.2	550	3.0

2.2.3 Masonry Infill Tests

1/3 scaled perforated masonry bricks having a dimensions of 60×85×85 mm were specially produced for this study. 500×500 mm masonry infill and CFRP retrofitted masonry infill samples were produced and tested in the laboratory in order to define the mechanical characteristics of infill wall. Since masonry infill is an anisotropic material, three different types of tests were conducted. The first one was in brick's holes direction, the second one was in the perpendicular direction of brick's holes and the third one was in diagonal direction.

2.2.3.1 Tests in the Direction of Masonry Brick's Holes

Unretrofitted and retrofitted infill wall samples were tested. The bricks holes were the same with the loading direction. The tested specimens are shown in Figure 2.8.

Figure 2.8: Compression tests in the brick's hole direction

The obtained axial stress-strain relationships are given in the Figure 2.9. The effect of retrofitting on strength and ductility can be seen from the figure.

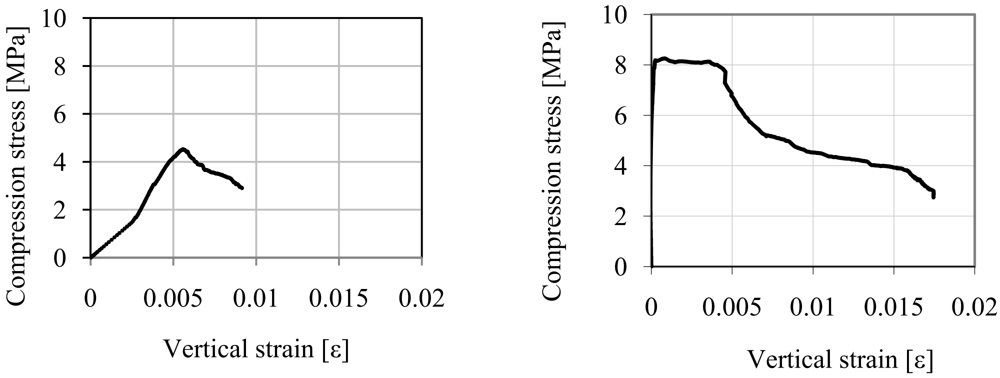

(a) Infill *(b)CFRP Retrofitted Infill*

Figure 2.9: Compression test results in the brick's hole direction

The modulus of elasticity which is the initial slope of the stress-strain relation was obtained as 3744 MPa.

2.2.3.2 Tests in the Perpendicular Direction of Masonry Brick's Holes

Bare and CFRP retrofitted infill samples were tested. Bricks holes were perpendicular to the loading direction. The tested specimens are shown in Figure 2.10.

Figure 2.10: Compression test in the brick's hole perpendicular direction

The obtained axial stress-strain relationships are given in the Figure 2.11. The effect of retrofitting on strength and ductility can be seen from the figure.

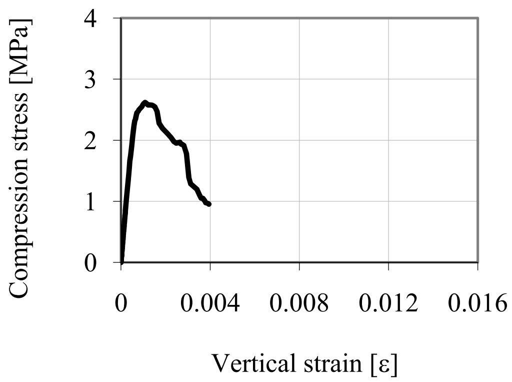

(a) Infill

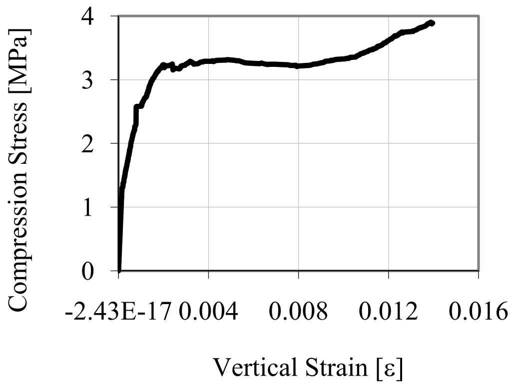

(b)CFRP Retrofitted Infill

Figure 2.11: Compression test results in the brick's hole perpendicular direction

2.2.3.3 Tests in the Diagonal Direction of Masonry Brick's Hole

This tests were conducted in order to determine infill's diagonal compression strength. The loading was applied to the samples in the diagonal direction. Infill and CFRP retrofitted infill samples are shown in Figure 2.12.

Figure 2.12: Diagonal shear test

The shear stress-strain relationships are given in Figure 2.13. The maximum shear strength for bare and retrofitted cases were determined as 0.9 MPa and 1.3 MPa, respectively.

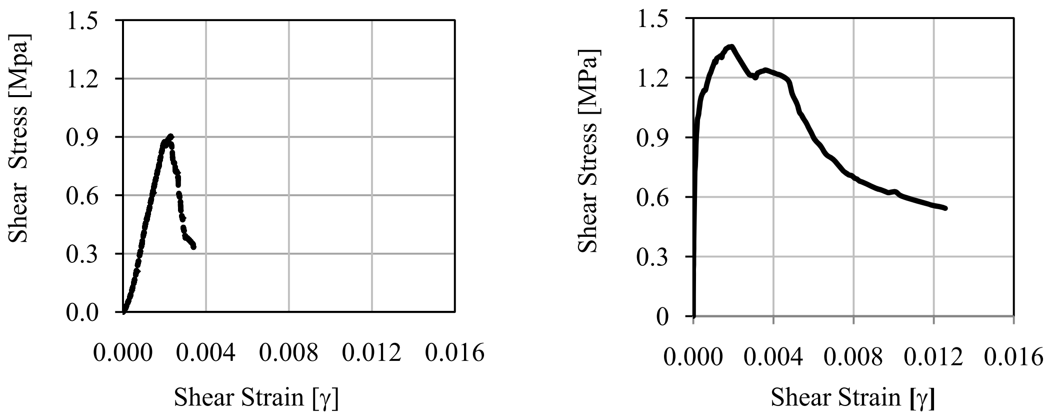

(b) Infill *(b)CFRP Retrofitted Infill*

Figure 2.13: Diagonal shear test results

The obtained test results are given together in Table 2.2.

Table 2.2: Masonry infill mechanical properties considered in analysis

Specimen	Hole's Direction		Hole's Perpendicular Direction		Diagonal Direction	
	f'_m [MPa]	ε'_m	f'_m [MPa]	ε'_m	τ [MPa]	γ
Infill	4.5	0.006	2.5	0.0015	0.9	0.002
CFRP Retrofitted Infill	7.5	0.0035	3.5	0.0035	1.3	0.0035

According to manufacturer data sheet, CFRP material tensile strength and modulus of elasticity are 3.9 GPa and 230 GPa, respectively.

3. ANALYTICAL MODEL

3.1 Analytical Software Used in Simulation

3.1.1 IDARC2D

For understanding the behavior of building structures during earthquake motions, significant researches have been carried out. Due to the inherent complexities that buildings have, often, researches have focused on understanding element behavior through component testing.

Cyclic behavior of specimen was modeled by improved nonlinear computer analysis program named IDARC2D which links experimental researches and analytical developments. IDARC2D includes the following analysis types: Quasi-static cyclic analysis, inelastic dynamic analysis, monotonic and adaptive pushover analysis and long-term loading analysis. Behavior of concrete and masonry infill members in IDARC2D is taken into account by two different hysteretic models, which are Polygonal Hysteretic Model (PHM), and Smooth Hysteretic Model (SHM).

The typical tri-linear moment curvature envelop (M-χ) have been used for the section of RC members and illustrated in Figure 3.1.

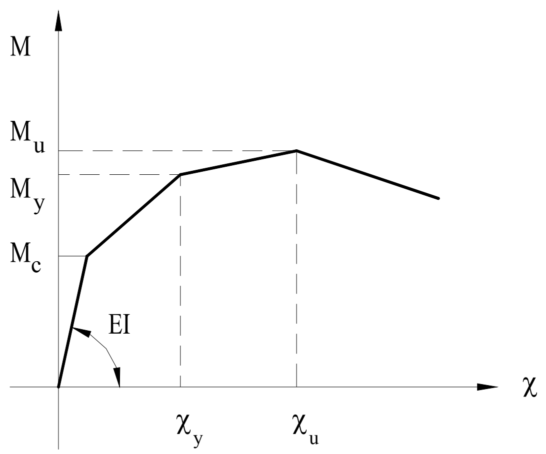

Figure 3.1: Tri-linear Moment-Curvature idealization

The idealized tri-linear M-χ relation shown in Figure 3.1 includes the following characteristics: EI (initial flexural stiffness), M_c (cracking moment), M_y (yield moment), M_u (ultimate moment), χ_y (yield curvature) and χ_u (ultimate curvature).

The infill panel is modelled in IDARC2D by the equivalent diagonal compression struts. The contribution of the infill panel is represented by bi-linear shear force-displacement envelope whose parameters depend on the material stress-strain relationships. The force-displacement relation of infill panel is shown in Figure: 3.2.

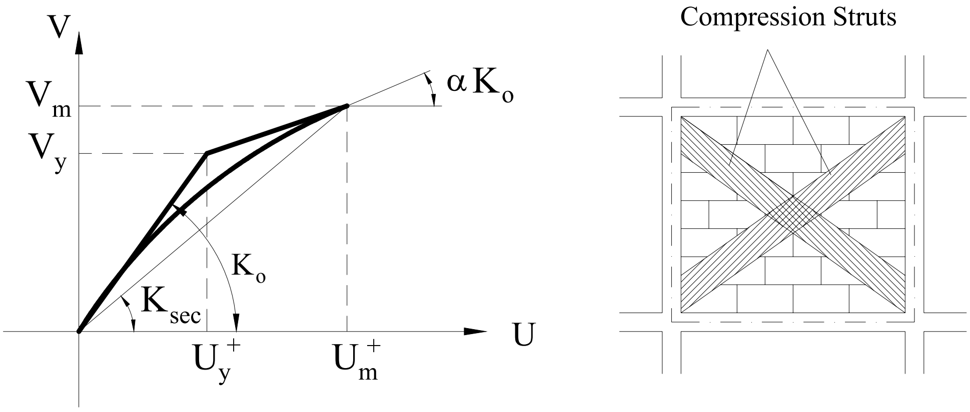

Figure 3.2: Infill panel lateral force-displacement relation

3.1.2 XTRACT

A cross-sectional analysis program of XTRACT was used for the creating of moment curvature envelopes for IDARC2D. XTRACT generates moment-curvature and axial force-moment interaction curves.

Mander concrete model was used in the analysis. Default strain values in XTRACT were used for unconfined concrete model. The strain at peak stress is taken as 0.2% and the crushing and spalling strains are taken as 0.4% and 0.6%, respectively. The unconfined concrete stress-strain diagram is given in Figure 3.3. The model is described in the following equations;

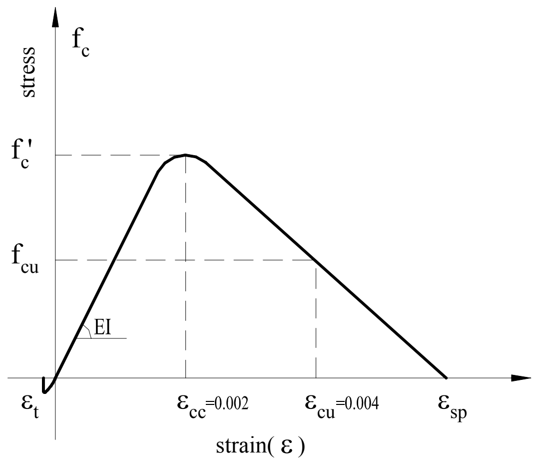

Figure 3.3: Stress-strain diagram for the Mander unconfined concrete model

For strain - $\varepsilon < 2 \cdot \varepsilon_t$ $\quad f_c = 0$ **[3.1]**

For strain - $\varepsilon < 0$ $\quad f_c = \varepsilon \cdot E_c$ **[3.2]**

For strain - $\varepsilon < \varepsilon_{cu}$ $\quad f_c = \dfrac{f_c' \cdot x \cdot r}{r - 1 + x^r}$ **[3.3]**

For strain - $\varepsilon < \varepsilon_{sp}$ $\quad f_c = f_{cu} + \left(f_{cp} - f_{cu}\right) \cdot \dfrac{\varepsilon - \varepsilon_{cu}}{\varepsilon_{sp} - \varepsilon_{cu}}$ **[3.4]**

$$x = \frac{\varepsilon}{\varepsilon_{cc}} \quad \textbf{[3.5]}$$

$$r = \frac{E_c}{E_c - E_{\sec}} \quad \textbf{[3.6]}$$

$$E_{\sec} = \frac{f_c'}{\varepsilon_{cc}} \quad \textbf{[3.7]}$$

Where ε is concrete strain, f_c is concrete stress, E_c is concrete modulus of elasticity, $E_{\sec}$ is secant modulus, ε_t is strain capacity in tension, ε_{cc} is strain at peak stress (0.2%), ε_{cu} is ultimate concrete strain (0.4%), ε_{sp} is spalling strain (0.6%), f_c' is 28-day compressive strength, f_{cu} is stress at ε_{cu} and f_{cp} is post spalling stress.

The formulation of confined concrete model is described in following equations and general stress-strain diagram is given in Figure 3.4.

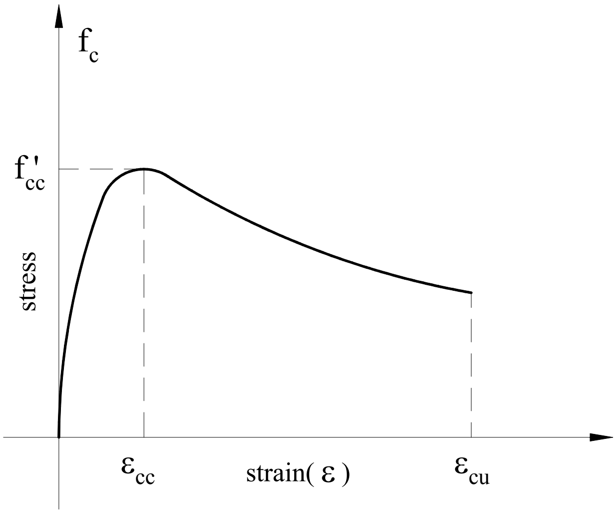

Figure 3.4: Stress-strain diagram for the Mander confined concrete model

For strain - $\varepsilon < 2 \cdot \varepsilon_t$ $\quad f_c = 0$

For strain - $\varepsilon < 0$ $\quad f_c = \varepsilon \cdot E_c$

For strain - $\varepsilon < \varepsilon_{cu}$ $\quad f_c = \dfrac{f'_{cc} \cdot x \cdot r}{r - 1 + x^r}$ **[3.8]**

$$x = \frac{\varepsilon}{\varepsilon_{cc}}$$

$$\varepsilon_{cc} = 0.002\left[1 + 5\left(\frac{f'_{cc}}{f'_c} - 1\right)\right] \qquad \textbf{[3.9]}$$

$$r = \frac{E_c}{E_c - E_{\sec}}$$

$$E_{\sec} = \frac{f'_{cc}}{\varepsilon_{cc}} \qquad \textbf{[3.10]}$$

Where f'_{cc} is confined concrete strength.

The formulation of bilinear with parabolic strain hardening steel model is described in following equations:

For strain - $\varepsilon < 2 \cdot \varepsilon_y$ $\quad f_s = E \cdot \varepsilon$ **[3.11]**

For strain - $\varepsilon < \varepsilon_{sh}$ $\qquad f_s = f_y$ **[3.12]**

For strain - $\varepsilon < \varepsilon_{su}$ $\qquad f_s = f_u - (f_u - f_y) \cdot \left(\frac{\varepsilon_{su} - \varepsilon}{\varepsilon_{su} - \varepsilon_{sh}} \right)^2$ **[3.13]**

Where ε is steel strain, f_s is steel stress, f_y is yield stress, f_u is rapture stress, ε_y is yield strain, ε_{sh} is strain at strain hardening, ε_{su} is failure strain E is modulus of elasticity.

For all specimens, strain at strain hardening is taken as 0.02 and ultimate strain is taken as 0.095. The typical stress-strain relationship of steel model is depicted in Figure 3.5.

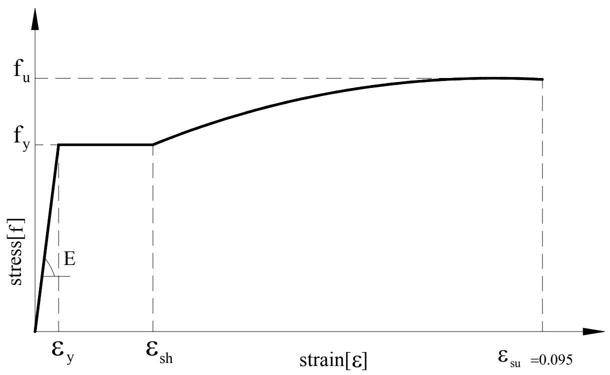

Figure 3.5: Stress-strain diagram for steel model

Trilinear moment-curvature relationships are obtained by using XTRACT. The typical column and beam moment curvature relations are given in Figure 3.6.

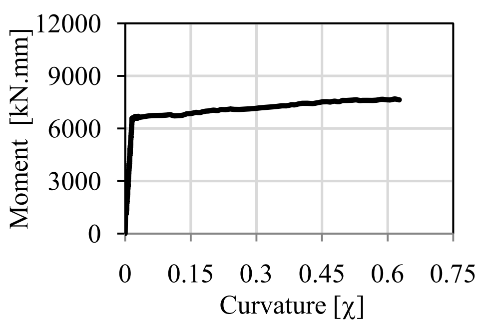

(a) Column Section

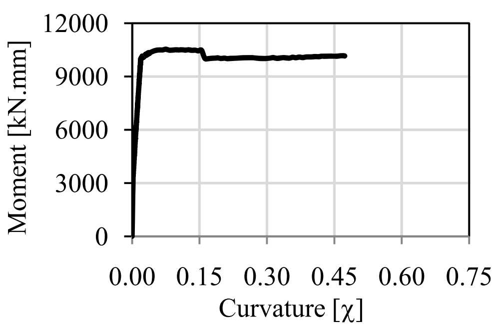

(b)Beam Section

Figure 3.6: The Typical Moment-Curvature Relation for Specimens

The reinforcement and confined concrete stress-strain relationships which express the failure mode in section are shown in Figure 3.7 and Figure 3.8, respectively. From the figures one can evaluate that column failure mechanism occurs due to reinforcement rupture and beam failure mechanism occurs due to crushing of confined concrete.

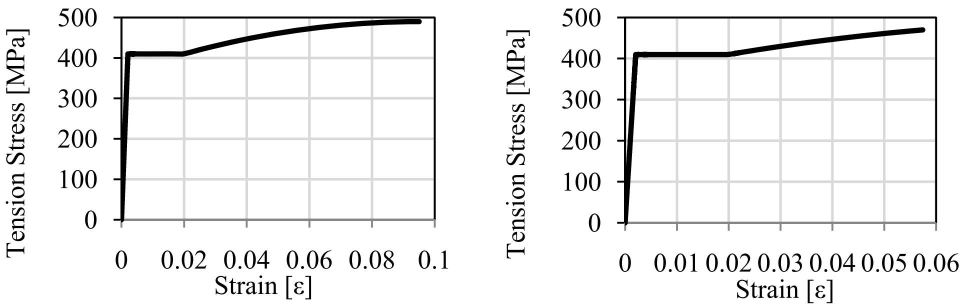

(c) Column Section *(b)Beam Section*

Figure 3.7: Column and Beam Re-bar Stress-Strain Relation

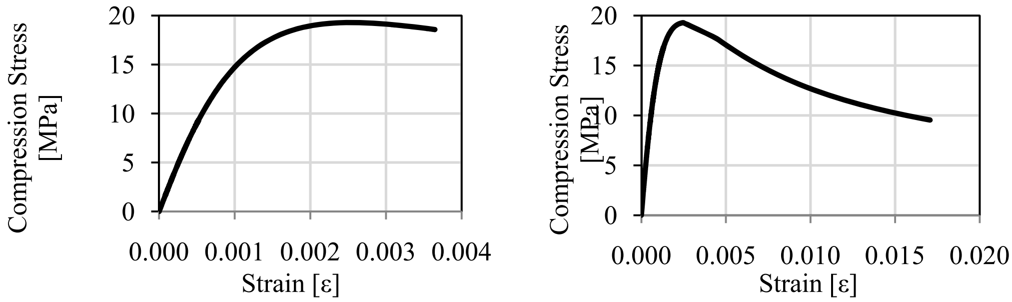

(a) Column Section *(b)Beam Section*

Figure 3.8: Column and Beam Concrete Stress-Strain Relation

3.2 Analytical Model for Bare Frame

The created analytical model for bare frame based on polygonal hysteretic model (PHM) with *concentrated plasticity*. Three types of PHM's are included in IDARC2D namely tri-linear, bilinear and vertex oriented. Depending on the results of the sensitivity analysis, it is obtained that tri-linear PHM is the convenient one for this study. The corresponding model includes stiffness degradation, strength deterioration and pinching effects.

Stiffness degradation expresses the decrease of the load-reversal slope due to increasing ductility. A corresponding stiffness degrading parameter in PHM (α) is defined having a range of 2 to 200. Strength deterioration includes an envelope degradation, which occurs when the maximum deformation attained in the past is exceeded, and continues energy based degradation. Corresponding parameters for strength deterioration are ductility based (β_1) and energy based (β_2) strength deterioration parameters. These parameters vary from 0.01 (no degrading) to 0.60 (severe degrading). Pinching hysteretic loops usually are the result of crack closure. Corresponding parameter for pinching is γ which varies from 0 (no slip) to 1.0 (severe slip). Mean values of the degradation parameters of hysteretic models were determined by comparing experimental and analytical results.

3.3 Analytical Model for Masonry Infill

3.3.1 The Force-Displacement Envelope for Masonry Infill

According to many researchers an infill wall can be represented by equivalent diagonal compression struts. The axial rigidity of these struts depends on the thickness, modulus of elasticity and width of the infill wall. The idealization of masonry infill are based on the study of Saneinejad and Hobbs, Figure 3.9.

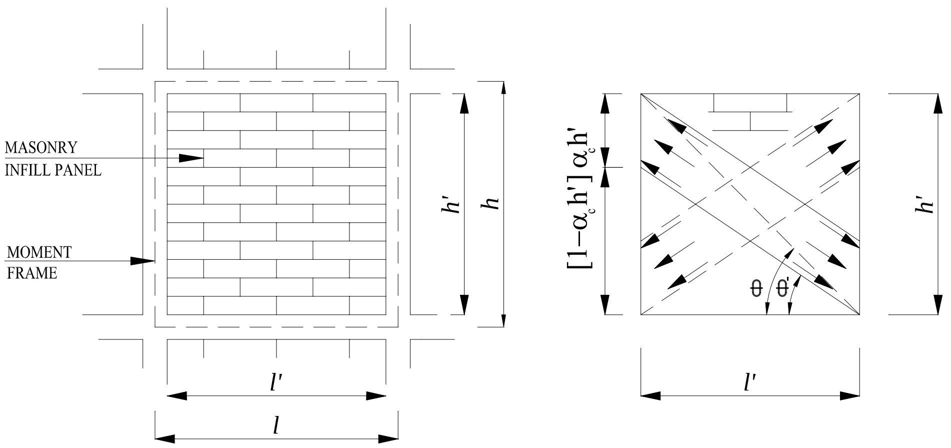

Figure 3.9: Equivalent diagonal strut model

In Figure 3.9, h is the height of the column measured on center of beam, $h^{'}$ is the height of the infill. l is the length of the beam measured center of columns. $l^{'}$ is length of the infill. r is aspect ratio and defined as follows.

$$r = h/l \qquad \textbf{[3.14]}$$

θ is sloping angle of infill and can be determined as

$$\theta = a\tan\left(h'/l'\right)$$ **[3.15]**

θ' is sloping angle of masonry diagonal strut at shear failure and was obtained from the relation:

$$\theta' = a\tan\left[\left(1-\alpha_c\right)\left(h'/l'\right)\right]$$ **[3.16]**

The upper bound or failure normal contact stress at the column-infill interface σ_{c0} and beam-infill interface σ_{b0} are calculated from Tresca Hexagonal Yield Criterion as:

$$\sigma_{c0} = \frac{f_c}{\sqrt{1+3\mu_f^2 r^4}}$$ **[3.17]**

$$\sigma_{b0} = \frac{f_c}{\sqrt{1+3\mu_f^2}}$$ **[3.18]**

Where μ_f is coefficient of friction of the masonry infill-frame interface and specified in ACI 530-88 [7] as $\mu_f = 0.45$.

f_c is effective (factored) compressive strength if the infill and calculated as

$$f_c = 0.6\phi f_m'$$ **[3.19]**

Where f_m' is prism strength of masonry.

The given formula for f_c is based on ACI 530-88 [7].

When the infilled frame is subjected to lateral loading, the comperssive strut cause compression at the infill-column and infill-beam interfaces. Saneinejad proposed rectangular stress block which takes into account this effect as shown in Figure 3.10.

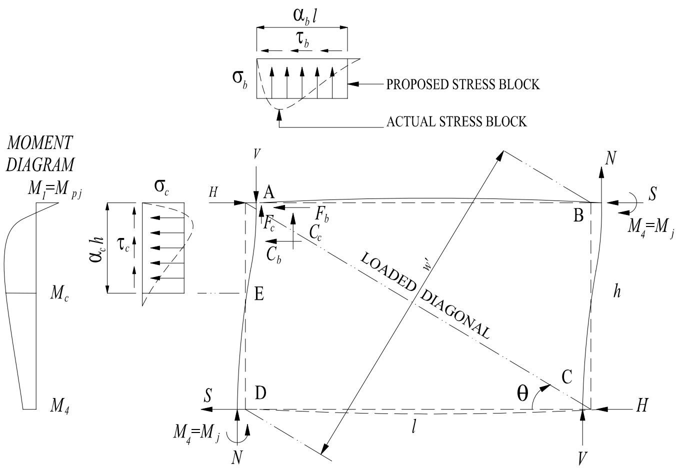

Figure 3.10: Masonry infill model

The length of stress block is defined as a portion of length of column or beam. If α is defined as normalized length of the interface contact length α_c and α_b correspond column and beam contact lengths, respectively. α_c can be determined as:

$$\alpha_c h = \sqrt{\frac{2M_{pj} + 2\beta_0 M_{pc}}{\sigma_{c0} t}} \leq 0.4h' \quad \textbf{[3.20]}$$

α_b can be determined as:

$$\alpha_b h = \sqrt{\frac{2M_{pj} + 2\beta_0 M_{pb}}{\sigma_{b0} t}} \leq 0.4h' \quad \textbf{[3.21]}$$

Where M_p is plastic moment capacity and subscripts *c* and *b* designates column and beam, respectively. M_{pj} is joint plastic resisting moment and taken as the least of the beam and the column plastic resisting moment.

The unloaded corners of the infill remain elastic when infill reach ultimate load. A coefficient is defined by Saneinejad based on finite element analysis and the resulting moment values of column and beam at the unloaded corners as follows:

$$M_c = \beta_c.M_{pc} \qquad M_b = \beta_b.M_{pb} \quad \textbf{[3.22]}$$

A value of β_0=0.2 is introduced as nominal or rather upper bound, value of the reduction factor of β_c and β_b

The permissible compressive stress of infill in its central region f_a is calculated as:

$$f_a = f_c \left[1 - \left(\frac{l_{eff}}{40t} \right)^2 \right] \quad \textbf{[3.23]}$$

Where l_{eff} is unsupported length of wall under diagonal compression stress and to be calculated as:

$$l_{eff} = \sqrt{\left[\left(1-\alpha_c\right)^2 h'^2 + l'^2 \right]} \quad \textbf{[3.24]}$$

The actual normal contact stress σ_c and σ_b are calculated using the following methodology:

If $A_c > A_b$ then

$$\sigma_b = \sigma_{b0} \Rightarrow \sigma_c = \sigma_{c0} \left[\frac{A_b}{A_c} \right] \quad \textbf{[3.25]}$$

If $A_b > A_c$ then

$$\sigma_c = \sigma_{c0} \Rightarrow \sigma_b = \sigma_{b0} \left[\frac{A_c}{A_b} \right] \quad \textbf{[3.26]}$$

Where

$$A_c = r^2 \sigma_{c0} \alpha_c \left(1 - \alpha_c - \mu_f r\right) \quad \textbf{[3.27]}$$

$$A_b = \sigma_{b0} \alpha_b \left(1 - \alpha_b - \mu_f r\right) \quad \textbf{[3.28]}$$

The contact shear stresses at the column-infill interface τ_c and beam-infill interface τ_b were given as, respectively:

$$\tau_c = \mu_f r^2 \sigma_c \quad \textbf{[3.29]}$$

$$\tau_b = \mu_f \sigma_b \quad \textbf{[3.30]}$$

Three types of failure mode can be classified which are corner crushing (CC), diagonal crushing (DC) and shear failure (SF). Diagonal and corner crushing strength can be calculated as follows:

$$V_m = A_d f_m^{'} \cos\theta \qquad \textbf{[3.31]}$$

Where A_d is cross-section area of the equivalent diagonal strut and given below:

$$A_d = \frac{\left[\left(1-\alpha_c\right)\alpha_c th \frac{\sigma_c}{f_c} + \alpha_b tl \frac{\tau_b}{f_c} \right]}{\cos\theta} \leq 0.5 \frac{th^{'} \frac{f_a}{f_c}}{\cos\theta} \qquad \textbf{[3.32]}$$

The left part of the Equation 3.32 corresponds to cross-section area for corner crushing mode and the right part corresponds to cross-section area for diagonal crushing mode.

Horizontal load carried by only infill at horizontal shear failure is given by Saneinejad as;

$$V_m = \frac{vtl^{'}}{\left(1-0.45\tan\theta^{'}\right)} < 0.83tl^{'} \qquad \textbf{[3.33]}$$

where v is cohesion or shear strength of infill wall.

Maximum lateral force carried by infill wall is the smallest value of the three distinct failure modes which are corner crushing, diagonal crushing and shear failure. The force displacement relationship of the infill panel is shown in Figure 3.11.

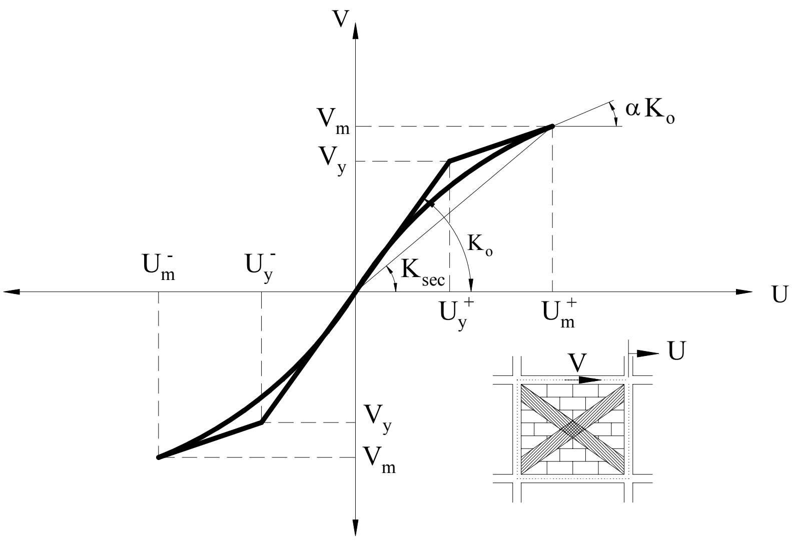

Figure 3.11: Strength envelope for masonry infill

In Figure 3.11, V_m is maximum lateral force carried by infill wall and calculated by the smallest value of Equations 3.31 and 3.33.

U_m is corresponding displacement for V_m. As described earlier V_m and U_m depend on the constitutive model which is shown in Figure 3.12.

$\varepsilon_m^{'}$ is corresponding strain for $f_m^{'}$

U_m is calculated from the following formula:

$$U_m = \frac{\varepsilon_m^{'} l_{eff}}{\cos\theta} \quad \textbf{[3.34]}$$

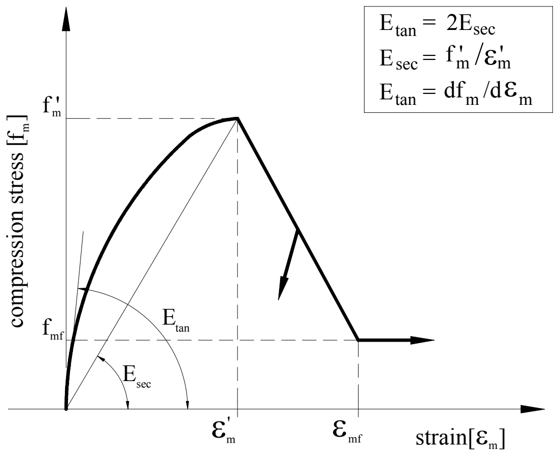

Figure 3.12: Constitutive model for masonry infill

K_{sec} is secant stiffness of the masonry infill at the peak load and defined as follows:

$$K_{sec} = \frac{V_m}{U_m} \quad \textbf{[3.35]}$$

The initial stiffness can be taken as twice the secant stiffness at the peak load untill a more consistent value is established for initial stiffness. And initial stiffness of the masonry infill and can be represented as:

$$K_0 = 2\left(\frac{V_m}{U_m}\right) \quad \textbf{[3.36]}$$

Lateral yield force of the infill panel can be determined as follows:

$$V_y = \frac{V_m - U_m K_0 \alpha}{(1-\alpha)} \quad \textbf{[3.37]}$$

Where α is post-yield stiffness ratio and taken as 1% .

Lateral yield displacement of the infill panel can be determined as follows:

$$U_y = \frac{V_m - U_m K_0 \alpha}{(1-\alpha) K_0} \qquad \textbf{[3.38]}$$

3.3.2 The Hysteresis Model for Masonry Infill

The response envelop of masonry infill are modeled in IDAR2D by its initial stiffness (K_0) and lateral yield force capacity V_y. The hysteretic behavior is represented by a smooth hysteretic model (SHM) based on the Wen-Bouc model. The input parameters for hysteretic model are A, β, γ, η, α, A_s, Z_s, $\overline{Z}$, s_k, s_{p1}, s_{p2} and μ_c.

A, β and γ are constants that control the shape of the generated hysteresis loops. The default values are taken for this parameters A=1, β=0.1 and γ=0.9. To satisfy viscoplastic conditions the present development assumes that $A = \beta + \gamma = 1.0$. The parameter η controls the rate of transition from the elastic to the yield state. A large value of η approximates a bilinear hysteretic curve, while a lower value will trace a smoother transition. Parameter α is post yielding stiffness ratio for infill panel which is defined as percent of initial stiffness. An important characteristic in the hysteretic response of infill panels is the loss of stiffness due to deformation beyond yield. s_k is a control parameter used to vary the rate of stiffness decay as a function of the current ductility, as well as the maximum attained ductility before the start of the current unloading or reloading cycle. A value of $s_k = 0$ simulates a non-degrading system. The parameters s_{p1} and s_{p2} control the rate of strength deterioration. μ_c is ductility capacity of infill panel. A_s is a control parameter to vary slip length which may be linked to the size of crack openings or reinforcement slip. The parameter Z_s, that controls the sharpness of the slip, is assumed to be independent from the response history. In order to shift the effective slip region to be symmetric about an arbitrary $Z = \overline{Z}$, the value of Z used for slip may be offset by a value $\overline{Z}$.

3.4 Methodology of the Study

The methodology used in this study can be summarized by a flow chart as follows. Material tests is the first step. Frame material tests consists of concrete compression test and steel tensile tests. The material test results were used as the input for XTRACT to obtain the moment-curvature envelopes. The nominal infill strength obtained by conducting compression tests. Infill dimensions and test results were used to obtain the infill force-displacement envelope. Sectional moment-curvature relations for frame members and shear force-displacement relation for infill panel were used in IDARC2D to simulate the behaviour.

Concrete compression strength, corresponding strain and modulus of elasticity were obtained from the compression test. Steel yield, ultimate strength, corresponding strains, modulus of elasticity were obtained from the tensile tests. Standart infill samples were tested in different directions and nominal infill strength and strain values are obtained.

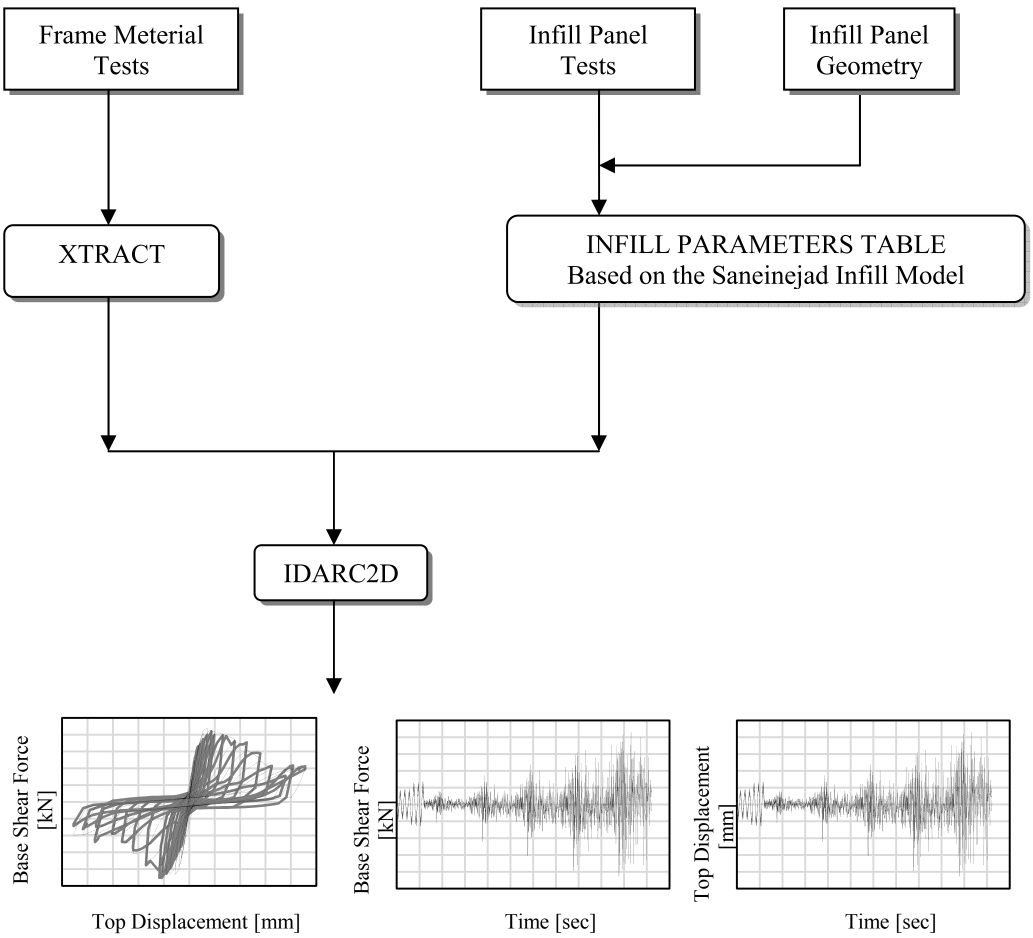

First step of the mothodology is summarized below:This step consist of a series of material tests.

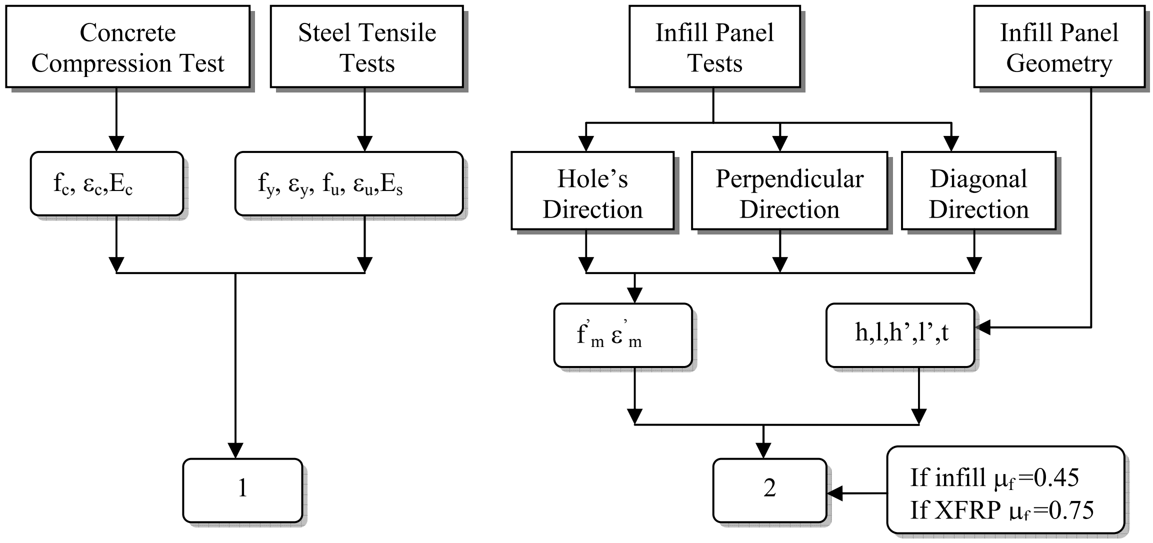

In the second step, frame member's moment-curvature envelopes were obtained in XTRACT by using the results of material tests to simulate hysteresis response in IDARC2D. Infill panel and CFRP retrofitted infill panel shear force-displacement envelopes were obtained by a calculation table defined in the previous pages, based on Saneinejad's infill wall model.

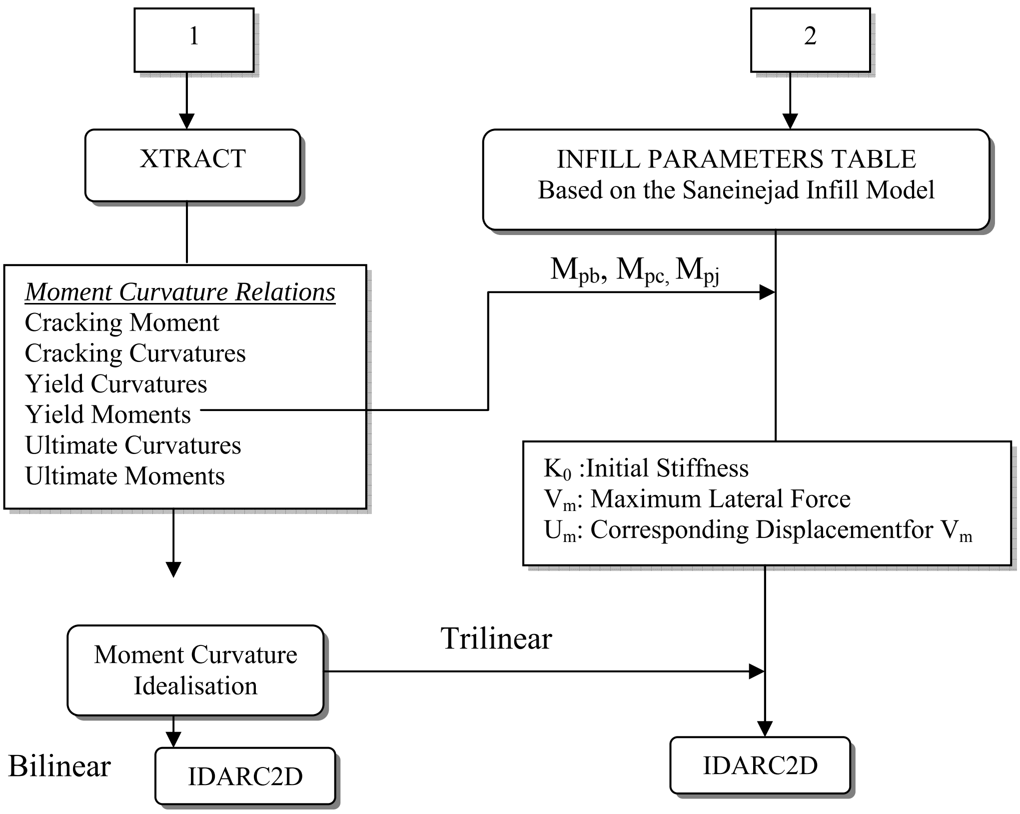

Polygonal Hysteretic Model [PHM] was used for bare frame. PHM was used for infilled frame columns and beam, Smooth Hysteretic Model [SHM] was used for masonry infill hysteresis. Mass-proportional damping was used for bare frame and stiffness-proportional damping type was used for infilled frames. Related procedure is summarized below.

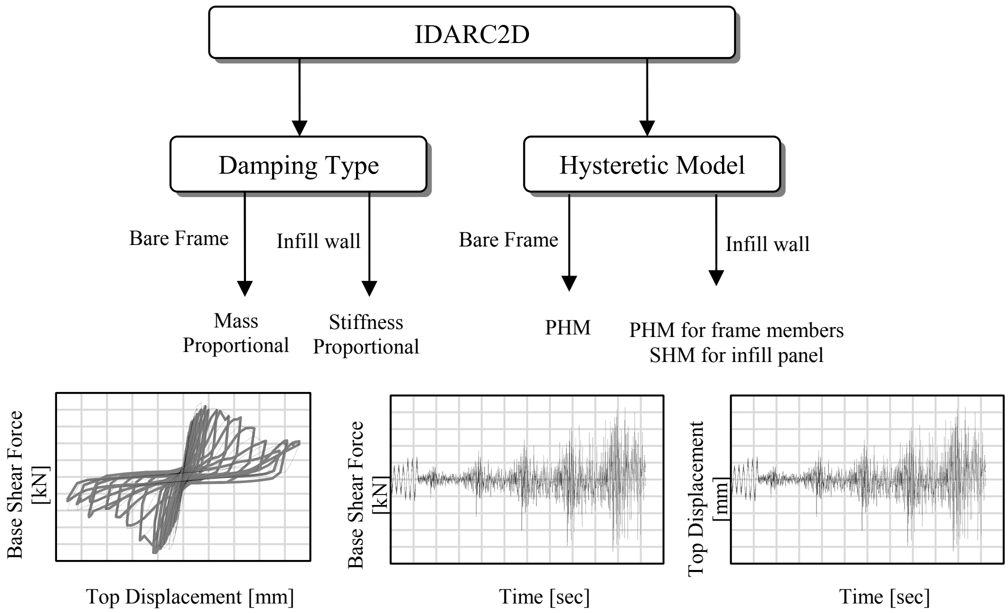

4. SIMULATION STUDY

Two set of analysis, which are quasi-static cyclic analysis and non-linear dynamic analysis, were conducted. Firstly, 1-cyclic and 3-cyclic quasi-static analysis were performed to determine hysteretic model parameters which consist of characteristics such as stiffness degradation, strength deterioration and pinching for each specimen type. Secondly, the reliability of determined hysteretic parameters were investigated by performing non-linear dynamic analysis for two mass levels which are nominated as low mass (8.5 kNs^2/m) and high mass (22.1 kNs^2/m) for each specimen.

The methodology for finding the hysteretic parameters can be explained as follows; first, PHM degrading parameters for bare frame were determined. Then, by using same model parameters for frame members, the SHM model parameters for infill panel and retrofitted infill panel were determined based on both series of experimental test results. The used hysteresis model types for specimens are listed in Table 4.1.

Table:4.1 Specimens hysteresis model used in simulation

Specimen	Columns and Beam Hysteretic Model	Infill Panel Hysteretic Model
Bare Frame	PHM	-
Infilled Frame	PHM	SHM
Cross-Braced Frame	PHM	SHM

4.1 Bare Frame

The analytical model for bare frame is idealized as 3 frame members which correspond two columns and a beam as shown in Figure 4.1.

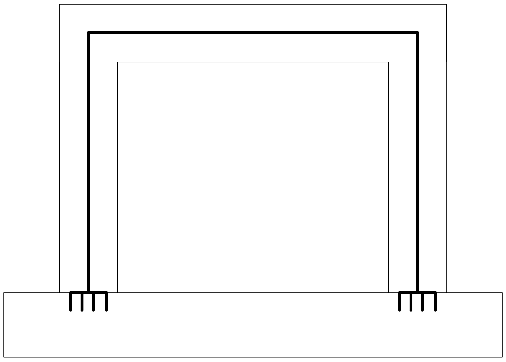

Figure 4.1: Analytical model of specimens

The concentrated plasticity is used in the nonlinear analysis of frame members. The typical moment curvature relations for columns and beam end sections were given in Figure 4.2.

In the analytical study, some assumptions were made depending on the experimental results. At the beginning of the analysis, the cracked stiffness was used depending on the photograph taken at a drift ratio of 0.072%, Figure 4.2, where some early cracks are seen.

Figure 4.2: The specimen photograph taken at % 0.072 drift ratio

The rigid-ends for column was not used because of the existency of the initial cracks shown in Figure 4.3.

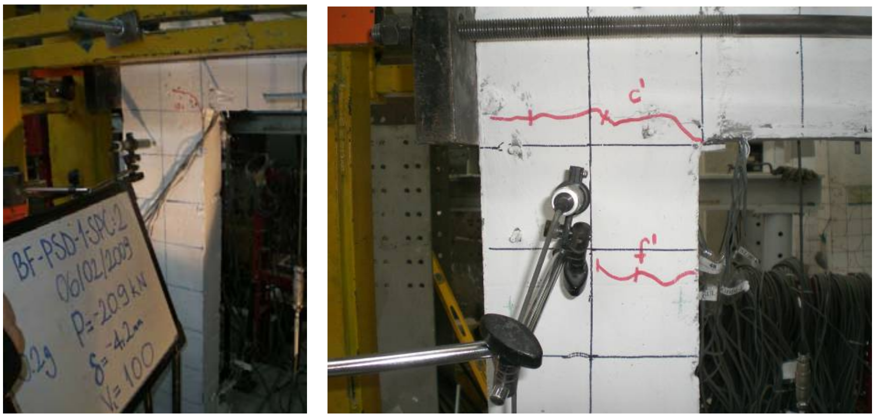

Figure 4.3: Observed cracks at column-beam intersections

4.1.1 Quasi-static Cyclic Analysis

Quasi-static cyclic analysis are performed by applying piecewise linear cyclic displacement history which was used in the experiments.

4.1.1.1 One-Cyclic Quasi-Static Analysis

The displacement pattern for one-cyclic quasi-static analysis is shown in Figure 4.4 .

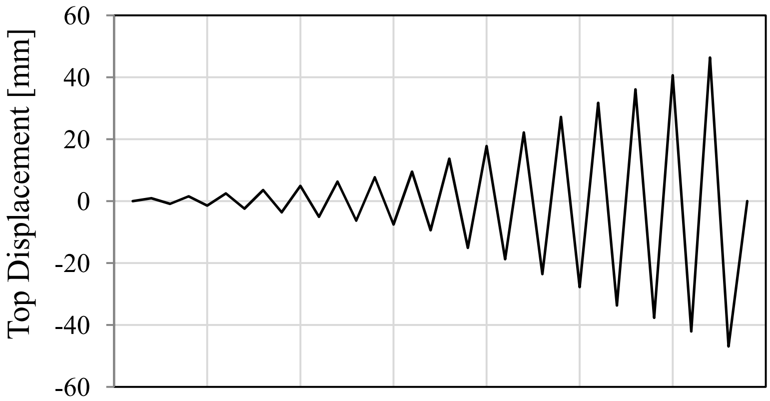

Figure 4.4: One-cyclic quasi-static displacement pattern

A calibration process is successfully completed to determine the optimum PHM degrading parameters by comparing the experimental and analytical force-displacement responses. The PHM degrading parameters and corresponding damage levels are given in Table 4.2.

Table 4.2: PHM parameters for frame members (colums and beam)

Parameter	Meaning	Value	Effect
α	Stiffness Degrading Parameter	10	Moderate
β_1	Ductility-Based Strength Degrading Parameter	0.01	No degrading
β_2	Energy-Based Strength Degrading Parameter	0.01	No degrading
γ	Slip or Crack Closing Parameter	0.30	Moderate

The calculated damage parameters demonstrate that there exist no strength deterioration whereas moderate stfifness degradation and moderate pinching were observed. In the experimental study, the concrete cover intended was 15 mm. Unfortunately, two re-bars moved from their original position and 40 mm concrete cover was observed at one face of columns, Figure 4.5. There exists quite difference between positive and negative shear force capacity of the specimen as shown in Figure 4.6. The moment-curvature relation of the columns was modified in the analytical model in order to reach similar force displacement relations with the experiment.

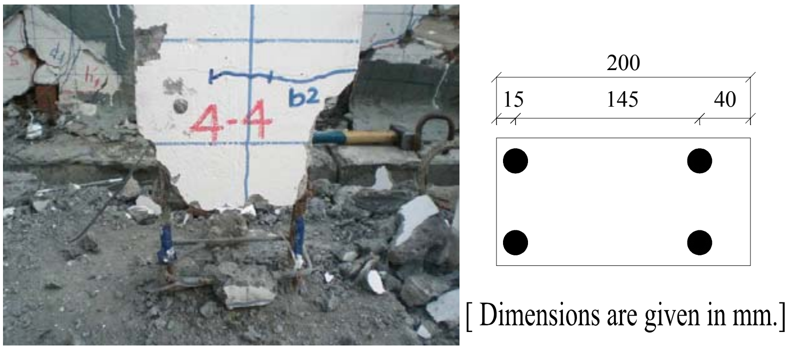

Figure 4.5: Constructional imperfection in columns

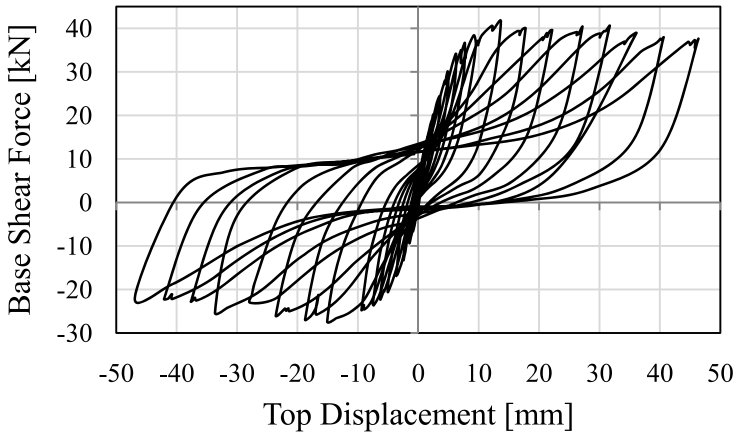

Figure 4.6: Difference in positive and negative shear capacity due to imperfection

The comparison of simulation with the experimently obtained top displacement versus base shear relation is illustrated in Figure 4.7.

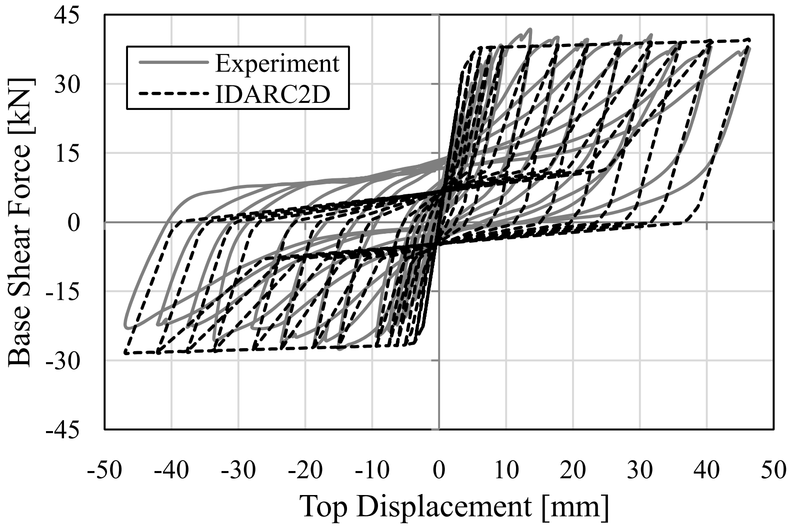

Figure 4.7: Base shear force- top displacement relation

Envelope curves of the experimental and analytical hysteresis for base shear force-top displacement are given in Figure 4.8.

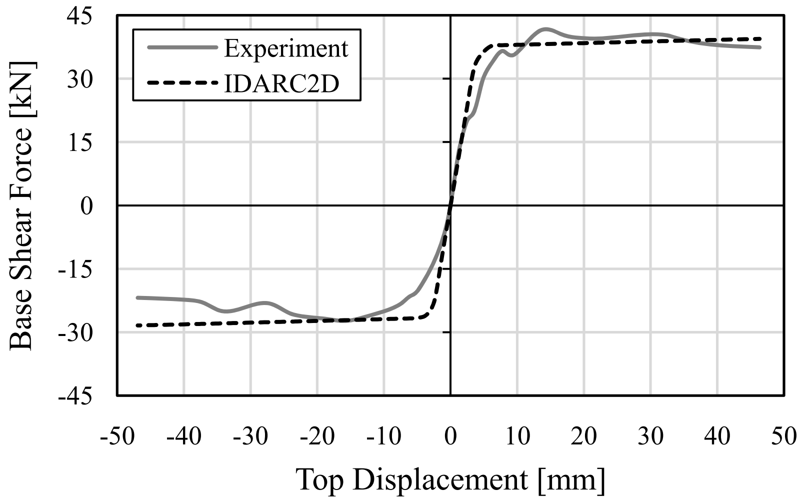

Figure 4.8: Envelope curves of the experimental and analytical hysteresis

The comparison of one-cyclic quasi-static test stiffness-drift ratio relationships of simulation and experiment are shown in Figure 4.9.

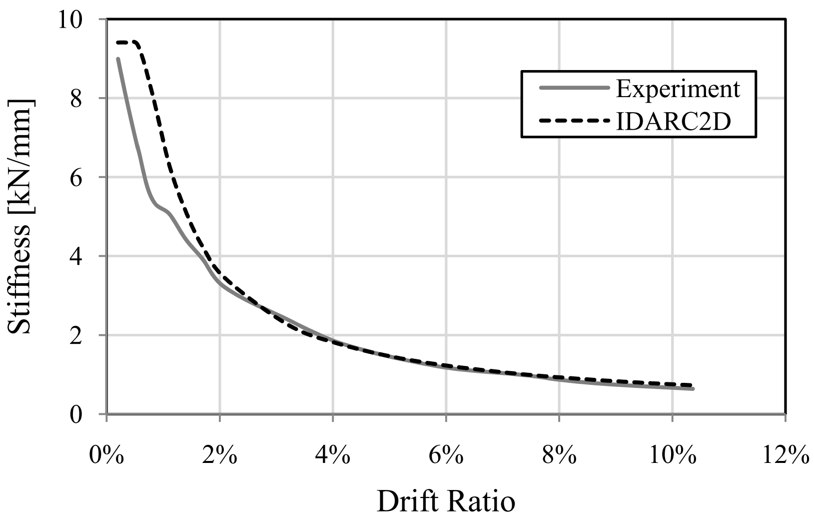

Figure 4.9: Lateral stiffness-drift ratio relations

The comparison of lateral stiffness for experiment and simulation is given in Figure 4.10.

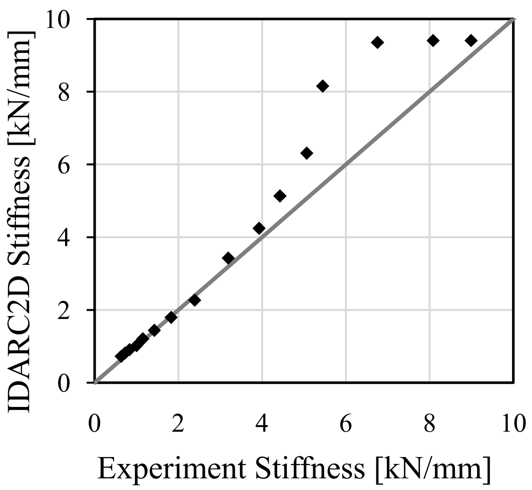

Figure 4.10: Comparison of lateral stiffness in experiment and analysis

Energy dissipation capacity is the sum of the area under the hysteretic loops in the base shear-top displacement relation diagram. Comperatively cumulative dissipated energy in experimental and analytical studies are given below.

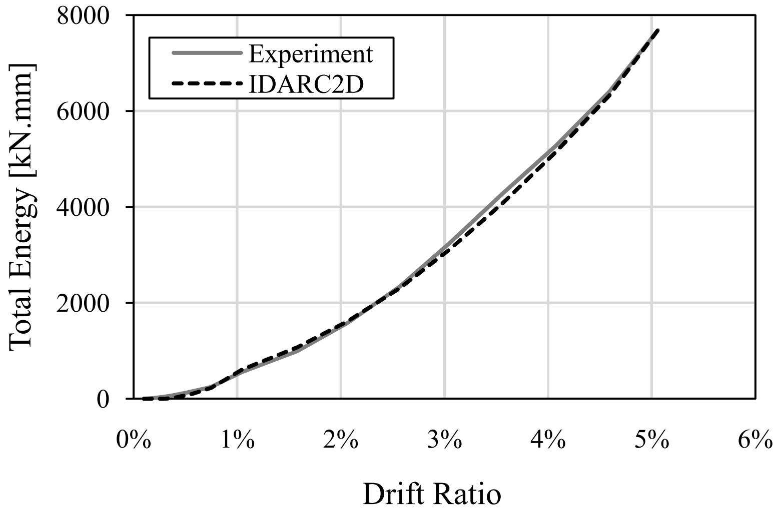

Figure 4.11: Experimental and analytical cumulative energy- drift ratio relations

The energy dissipated at each displacement cycle is given in Figure 4.12. As seen the dissipiated energy values are sufficently close in experiment and analytical works.

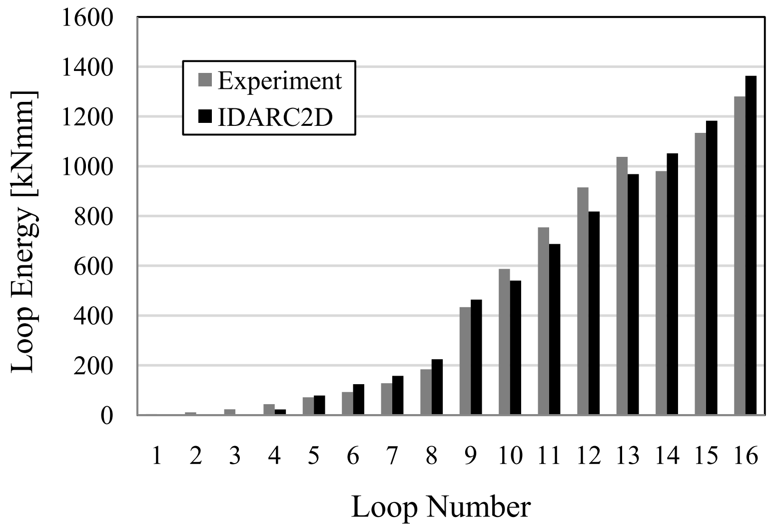

Figure 4.12: Dissipated energy at each experimental and analytical cycles

4.1.1.2 Three-Cyclic Quasi-static Analysis

The quasi-static displacement pattern in which three repetition is existing for each diplacement target is illustrated in Figure 4.13.

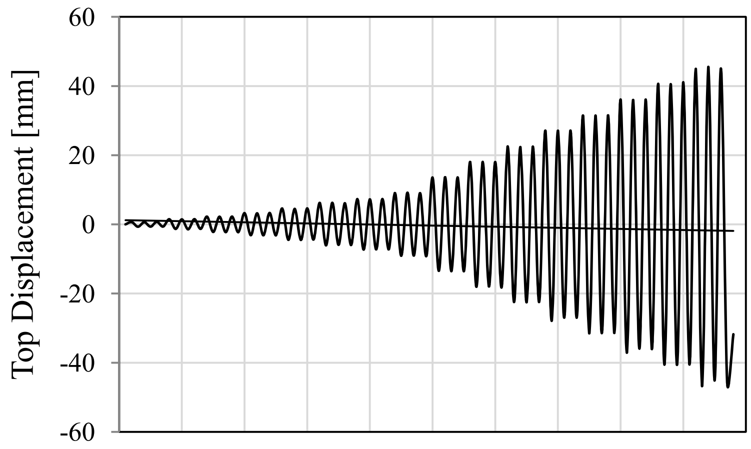

Figure 4.13: Three-cyclic quasi-static displacement pattern

The comparison of experimental and analytical base shear versus top displacement relations obtained by using three-cyclic displacement pattern are shown in Figure 4.14.

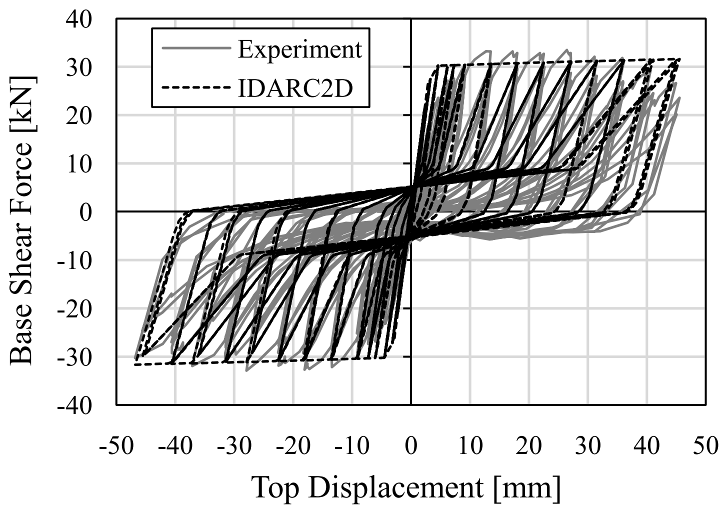

Figure 4.14: Base shear force- top displacement relation

In the analytical study, the degrading parameter of γ was taken as 0.23. Because the damage accumulation in three-cyclic test is more severe than one-cyclic test. The photographs seen in Figure 4.15 shows the final damage states at the end of tests for two different loading cases.

(a)One-cyclic

(b) Three-cyclic

Figure 4.15: Final damage states

Envelope curves of the experimental and analytical hysteresis of base shear-top displacement are given in Figure 4.16.

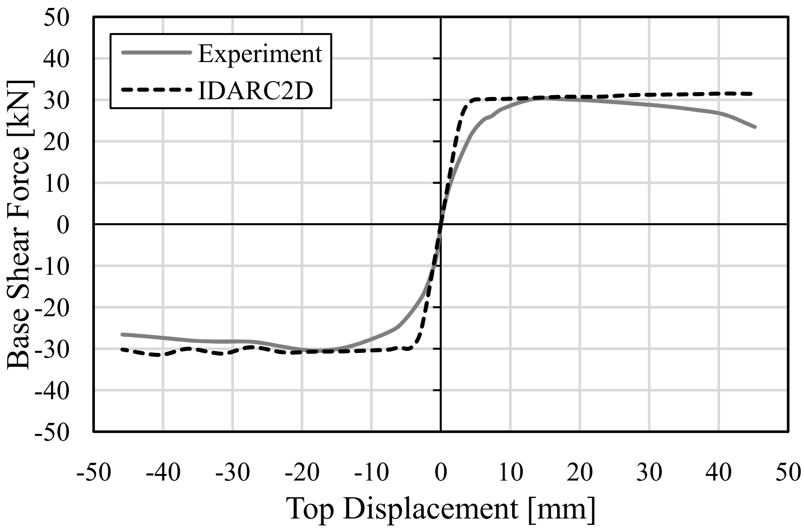

Figure 4.16: Envelope curves of the experimental and analytical hysteresis

The comparison of lateral stiffness versus story drift ratio relationships is given in Figure 4.17.

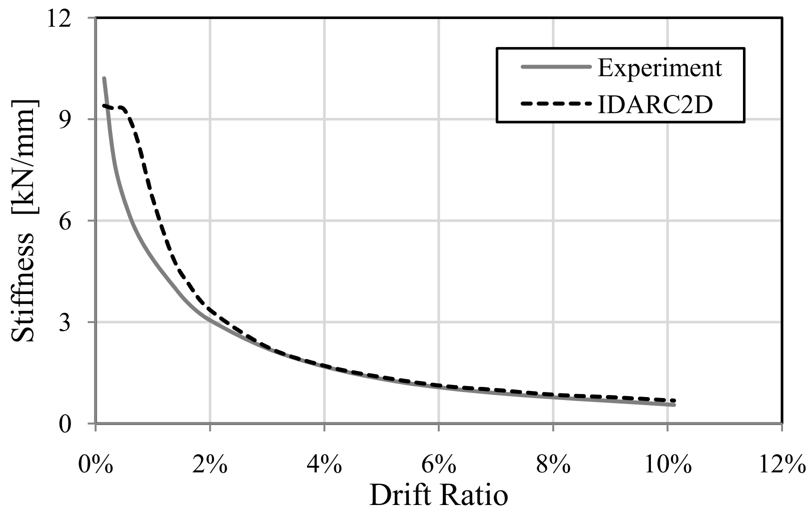

Figure 4.17: Lateral stiffness-drift ratio relations

The lateral stiffness obtained from the experiment and analytic work has been compared for varios drift levels and given in Figure 4.18.

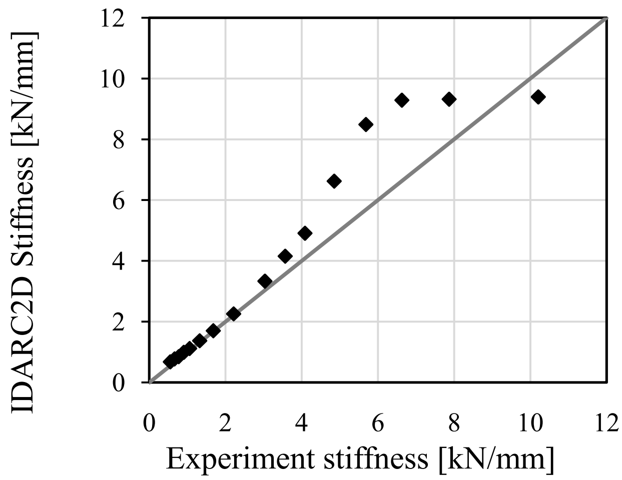

Figure 4.18: Comparison of lateral stiffness in experiment and analysis

Cumulative dissipated energy obtained from the experimental and analytical works are given in Figure 4.19 comperatively.

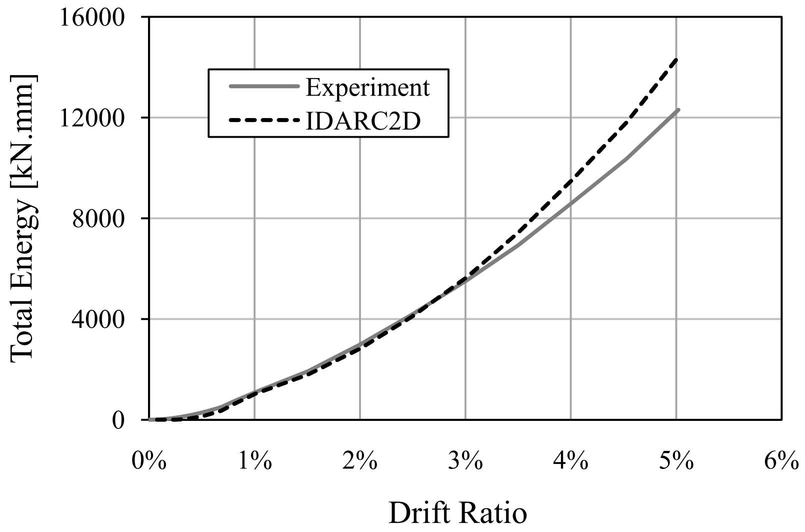

Figure 4.19: Experimental and analytical cumulative energy- drift ratio relations

The cumulative dissipated energy in experiment is coincide with analytical results until a drift ratio of 3%. The cumulative error in total dissipated energy is 14%. The energy dissipated at each displacement cycle is given in Figure 4.20.

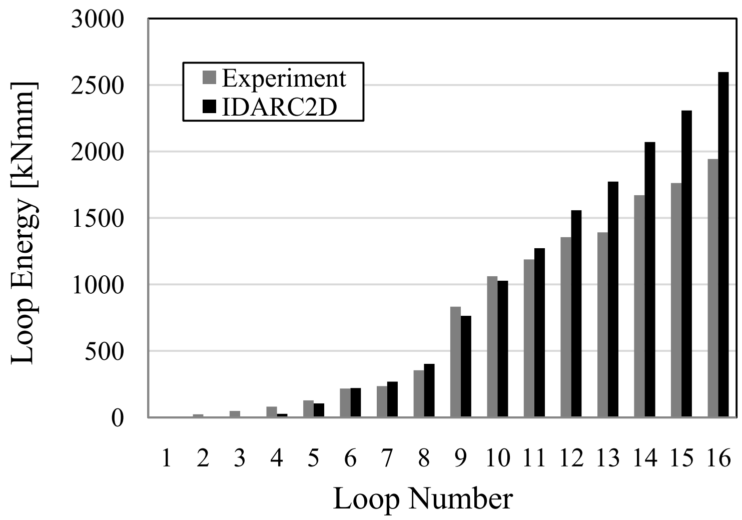

Figure 4.20: Dissipated energy at each experimental and analytical cycles

4.1.2 Non-linear Time History Analysis

Non-linear time history analyses for two mass conditions which are low mass (8.5 kNs^2/m) and high mass (22.1 kNs^2/m) have been performed to compare with the results of corresponding PsD tests. The damping is modeled as mass proportional and taken as 5% of the critical damping.

Base shear force lateral top displacement relations for 0.2 and 0.4 PGA levels are given in Apendix: A1. Lateral top displacement histories for 0.2 and 0.4 PGA levels are given in Apendix: A4. Base shear force histories for 0.2 and 0.4 PGA levels are given in Apendix: A7.

4.1.2.1 Low-Mass Dynamic Case

In PSD experiments, specimen was subjected to a series of acceleration records. Firstly, a sinusoidal type acceleration record was used, Figure 4.21. The time increment and total duration of the record are 0.02 sec and 6 sec, respectively.

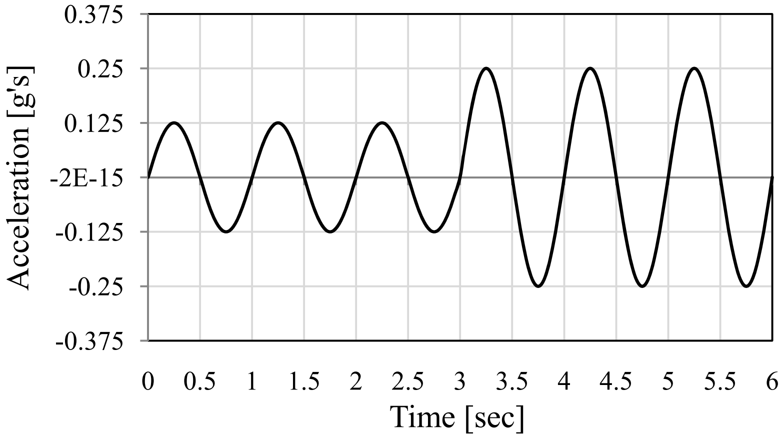

Figure 4.21: Sinusoidal wave acceleration record

Secondly, the modified Duzce Earthquake acceleration record was applied repeatedly for increasing peak accelerations which are 0.2g, 0.4g, 0.6g. The modified Duzce Earthquake acceleration record sampled by 0.01 sec time intervals and the duration of record is 10 sec. The modified Duzce Earthquake acceleration record for 0.2 PGA level is given in Figure 4.22.

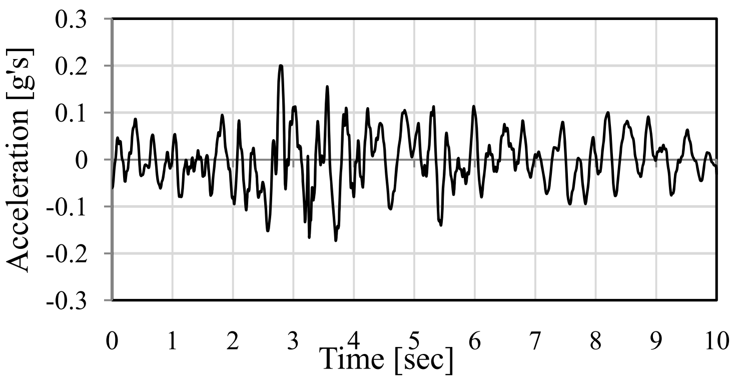

Figure 4.22: The modified Duzce Earthquake PGA=0.2g

The complate acceleration record that applied to bare frame is given in Figure 4.23. Total duration is 36 seconds which include a sinus wave and three modified Duzce Earthquake with increasing PGA values of 0.2g, 0.4g and 0.6g, respectively.

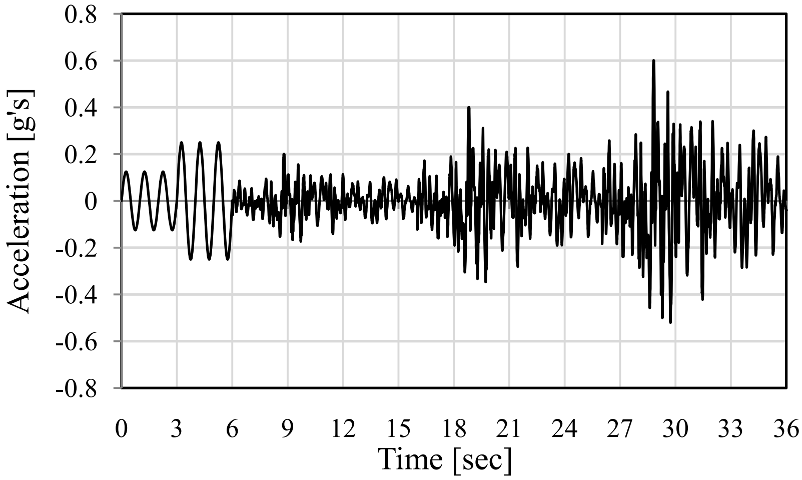

Figure 4.23: Acceleration record used in low mass case

The numerical integration time step in the analytical work is selected as 0.00005 (Δt/200) sec to assure numerical stability. The performance of the hysteretic model is investigated by three relations which are time-displacement, time-base shear and force-displacement. The comparison of top displacement-base shear relations are given in Figure 4.24.

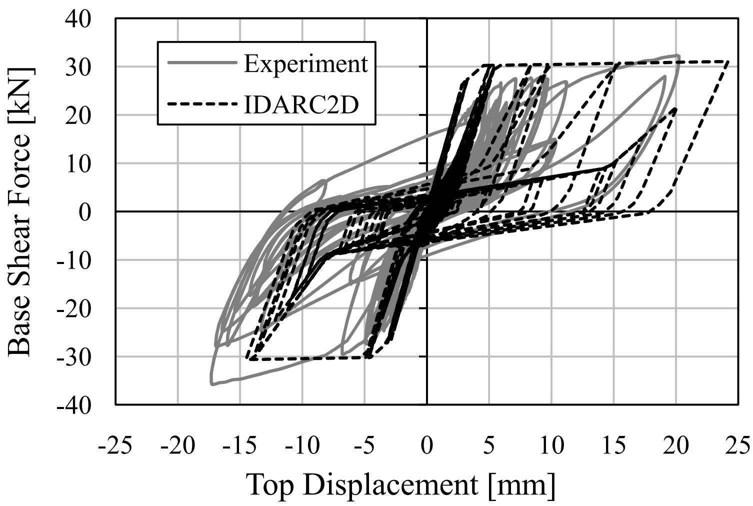

Figure 4.24: Base shear force- top displacement relation

The comparison of top displacement history is given in Figure 4.25.

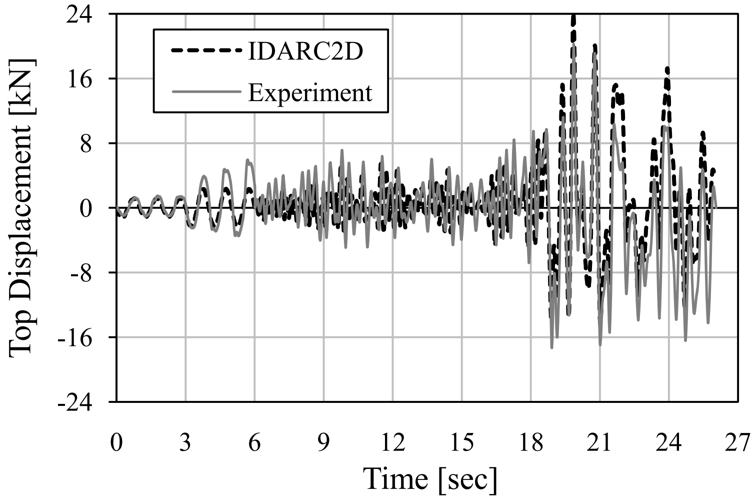

Figure 4.25: Lateral top displacement history for low mass case

The base shear force history obtained analytically is compared with the experimental one, Figure 4.26.

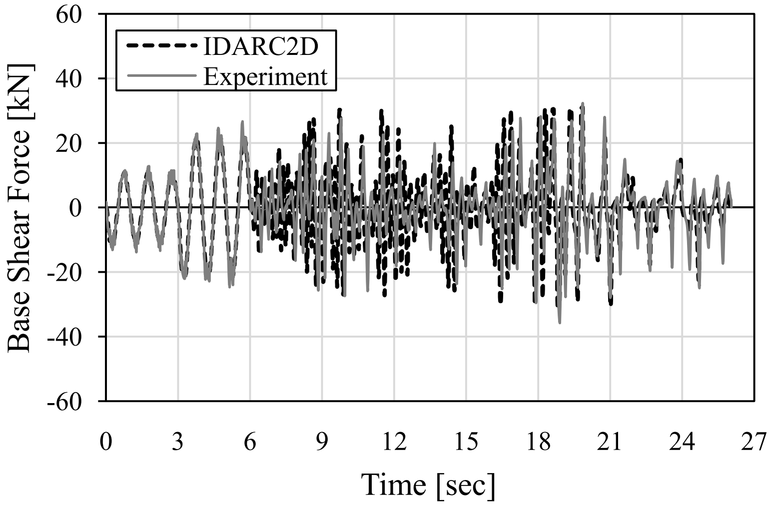

Figure 4.26: Base shear force history for low mass case

4.1.2.2 High-Mass Dynamic Case

The full acceleration record that applied to bare frame is given in Figure 4.27. Total duration is 32 seconds which include a triangular wave and two modified Duzce Earthquake with increasing PGA values of 0.2g and 0.4g, respectively.

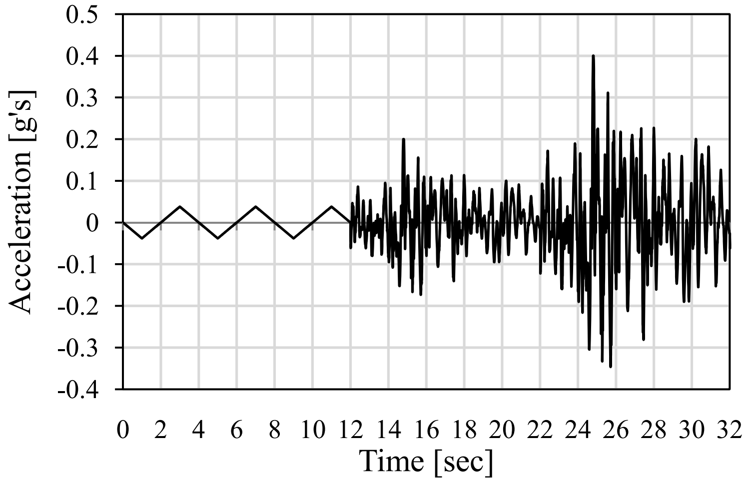

Figure 4.27: Acceleration record used in low mass case

The comparison of top displacement versus base shear force relations are given in Figure 4.28.

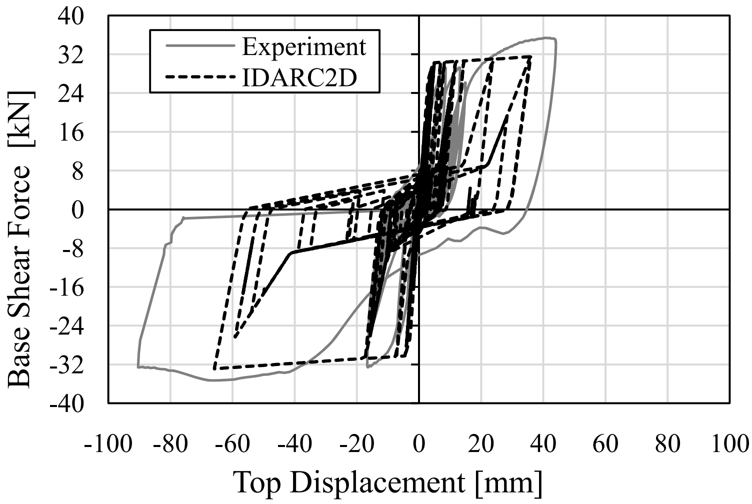

Figure 4.28: Base shear force- top displacement relation

The comparison of top displacement history is given in Figure 4.29.

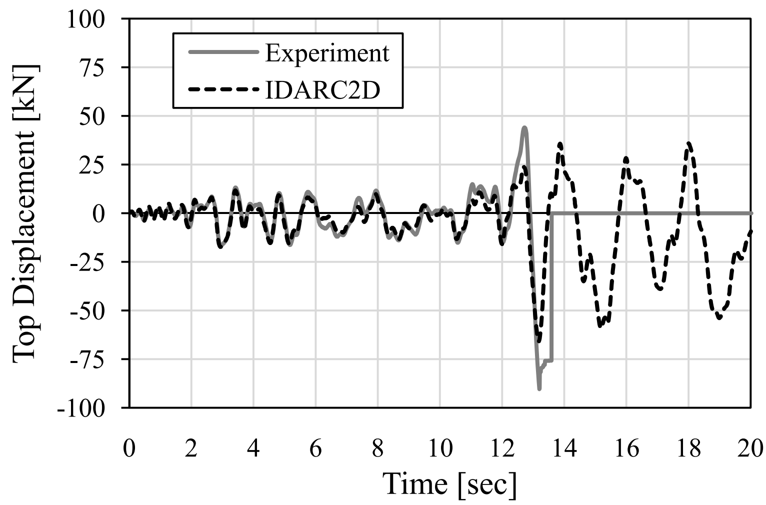

Figure 4.29: Lateral top displacement history for high mass case

The comparison of base shear history is given in Figure 4.30.

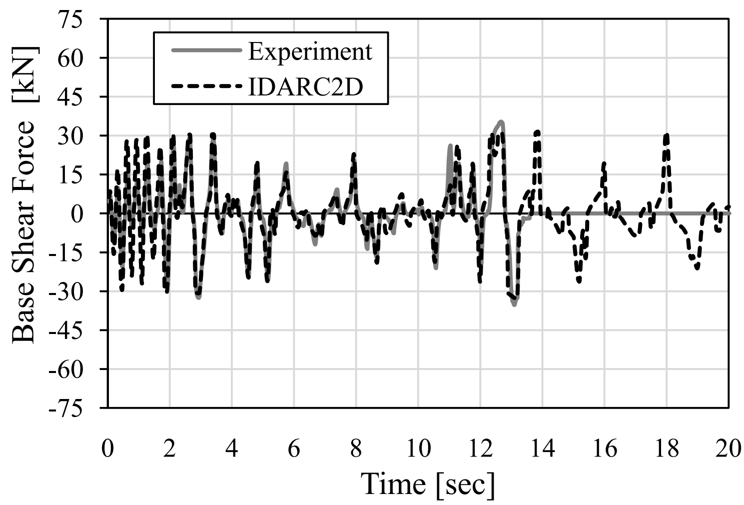

Figure 4.30: Base shear force history for high mass case

4.2 INFILLED FRAME

The infill panel is modeled by equivalent diagonal compression struts. The contribution of infill panel to bare frame is taken into account as a bilinear shear spring. The initial stiffnesss K_0 and lateral yield force capacity V_y of infill panel is calculated in Table 4.3.

The compression strength of masonry f_c is taken from the infill panel tests of 500 × 500 mm, [8]. The average of compressive strengths obtained in two main directions is 4.5 MPa and the corresponding strain value is 0.006. Basic shear strength of masonry v is 1.1 MPa which is specified in ACI 530-88.

Lateral yield force V_y and initial stiffness K_0 are 80.8 kN and 19.4 kN/mm which are close to the calculated values of 77.0 kN and 17.7 kN/mm in Table 4.3.

The following assumptions are used in the analytical study. Tri-linear moment curvature idealization was used in the analytical model. Initial cracks were not existing at the top and bottom sections of the columns, see the photograph taken at 0.078% drift level in Figure 4.33. Therefore gross-sectional flexural rigidity is used as the initial rigidity for RC members.

Figure 4.31: Specimen state at 0.078% story drift

At top end of the columns, a rigid end having 100 mm depth was taken into consideration. The photograph taken at 0.16% drift level shows no crack in and around the beam-column connection, Figure 4.32.

Table: 4.3 : Strength and Stiffness Calculation for Infill Panel

Parameter	Meaning	Value	Unit
h	Height of column measured on center of beams	900	mm
h'	Height of infill	800	mm
l	Length of column measured on center of columns	1133	mm
l'	Length of infill	933	mm
r	Aspect Ratio	0.7944	
θ	Sloping angle of diagonal infill	0.7088	
θ'	Sloping angle of masonry diagonal strut at shear failure	0.5740	
μ_f	**Coefficient offriction of the frame-infill interface**	**0.45**	
f_m'	Prism strength of masonry	4.5	MPa
f_m	Effective(factored) compressive strength of infill	4.5	MPa
σ_{c0}	Column-infill nominal (upper bound) uniform contact normal stress	4.0	MPa
σ_{b0}	Beam-infill nominal (upper bound) uniform contact normal stress	3.5	MPa
M_{pc}	Plastic resisting moment of the column	6592	kN.mm
M_{pb}	Plastic resisting moment of the beam	10300	kN.mm
M_{pj}	Joint plastic resisting moment	6592	kN.mm
t	Infill thickness	80	mm
α_c	Normalized contact length of column-infill interface	0.25	
α_b	Normalized contact length of beam-infill interface	0.22	
A_c	Column-Infill interface contact stress	2.0	MPa
A_b	Beam-Infill interface contact stress	3.0	MPa
σ_c	Actual normal stress column-infill interface	4.0	MPa
σ_b	Actual normal stress beam-infill interface	2.7	MPa
τ_c	Contact shear stress column-infill interface	1.1	MPa
τ_b	Contact shear stress beam-infill interface	1.2	MPa
l_{eff}	Effective length of the equilavent diagonal struts	1111	mm
f_a	Permissible stress	3.9	MPa
A_d	Area of the equilavent diagonal struts	22768	mm^2
v	Basic shear strength or cohesion of masonry	1.1	MPa
V_m	Maximum lateral force	77.78	kN
ε_m'	Corresponding strain for masonry prism strength	0.006	
U_m	Corresponding displacement for V_m	8.87	mm
$\boldsymbol{K_0}$	**Initial stiffness**	**17.71**	**kN/mm**
α	Post-yield stiffness ratio	0.01	
$\boldsymbol{V_y}$	**Lateral yield force**	**76.99**	**kN**
U_y	Lateral yield displacement	4.34	mm

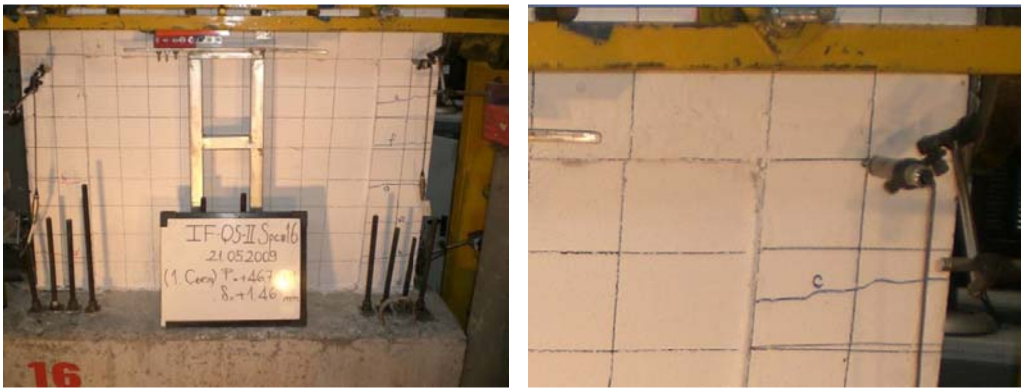

Figure 4.32: Specimen state at 0.16% story drift

4.2.1 Quasi-static Cyclic Analysis

4.2.1.1 One-Cyclic Quasi-static Analysis

The applied displacement pattern for one-cyclic static test is given below:

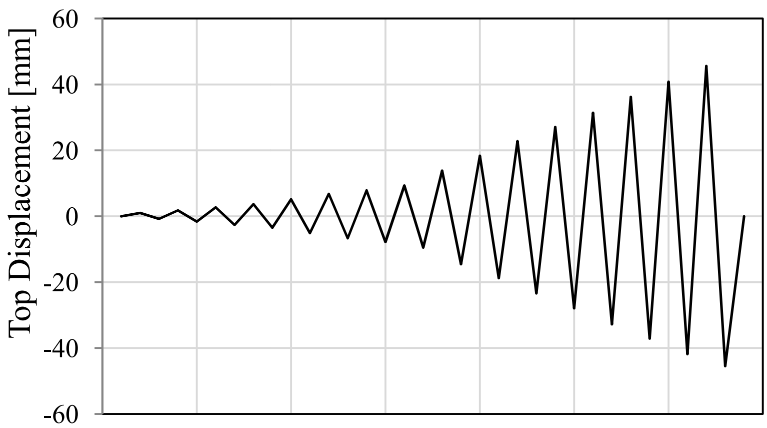

Figure 4.33: One-cyclic quasi-static displacement pattern

A calibration process is successfully accomplished to determine the smooth hysteretic model (SHM) parameters in IDARC2D for infill panel by comparing the experimental and analytical force-displacement relations. The obtained parameters are listed in the Table 4.4. The polygonal hysteretic model (PHM) parameters used for the RC frame members are the same obtained for bare frame.

Table: 4.4 : SHM paramaters for infill panel

Parameter	Meaning	Value
K_0	Initial Elastic Stiffness of Infill Panel	19.4 kN/mm
V_y	Lateral Yield Capacity	80.8 kN
A	Parameter A in Wen's Model	1.0
β	Parameter β in Wen's Model	0.1
γ	Parameter γ in Wen's Model	0.9
η	Parameter η in Wen's Model	2.0
α	Post Yielding stiffness Ratio	0.001
A_s	Control parameter for slip length	0.83
Z_s	Parameter that controls the sharpness of the slip	0.20
$\overline{Z}$	Offset value for slip response	0.0
s_k	Control parameter to vary the rate of stiffness decay	0.001
s_{p1}	Parameter to control the rate of strength deterioration	0.01
s_{p2}	Parameter to control the rate of strength deterioration	1.0
μ_c	Ductility capacity of infill panel	7.5

Top displacement-base shear relationships obtained in the experimental and analytical studies are shown in Figure 4.34.

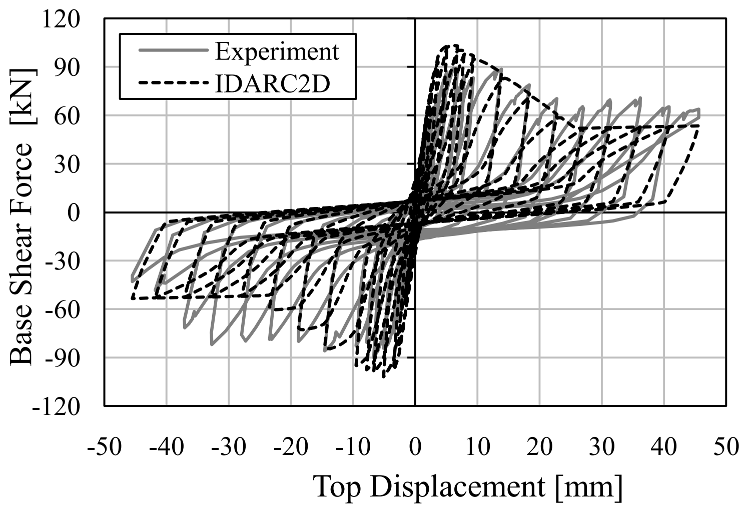

Figure 4.34: Base shear force-top displacement relations

Envelope curves of the hysteresis are illusrated in Figure 4.35. The general form of the analytical curve is similar to the experimental one.

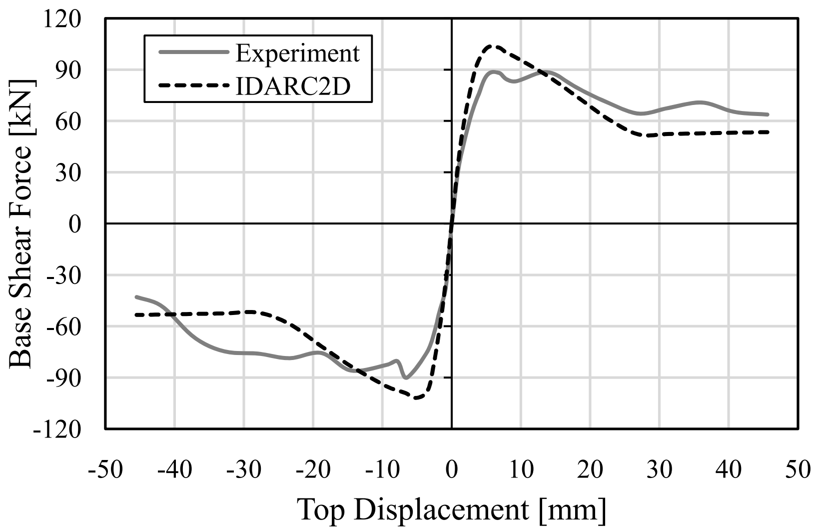

Figure 4.35: Envelope curves of the experimental and analytical hysteresis

The comparison of lateral stiffness versus story drift ratio relation obtained in experimental and analytical studies is given together in Figure 4.36.

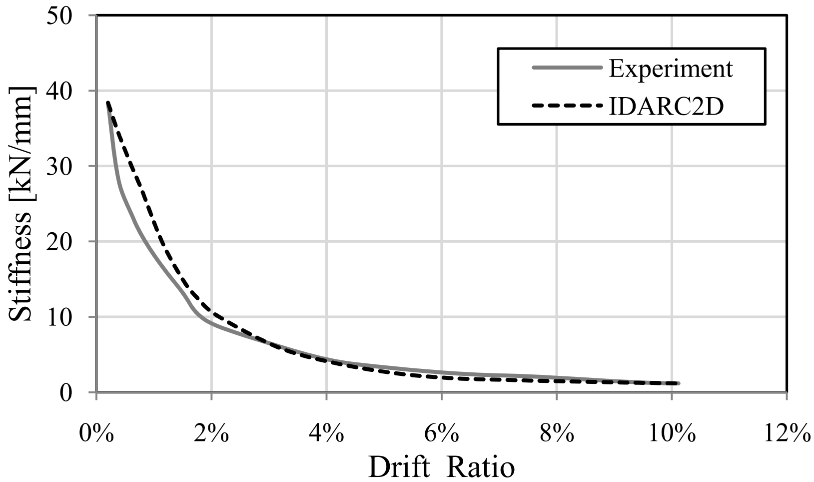

Figure 4.36: Lateral stiffness-drift ratio relations

The comparison of the lateral stiffness obtained for different displacement cycles is given in Figure 4.37. If a point coincides on the line with a slope of 45^0, it means that the lateral stiffness obtained from the experimental and analytical works are equal to each other. From Figure 4.37, one can evaluate that lateral stiffness of analytical model is relatively greater than the experiment.

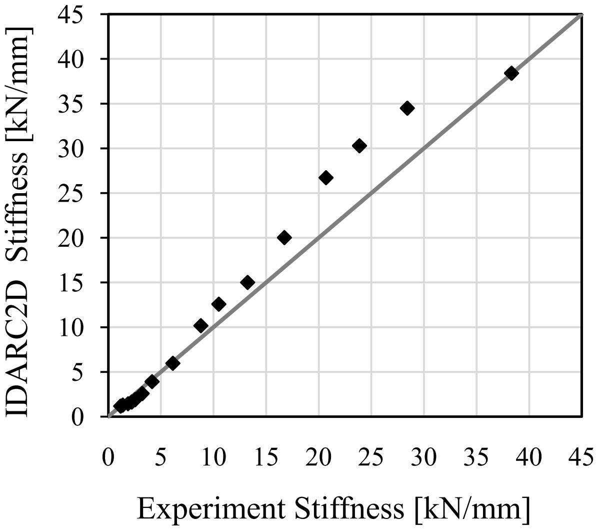

Figure 4.37: Comparison of lateral stiffness in experiment and analysis

The comparison of cumulative dissipated energy obtained from analytical and experimental studies is shown in Figure 4.38. The cumulative relative error in final stage is around 13%.

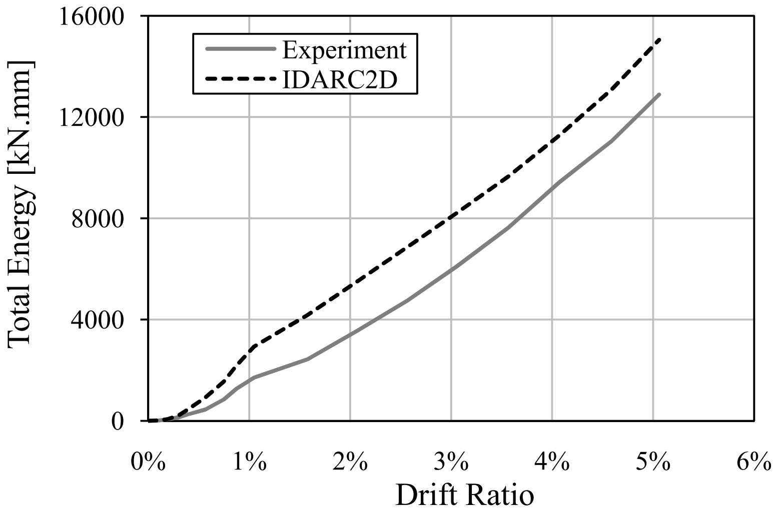

Figure 4.38: Experimental and analytical cumulative energy- drift ratio relations

The hysteretic energy dissipated at each cycles in experimental and analytical works is given in Figure 4.39. It is clearly seen that dissipated energies at experimental and analytical loops sufficently close each other.

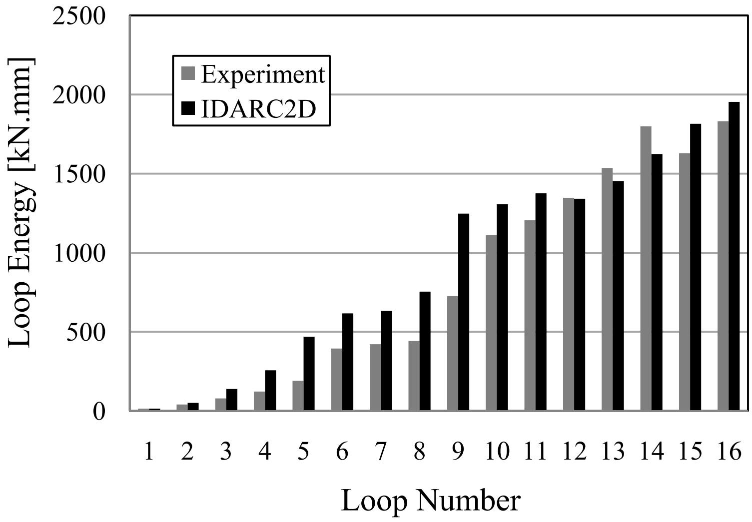

Figure 4.39: Dissipated energy at each experimental and analytical cycles

4.2.1.2 Three-Cyclic Quasi-static Analysis

The quasi-static displacement pattern in which three cycles for each ductility level are repeating is given below:

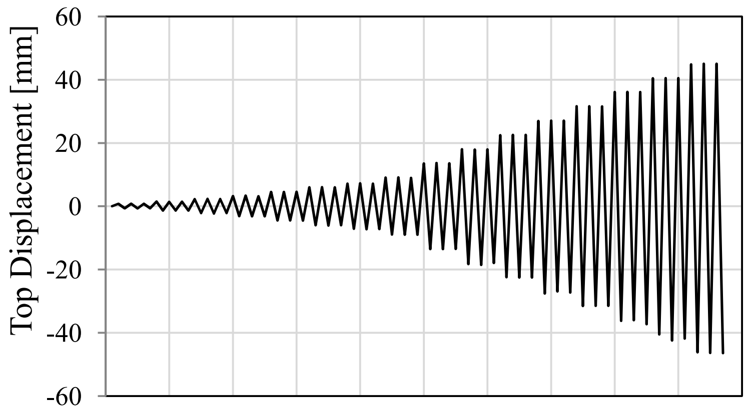

Figure 4.40: Three-cyclic quasi-static displacement pattern

Similar to bare frame, quasi-static displacement pattern in which three cycles for each ductility level are repeating caused more damage on the frame members compared with one-cyclic quasi-static test. After a calibration process, the PHM strength degrading parameters ($\beta_1 = \beta_2$) for the frame members were determined as 0.30 instead of 0.01 obtained for one-cyclic quasi-static test. The comparison of top displacement versus base shear relationships of simulation and experiment is illustrated in Figure 4.41.

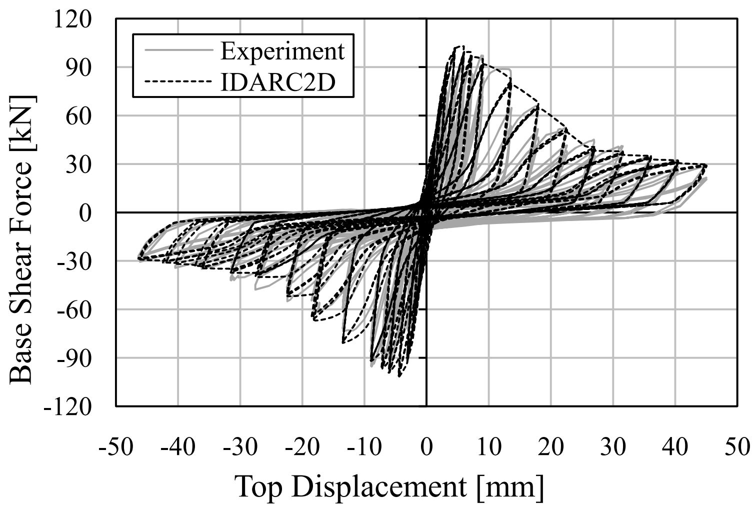

Figure 4.41: Base shear force-top displacement relations

Envelope curves of the experimental and analytical hysteresis for base shear force versus top displacement are given in Figure 4.42.

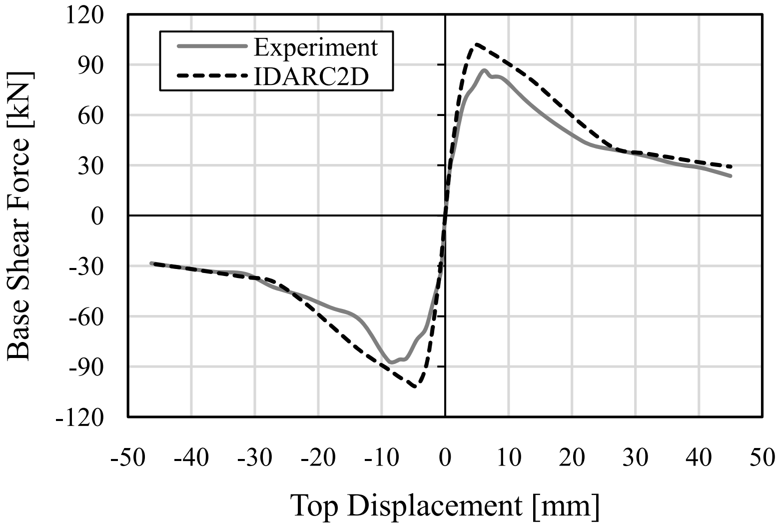

Figure 4.42: Envelope curves of the experimental and analytical hysteresis

The comparison of lateral stiffness obtained from experiment and analytical works are made for various drift ratios, Figure 4.43.

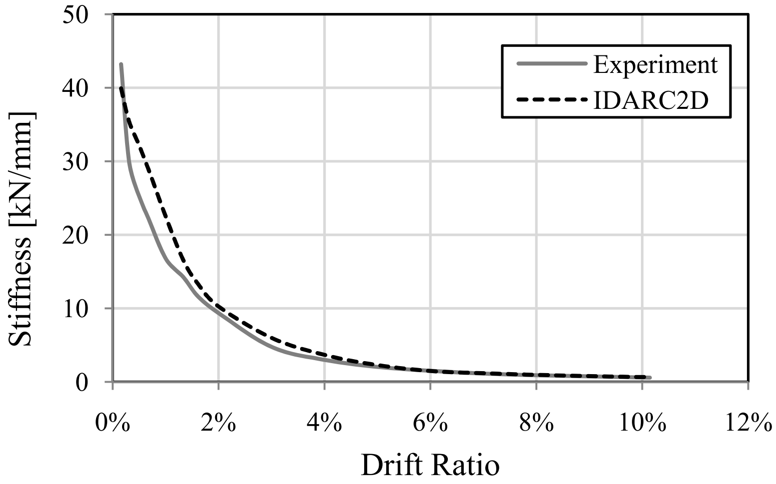

Figure 4.43: Lateral stiffness-drift ratio relations

The comparison of the average lateral stiffnesses at each displacement cycles is given in Figure 4.44. The points are positioned generally above the 45° line. It means that the lateral stiffness obtained from the analytical work is a slightly greater than the ones obtained in the experimental work.

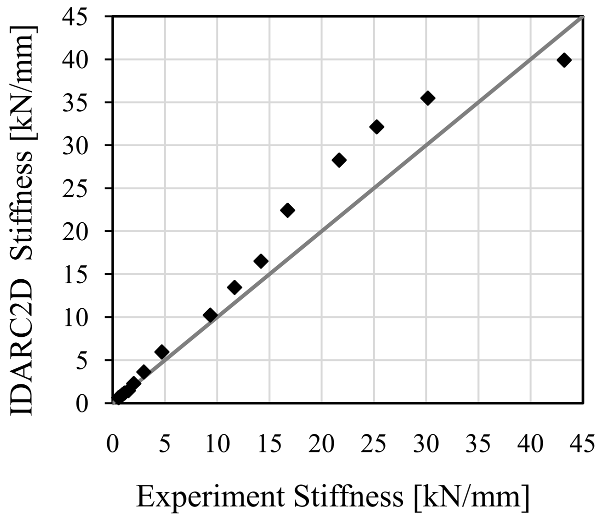

Figure 4.44: Comparison of lateral stiffness in experiment and analysis

The comparison of cumulative dissipated energy obtained in the analytical and experimental work is made in Figure 4.45. The cumulative relative error in final stage is around 17%.

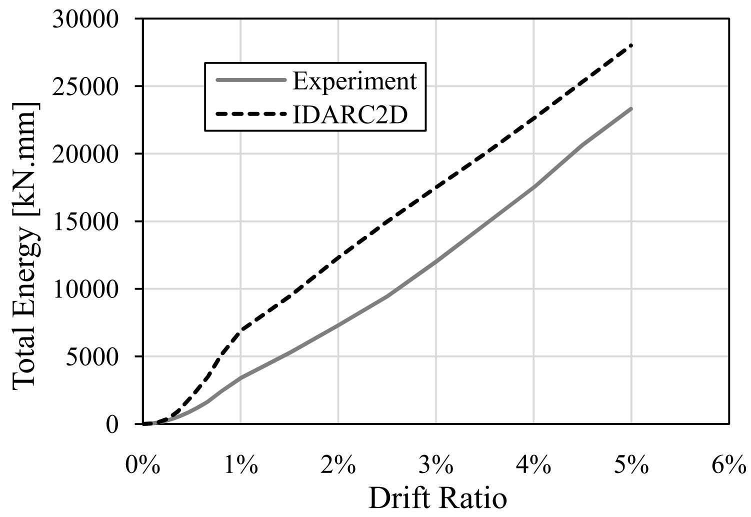

Figure 4.45: Experimental and analytical cumulative energy- drift ratio relations

The hysteretic energy dissipated at each cycles in experimental and analytical works is given in Figure 4.46. It is seen that there is quite differences between experimental and analytical results.

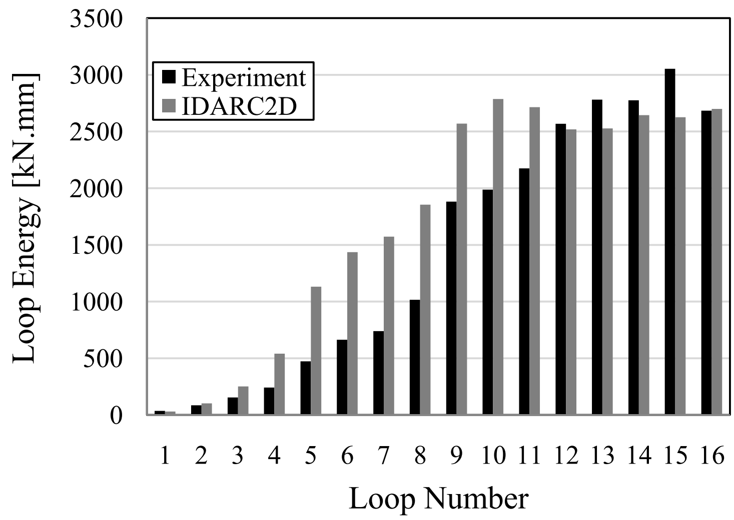

Figure 4.46: Dissipated energy at each experimental and analytical cycles

4.2.2 Non-linear Time History Analysis

Stiffness proportional damping is used in nonlinear time history analysis performed in IDARC2D. Base shear force-lateral top displacement relations for 0.2 and 0.4 PGA levels are given in Apendix: A2. Lateral top displacement histories for 0.2 and 0.4 PGA levels are given in Apendix: A5. Base shear force histories for 0.2 and 0.4 PGA levels are given in Apendix: A8.

4.2.2.1 Low-Mass Dynamic Case

The specimen was subjected to successive acceleration records. A sinusoidal wave which consists of three 0.25g and three 0.375g cycles was applied initially, Figure 4.47. The time intervals of the sine wave is 0.02 sec and the total duration is 6 sec.

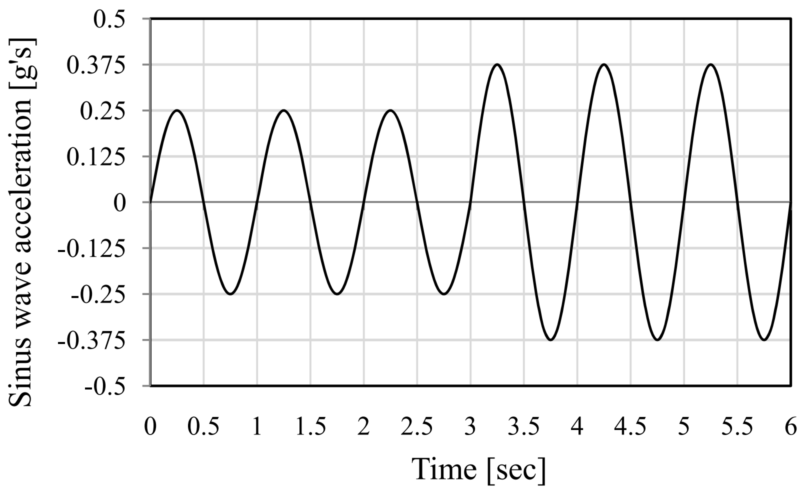

Figure 4.47: Sinusoidal wave acceleration record

The modified Duzce acceleration record is used with increasing intensities of 0.2g, 0.4g, 0.6g, 0.8g.

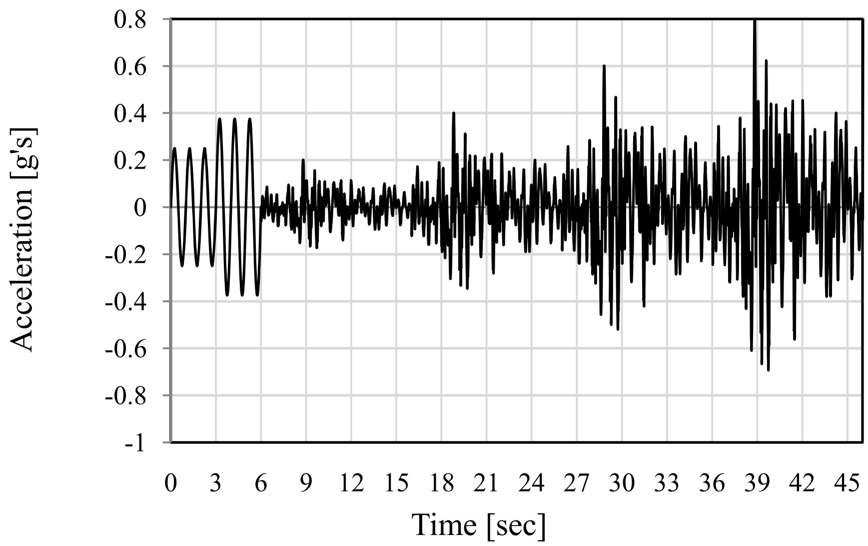

Figure 4.48: Acceleration record used in low mass case

The damage parameters obtained for the quasi-static displacement pattern has been used in nonlinear time history analysis. Because of the initial cracks observed in experiment, initial stiffness of the infill panel is taken as 12.0 kN/mm instead of 19.4 kN/mm.

The comparison of top displacement versus base shear relations for low mass case is given in Figure 4.49.

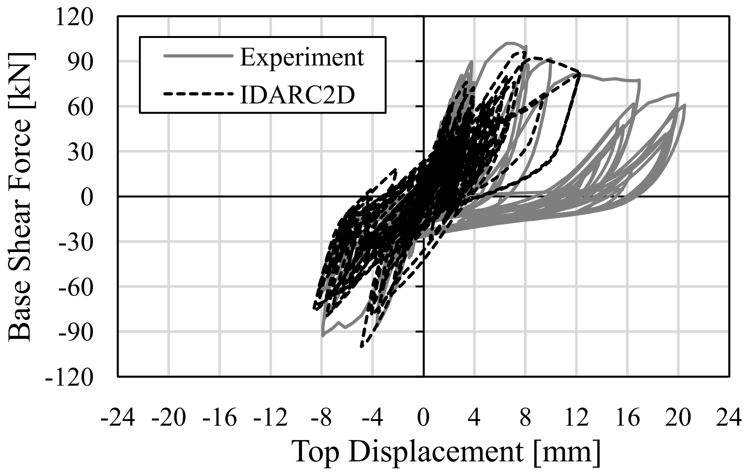

Figure 4.49: Base shear force-top displacement relations

Top displacement and base shear history are given in Figures 4.50, 4.51.

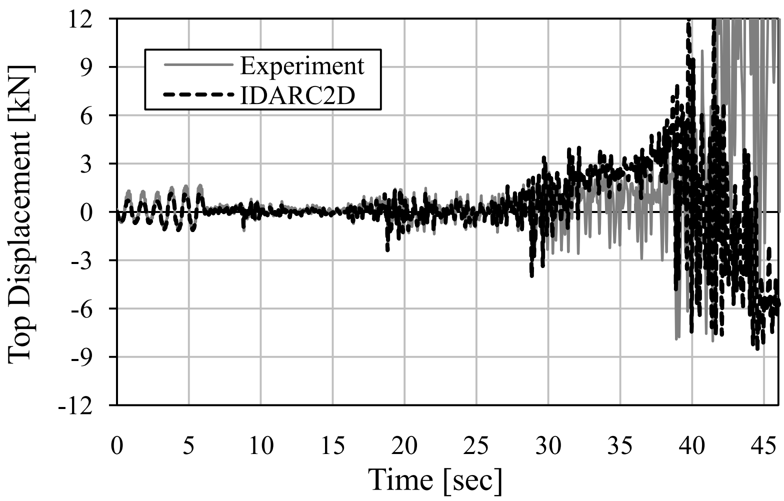

Figure 4.50: Lateral top displacement history for low mass case

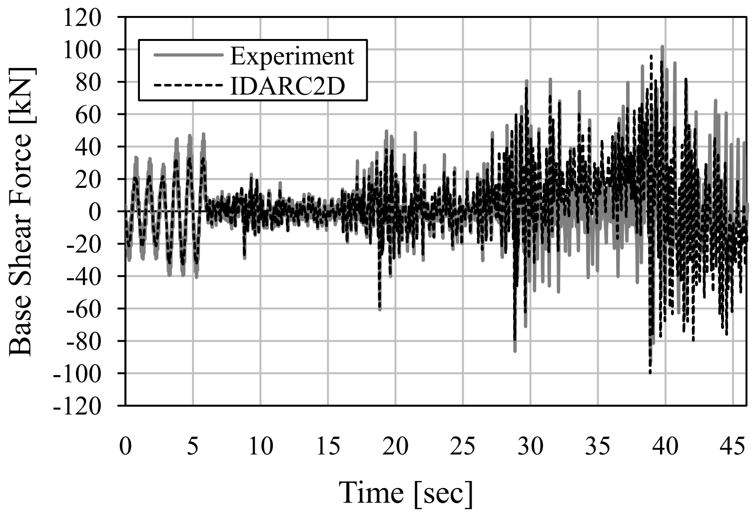

Figure 4.51: Base shear force history for low mass case

4.2.2.2 High-Mass Dynamic Case

The complate acceleration record that applied to infilled frame is given in Figure 4.52. Total record length is 32 seconds and it includes successive triangular wave and the modified Duzce Earthquake with increasing intensity.

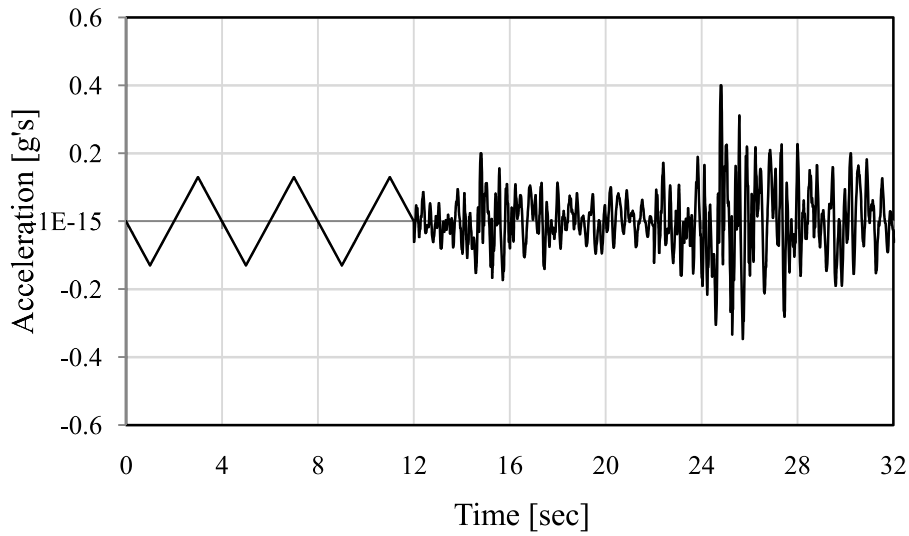

Figure 4.52: Acceleration record used in high mass case

The comparison of top displacement versus base shear relations for high mass case is given in Figure 4.53.

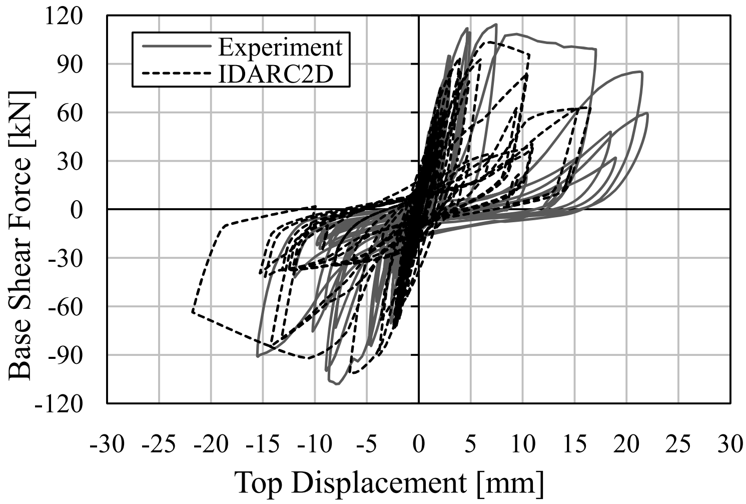

Figure 4.53: Base shear force-top displacement relations

Top displacement and base shear history are given in Figures 4.54, 4.55.

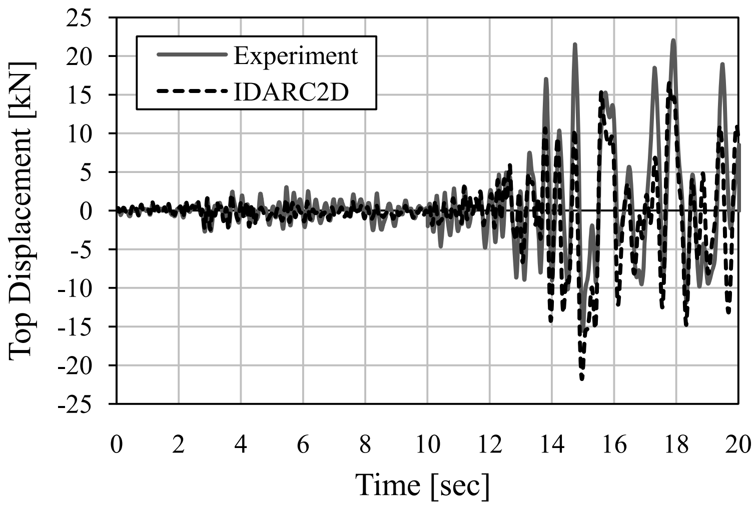

Figure 4.54: Lateral top displacement history for high mass case

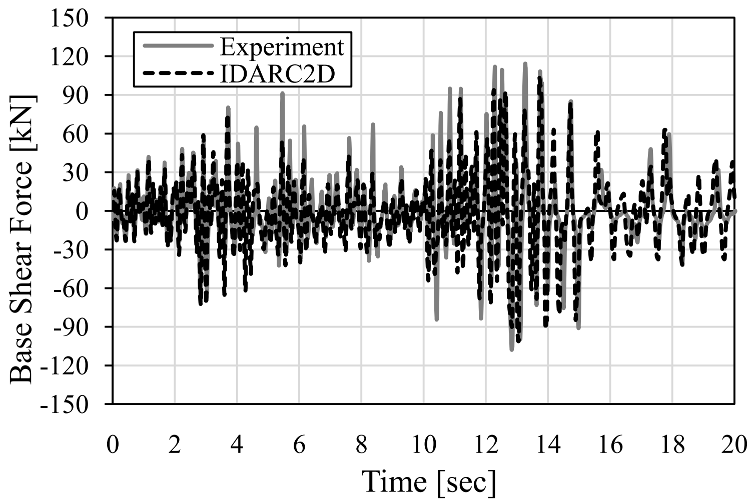

Figure 4.55: Base shear history for high mass case

4.3 RETROFITTED INFILLED RC FRAME

The methodology for modeling cross-braced type retrofitted infill panel is same with the created analytical model for infill panel.

Compresion strength of infill wall $f_m^{'}$, is taken from the material tests of 500 × 500 mm CFRP confined panels. The average of the compression strengths obtained in two perpendicular directions of the panels is 7.5 MPa and the corresponding strain is 0.0035. Basic shear strength of infill wall is 1.1 MPa, [8].

Lateral yield force V_y and initial stiffness K_0 are calculated as 109 kN and 42.1 kN/mm (Table 4.5) whereas initial stiffnes value of 42.1 kN/mm is consistent with the three-cyclic quasi-static test. The calculated stiffness values for all analysis cases for the retrofitted infilled frames are given in Table 4.6.

Table: 4.5 : Strength and Stiffness Calculation for Retrofitted Infilled Frame

Parameter	Meaning	Value	Unit
h	Height of column measured on center of beams	900	mm
h'	Height of infill	800	mm
l	Length of column measured on center of columns	1133	mm
l'	Length of infill	933	mm
r	Aspect Ratio	0.7944	
θ	Sloping angle of diagonal infill	0.7088	
θ'	Sloping angle of masonry diagonal strut at shear failure	0.6042	
μ_f	**Coefficient of friction of the frame-infill interface**	**0.55**	
f_m'	Prism strength of masonry	7.5	MPa
f_m	Effective(factored) compressive strength of infill	7.5	MPa
σ_{c0}	Column-infill nominal (upper bound) uniform contact normal stress	6.4	MPa
σ_{b0}	Beam-infill nominal (upper bound) uniform contact normal stress	5.4	MPa
M_{pc}	Plastic resisting moment of the column	6592	kN.mm
M_{pb}	Plastic resisting moment of the beam	10300	kN.mm
M_{pj}	Joint plastic resisting moment	6592	kN.mm
t	Infill thickness	80	mm
α_c	Normalized contact length of column-infill interface	0.19	
α_b	Normalized contact length of beam-infill interface	0.18	
A_c	Column-Infill interface contact stress	3.0	MPa
A_b	Beam-Infill interface contact stress	4.0	MPa
σ_c	Actual normal stress column-infill interface	6.4	MPa
σ_b	Actual normal stress beam-infill interface	4.3	MPa
τ_c	Contact shear stress column-infill interface	2.2	MPa
τ_b	Contact shear stress beam-infill interface	2.3	MPa
l_{eff}	Effective length of the equilavent diagonal struts	1133	mm
f_a	Permissible stress	6.5	MPa
A_d	Area of the equilavent diagonal struts	19340	mm^2
v	Basic shear strength or cohesion of masonry	1.1	MPa
V_m	Maximum lateral force	110.11	kN
ε_m'	Corresponding strain for masonry prism strength	0.0035	
U_m	Corresponding displacement for V_m	5.23	mm
$\boldsymbol{K_0}$	**Initial stiffness**	**42.13**	**kN/mm**
α	Post-yield stiffness ratio	0.01	
$\boldsymbol{V_y}$	**Lateral yield force**	**109**	**kN**

Table: 4.6 : The differencies between analysis cases for retrofitted infilled frames

Analysis case	**Initial Elastic Stiffness (kN/mm)**	**Ductility (μ_c)**
1-cyclic quasi-static	20	10
3-cyclic quasi-static	42	20
Low-mass nonlinear time history	20	10
High-mass nonlinear time history	32	16

The determined damage parameters used for cross-braced member are the same with thus used for infill panel element except for the control parameter of strength deteration (s_{k1}). This parameter is taken as 1.0 for cross-braced member and 0.01 for infill panel member.

4.3.1 Quasi-static Cyclic Analysis

The rigid-end assumption and trilinear moment-curvature relationship is used for frame members as used in infilled frame.

4.3.1.1 One-Cyclic Quasi-static Analysis

The applied displacement pattern for one-cyclic static test is given below:

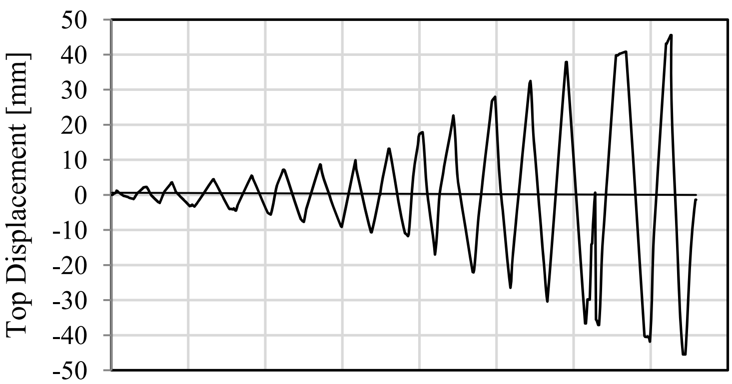

Figure 4.56: One-cyclic quasi-static displacement pattern

Top displacement versus base shear hysteresis obtained for one-cyclic quasi-static test are compared in Figure 4.57. The envelop curves for experimental and analytical works are also given in Figure 4.58. From these diagrams, one can evaluate that initial stiffness, ultimate strength and descending branch are consistent each other.

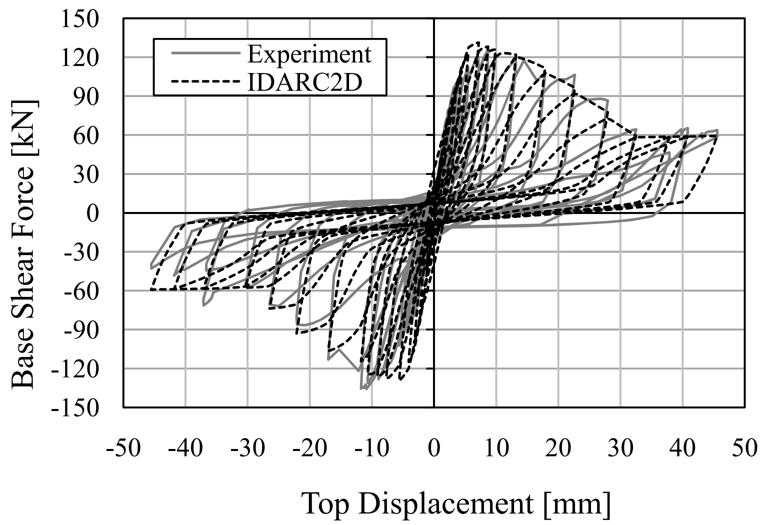

Figure 4.57: Base shear force-top displacement relations

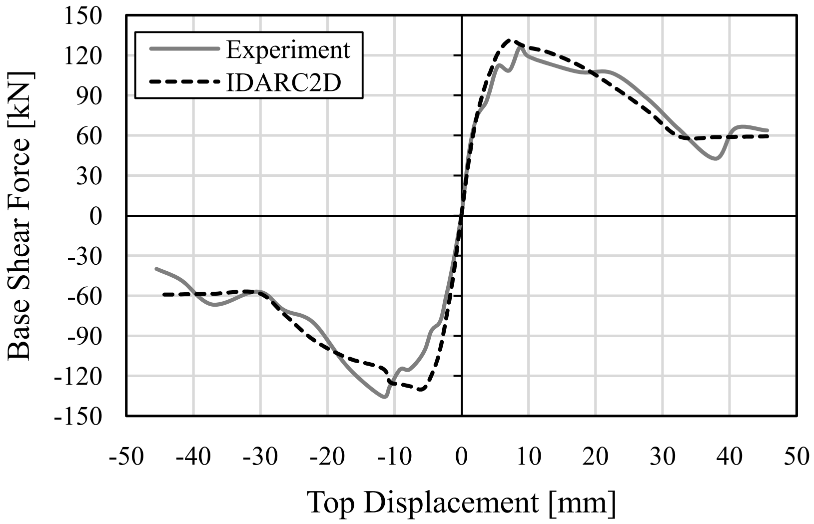

Figure 4.58: Envelope curves of the experimental and analytical hysteresis

The comparison of stiffness-drift ratio relation for one-cyclic quasi-static test is illustrated in Figure 4.59.

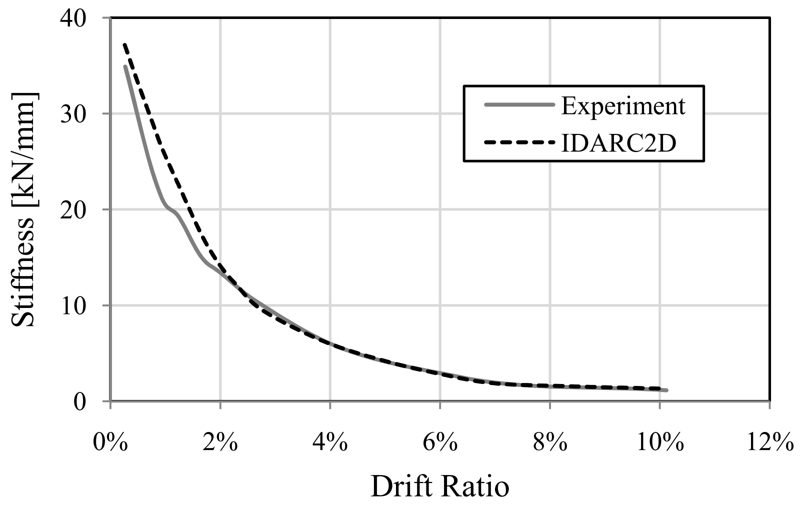

Figure 4.59: Lateral stiffness-drift ratio relations

The comparison of the calculated lateral stiffness obtained for each displacement cycle is also given in Figure 4.60.

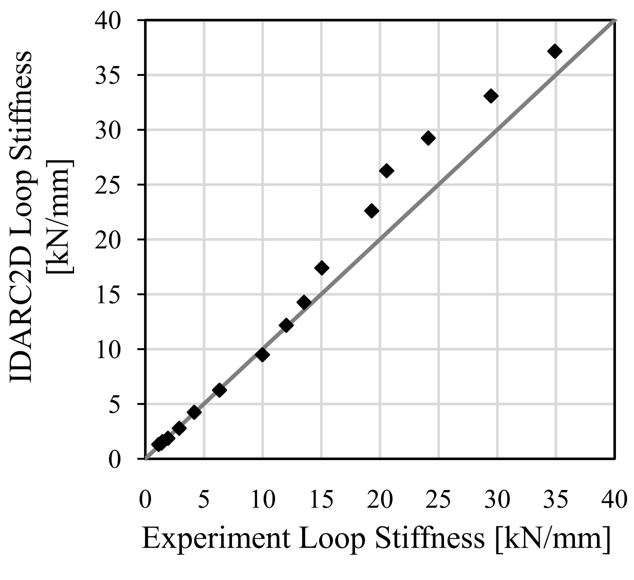

Figure 4.60: Comparison of lateral stiffness in experiment and analysis

The comparison of the cumulative dissipated energy versus story drift relation obtained in the experimental and analytical works is shown in Figure 4.61. The cumulative relative error in total dissipated energy is around 3%.

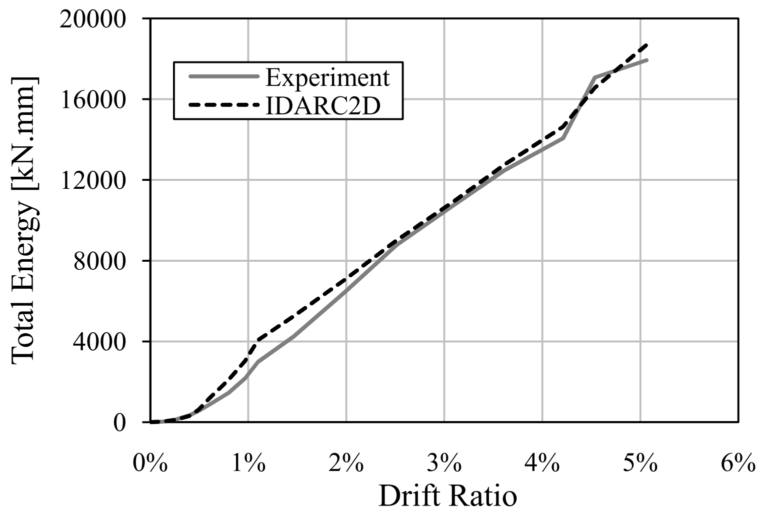

Figure 4.61: Experimental and analytical cumulative energy- drift ratio relations

The dissipated energies at each displacement cycles are compared in Figure 4.62.

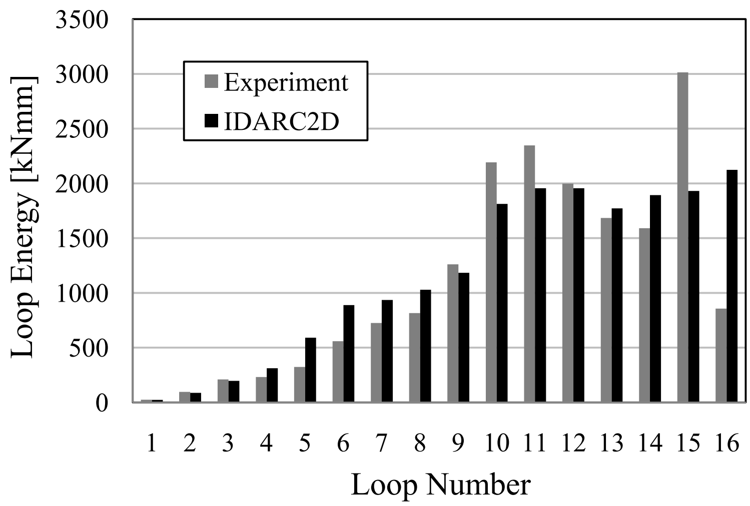

Figure 4.62: Dissipated energy at each experimental and analytical cycles

4.3.1.2 Three-Cyclic Quasi-static Analysis

The applied displacement pattern for three-cyclic quasi-static test is given below:

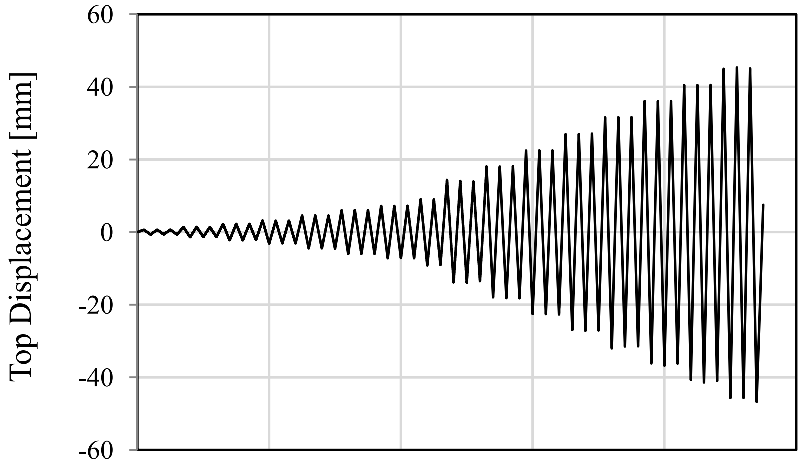

Figure 4.63: Three-cyclic quasi-static displacement pattern

Three-cyclic quasi-static displacement pattern caused more damage to the specimen compared with one-cyclic quasi-static displacement protocol. Based on the calibration process, the PHM strength degrading parameters ($\beta_1 = \beta_2$) for the frame members were determined as 0.20 instead of the value of 0.01 used for one-cyclic quasi-static test.

The comparison of top displacement-base shear relationships obtained in the experimental and analytical works is given in Figure 4.64.

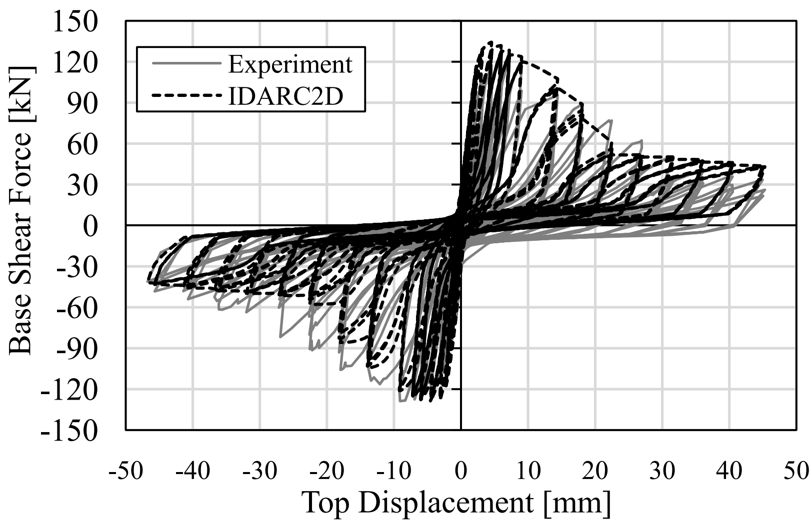

Figure 4.64: Base shear force-top displacement relations

Envelope curves of the experimentally and analytically obtained base shear versus top displacement relations are given in Figure 4.65.

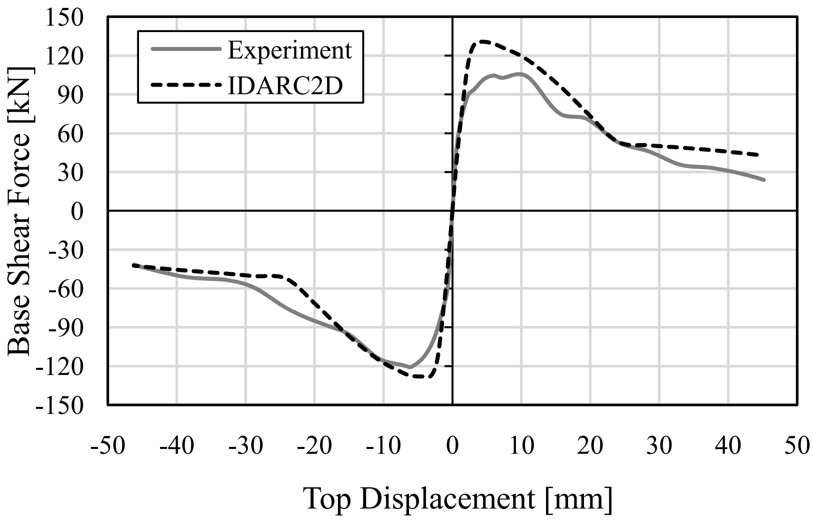

Figure 4.65: Envelope curves of the experimental-analytical hysteresis

The comparison of lateral stiffness versus story drift relation for three-cyclic quasi-static test is illustrated in Figure 4.66.

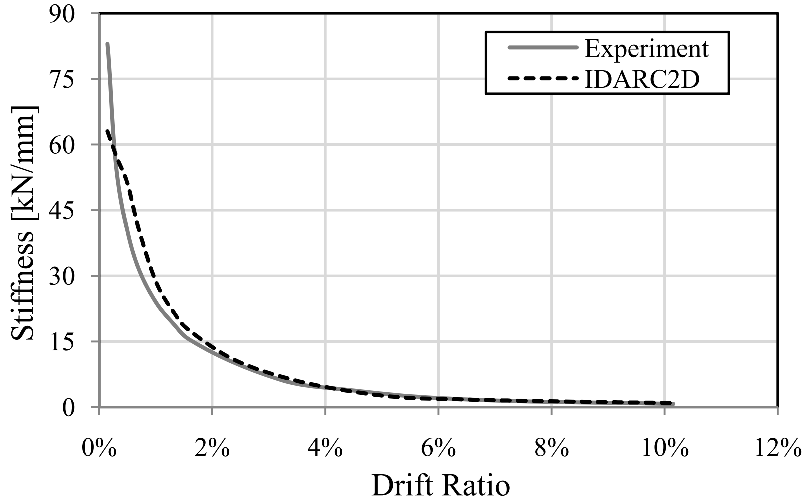

Figure 4.66: Lateral stiffness-drift ratio relations

The comparison of lateral stiffnesses at each displacement cycles for experiment and analytical cases is made in Figure 4.67. The points shown are the average value of the three cycles.

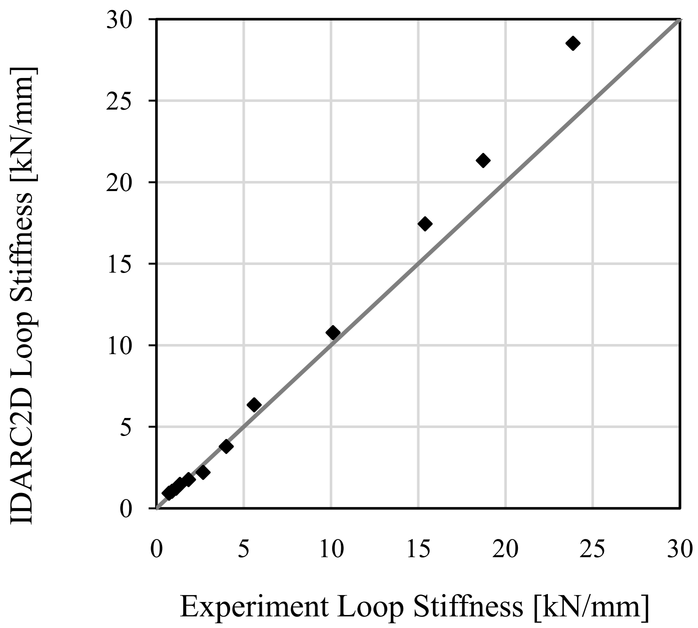

Figure 4.67: Comparison of lateral stiffness in experiment and analysis

The comparison of the cumulative dissipated energy calculated for the experimental and analytical cases is illustrated in Figure 4.68. The cumulative error in total dissipated energy is around 14%.

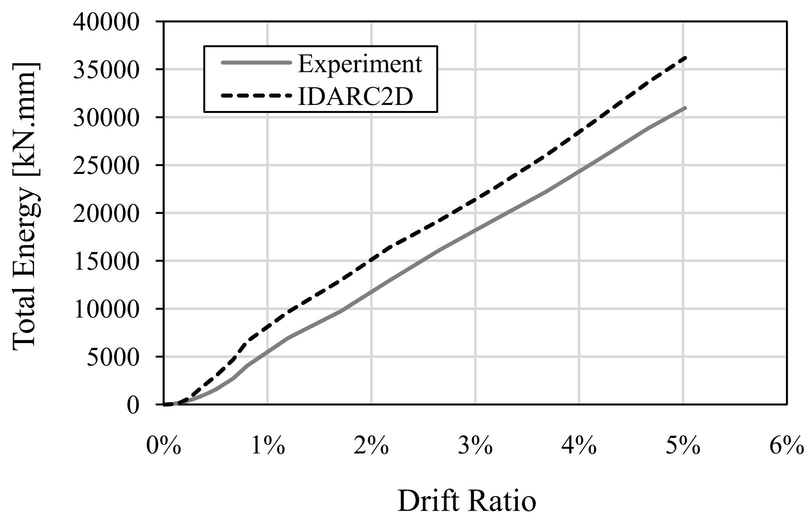

Figure 4.68: Experimental and analytical cumulative energy- drift ratio relations

The dissipated energies calculated for each displacement cycles are given in Figure 4.69.

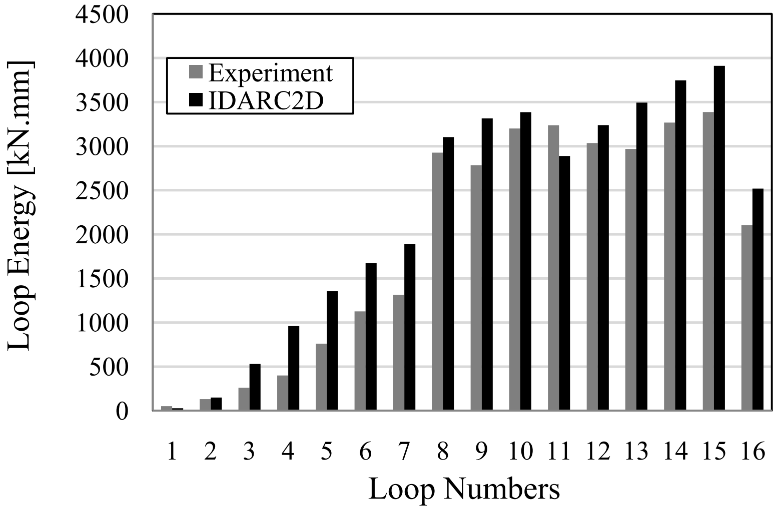

Figure 4.69: Dissipated energy at each experimental and analytical cycles

4.3.2 Non-linear Time History Analysis

Stiffness proportional damping type is used in nonlinear time history analysis contrary to mass proportional damping type used in bare frame.

Base shear force-lateral top displacement relations for 0.2 and 0.4 PGA levels are given in Apendix: A3. Lateral top displacement histories for 0.2 and 0.4 PGA levels are given in Apendix: A6. Base shear force histories for 0.2 and 0.4 PGA levels are given in Apendix: A9.

4.3.2.1 Low-Mass Dynamic Case

The specimen was subjected to consecutive acceleration records. A sinusoidal wave which was also used for infilled frame (Figure 4.49), was applied first. Then the acceleration record of Duzce Earthquake was repeated with the incremental PGA.

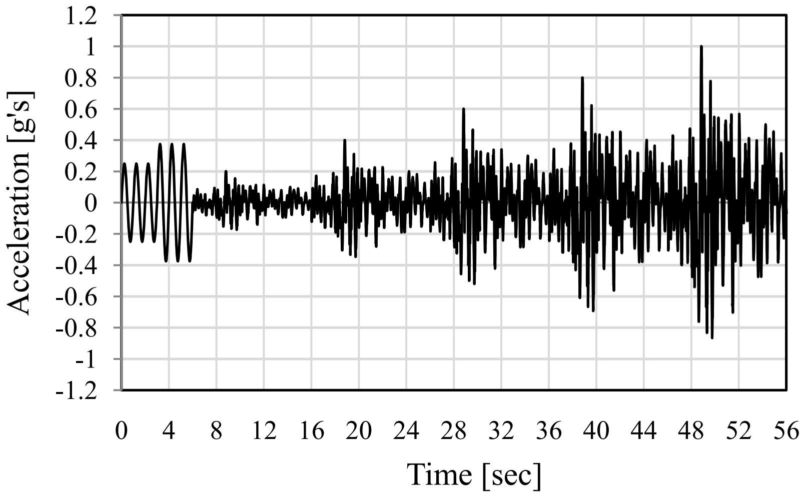

Figure 4.70: Acceleration record used in low mass case

The comparison of top displacement versus base shear history is given in Figure 4.71.

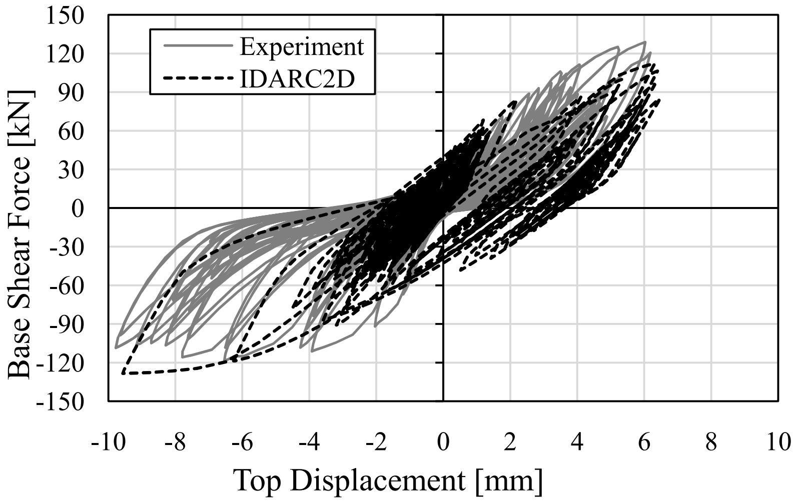

Figure 4.71: Base shear force-top displacement relations

Top displacement history obtained in the experimental and analytical works are compared in Figure 4.72.

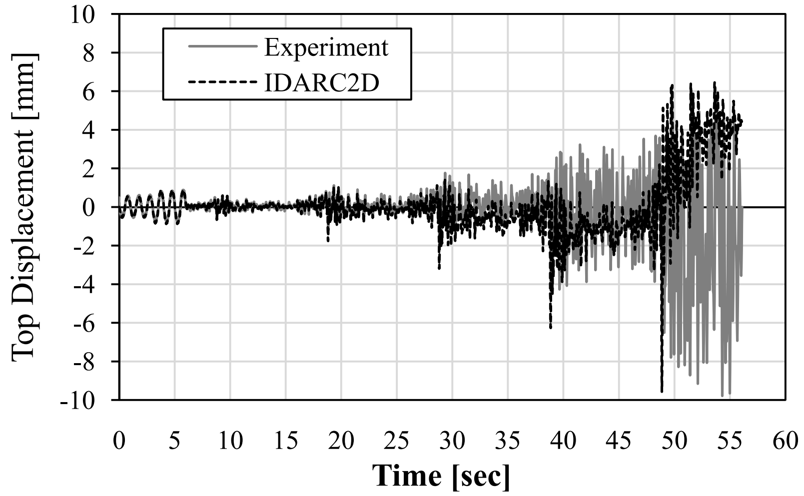

Figure 4.72: Lateral top displacement history for low mass case

Base shear histories obtained in the experimental and analytical works are compared in Figure 4.73.

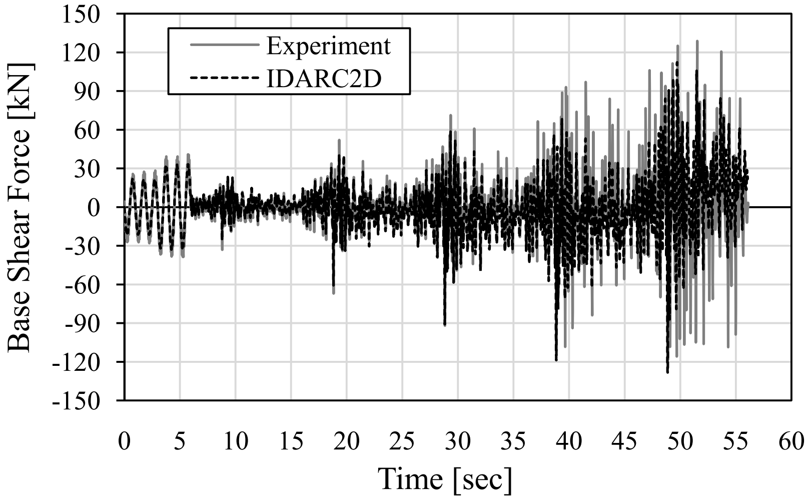

Figure 4.73: Base shear force history for low mass case

4.3.2.2 High-Mass Dynamic Case

The specimen was subjected to consecutive acceleration records. A triangular wave was applied first. Then the acceleration record of Duzce Earthquake was repeated with the incremental PGA, Figure 4.74.

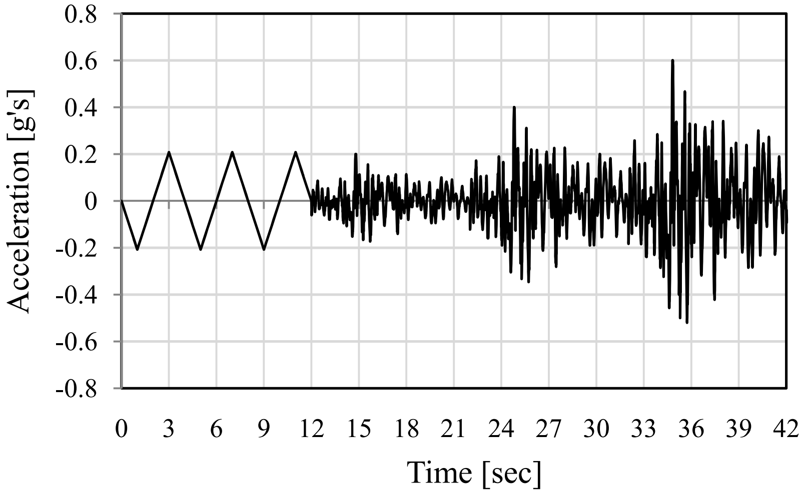

Figure 4.74: Acceleration record used in high mass case

The comparison of top displacement versus base shear history is given in Figure 4.75.

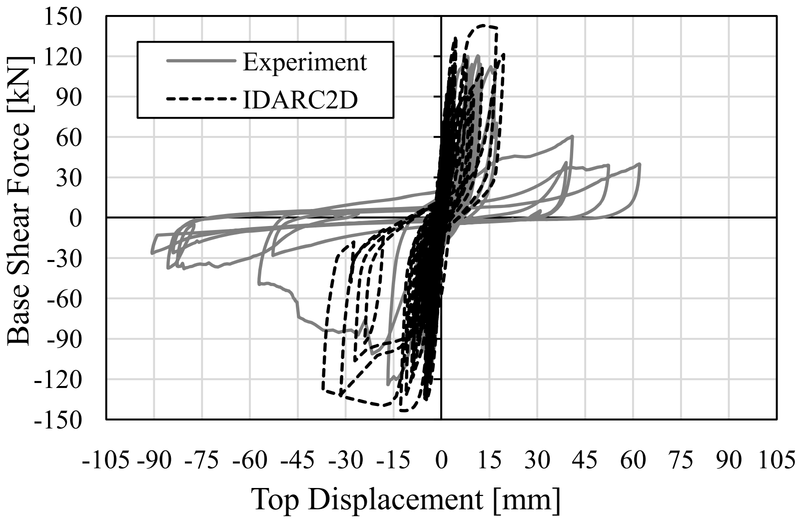

Figure 4.75: Base shear force-top displacement relations

Top displacement histories obtained in the experimental and analytical works are compared in Figure 4.76.

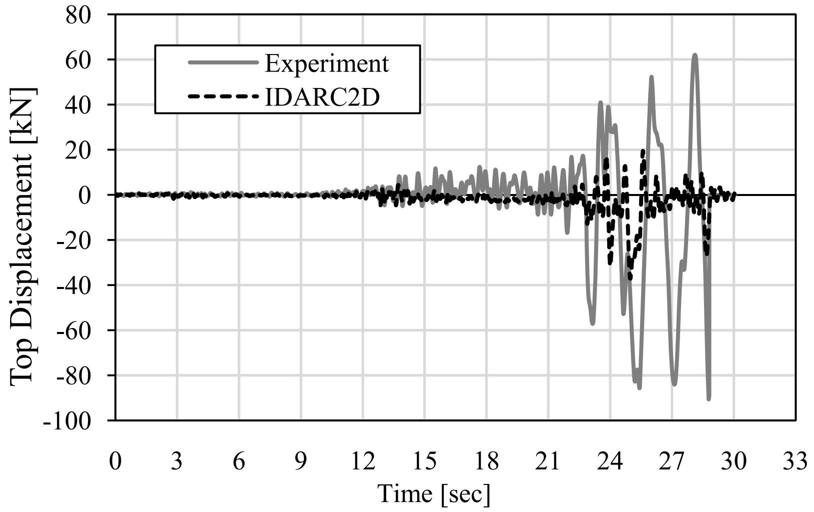

Figure 4.76: Lateral top displacement history for high mass case

Base shear histories obtained in the experimental and analytical works are compared in Figure 4.77.

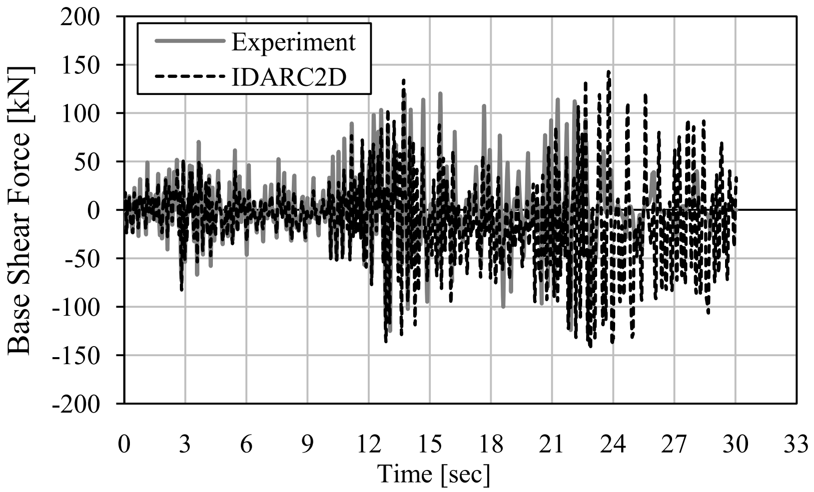

Figure 4.77: Base shear force history for high mass case

5. CONCLUSIONS AND RECOMMENDATIONS

This thesis aimed to simulate the results of various experiments which were conducted in Structural Earthquake Engineering Laboratory of ITU. The experiments consists of three groups of specimens which are the reference bare frame, the infilled frame and the retrofitted infilled frame (cross-braced frame) with CFRP sheets. Each group of specimens was tested in the laboratory by using quasi-static and pseudo-dynamic testing techniques. The quasi-static tests were performed with gradually increasing displacement based one cyclic and three cyclic reversals. Pseudo-dynamic tests were performed for two different inertia mass condition. The simulation study was performed by using IDARC2D software.

Based on the quasi-static experiments the performances of hysteretic model parameters for each group of specimens were evaluated in terms of stiffness, strength, absorbed energy and ductility. The correctness of the hysteretic model parameters were inspected with pseudo-dynamic test results by performing non-linear time history analysis. According to the nonlinear time history analysis result, it can be concluded that the analytical assumption made on the hysteretic model parameters, works well with the experimental results up to 1% story drift ratio.

The following conclusions can be driven according to the simulation study;

For all of the analytical models, there are some common assumptions. The concentrated plasticity assumption is made for the all models. Regarding the hysteresis properties of the frame members, tri-linear polygonal hysteretic model (PHM) is selected.

1- The frame members namely beam and column's sectional behavior (moment-curvature) were idealized as bilinear envelope that is formed with two critical co-ordinates yielding and ultimate points. The supposed tri-linear polygonal hysteretic model (PHM) degrading parameters that are extracted from the quasi-static tests are α=10, β_1=0.01, β_2=0.01 and γ=0.30. The defined PHM degrading parameters result in a well convergence with the nonlinear time history analysis. Therefore they are strongly recommended to be used as hysteretic model parameters in the frame members.

In the nonlinear time history analysis of bare frame, 5% mass proportional damping was used. The stiffness values obtained analytically and experimentally are nearly the same for higher drift ratios. The analytical energy dissipation variation is also adequately close to those of obtained in experiments. The hysteretic model parameters those are used in three cyclic quasi-static tests were also same with the one cyclic quasi-static test except just only one "γ" parameter. This parameter is taken "0.3" in three cyclic tests instead of 0.23 used in one-cyclic tests.

2- A tri-linear moment-curvature relation is assumed for the frame members namely columns and beam. The moment-curvature relation consists of the characteristic coordinates of cracking, yielding and ultimate points. Due to the fact that the column section is not cracked at the very beginning of the tests for the infilled frame case. Therefore the initial stiffness of the frame members is used as non-cracked stiffness. For infilled frames, rigid ends of the members are taken into account. The hysteretic degrading parameters of the members of infilled frame are the same with the one that are used in bare frame (α=10, β_1=0.01, β_2=0.01 and γ=0.30).

The infill panel is modeled by using equivalent diagonal compression struts. The contribution of infill panel is taken into account indirectly as a bilinear shear-spring. The initial stiffness K_0 and lateral yield force capacity V_y of infill panel is calculated by using Saneijad's model. The inputs of this analytical model are h (height of column measured on center of beams), l (length of column measured on center of columns), h' (height of infill), l'(length of infill), μ_f (friction co-efficient of the frame/infill interface), f_m' (prism strength of masonry), ε_m' (corresponding strain for prism strength of masonry), t (infill wall thickness), M_{pc} (plastic resisting moment of column), M_{pb} (plastic resisting moment of beam), M_{pj} (joint plastic resisting moment), α (post yield stiffness ratio). ε_m' and f_m' are strain and strength values determined from singular brick element experiments. A reduced strength value of f_c is used for the infill panel. Instead of using unique brick experiment, the strain and stress values of $\varepsilon_m' = 0.006$ and $f_m' = 4.5\,\mathrm{MPa}$ are obtained from the compression tests performed on the masonry walls which were 500×500 mm in size. μ_f is taken as 0.45 which is specified in ACI 530-88. M_{pj} is the minimum of column and beam plastic resisting moment capacities. Thickness of infill wall consists of the infill and mortar thickness at two faces. A smooth hysteretic model (SHM) based on Wen-Bouc model is used for infill panel. Calculated degrading parameters for one-cyclic quasi-static tests are: $A=1$, $\beta=0.1$, $\gamma=0.9$, $\eta=2$, $\alpha=0.001$, $A_s=0.83$, $Z_s=0.20$, $\bar{Z}=0$, $s_k=0.001$, $s_{p1}=0.01$, $s_{p2}=1.0$ and $\mu_c=7.5$.

This parameters yield adequate accuracy in NTHAs and recommended to be used as hysteretic model parameters for infill panel. In NTHAs 5% stiffness proportional damping is assumed. The stiffness and absorbed energy calculated from simulation study are compared with one-cyclic quasi-static experimental results. The stiffness values calculated from simulation are in good agreement with the experimental results. The cumulative relative error in terms of absorbed energy in final stage is around 13%. In three cyclic quasi-static tests strength degrading parameters for frame members are calibrated as $\beta_1=\beta_2=0.30$. The other degrading parameters for frame members and infill panel are taken as the same with thus used in one-cyclic quasi-static tests. The stiffness values calculated from three cyclic simulations are in good agreement with the experimental results. The cumulative relative error in terms of absorbed energy in final stage is around 17%.

3- The analytical model prepared for the infilled frame retrofitted by CFRP is same with infilled frame's except some minor revisions. The parameters representing the contribution of CFRP retrofitting is compression strength, ductility and friction coefficient for infill wall-frame interface.

Tri-linear moment curvature relations, rigid end assumption and the same hysteretic model parameters (PHM) ($\alpha=10$, $\beta_1=0.01$, $\beta_2=0.01$ and $\gamma=0.30$) are used in the analytical model of retrofitted infilled frame with CFRP sheets.

The contribution of CFRP sheets to infill panel is taken into account by changing the input values of ε_m', f_m' and μ_f. The stress-strain values of $\varepsilon_m'=0.0035$ and $f_m'=7.5\,\text{MPa}$ are taken from the tests of 500×500 mm masonry prisms.

If one wish to use the approximate characteristics for the retrofitted infill panel, the infill panel strength must be multiplied by a constant of 7.5/4.5 ≅ 1.65 and the infill panel strain must be divided by 2. The friction coefficient μ_f which is used for infill wall-frame interface, is taken as 0.55 instead of 0.45. All the other parameters in order to calculate the initial stiffness K_0 and shear force V_y are the same with the infilled frame.

The calculated smooth hysteretic model (SHM) parameters are also same for the case of infill wall except for the parameters μ_c and S_{p1}. μ_c should be taken as 20 if the initial damage does not exist. S_{p1} is taken as 1.0 in the retrofitted infill panel instead of 0.01 used in infill panel.

These parameters yield accurate results in NTHAs and it is recommended to be used as hysteretic model parameters for retrofitted infilled frame (cross-braced frame) with CFRP sheets. In NTHAs 5% stiffness proportional damping is used. The stiffness and dissipated energy calculated from the simulation are compared with one-cyclic quasi-static experimental results. The stiffness and dissipated energy values calculated from simulation are in good agreement with the experimental results. The observed relative errors are not significant. In three cyclic quasi-static tests, strength degrading parameters for the frame members are calibrated as β_1=β_2=0.20. The other degrading parameters for frame members and infill panel are taken as the same with thus used in one-cyclic quasi-static tests. The stiffness values calculated from three cyclic simulations are in good agreement with experimental results. The cumulative error in total dissipated energy is around 14%.

REFERENCES

[1] **Reinhorn, A.M., Kunnath, S.K., Valles, R.E.**, 1994. IDARC2D V6.1 A Program for the Inelastic Damage Analysis of Buildings, *National Center for Earthquake Engineering Research*, Buffalo.

[2] **XTRACT V3.0.7**., 2006. Cross-sectional Structural Analysis of Components. Imbsen Software Systems, Sacramento, CA.

[3] **Madan, A., Reinhorn, A.M., , Mander, J.B., Valles, R.E.** 1997. Modeling of Masonry Infill Panels for Structural Analysis, *Journal of Structural Engineering*, 1295-1302.

[4] **Saatcioglu, M., Serrato, F., Foo, S.,** 2005. Seismic Performance of Masonry Infill Walls Retrofitted with CFRP Sheets, *ACI,* 341- 354.

[5] **Saneinejad, A., Hobbs, B.,** 1995. Inelastic Design of Infılled Frames, *ASCE, Journal of Structural Engineering*, 634- 650.

[6] **Yuksel, E., Ozkaynak, H., Buyukozturk, O., Yalcin, C., Dindar, A.A., Surmeli, M., Tastan, D.,** 2009. Performance of Alternative CFRP Retrofitting Shemes *Used in Infilled RC Frames, Construction and Building Materials,24, PP.596-609, (2009).*

[7] **ACI 530-88.** Building Code for Masonry Structures & Specification for Masonry Structures.

[8] **Ozsayin, B.** 2009. Karbon Lifli Polimerlerle Güçlendirilmiş Boşluklu Tuğla Duvarların Mekanik Özellikleri M.Sc. Thesis to be submitted to Graduate School of ITU.

[9] **Polyakov, S.V.** 1960. On the Interaction Between Masonry Filler Walls and Enclosing Frame When Loaded in the Plane of the Walls.

[10] **Bertero, V. And Brokken, S.** 1983. Infill In Seismic Resistant Building. Journal of the Structural Engineering,*ASCE,Vol.No 6.*

[11] **Mander, J.B., Nair, B.,** 1994. Seismic Resistance of Brick-infilled Steel Frames with or without Retrofit, *TMS Journal*.

[12] **Dhanasekar, M. and Page, A.W.** (1986)**.** "The Influence of Brick Masonry Infill Properties on The Behaviour of Infilled Frames". *Proc Inst of Civil Engrs,London*.

[13] **Holmes, M.** (1961). ''Steel frame with brickwork and concrete infilling''. *Proc.Inst of Civil Engrs,London*.

[14] **Mainstone, J.R.** (1971). ''On the stiffness and strength of infilled frames. *Proceedings of Instutition of civil engineers*.

APPENDICES

APPENDIX A.1 : Bare Frame Base shear force-top displacement relations

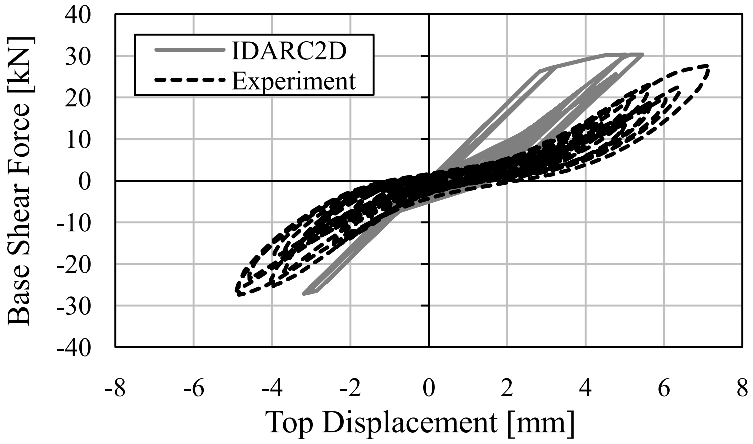

Figure A.1: Low mass 0.2 PGA

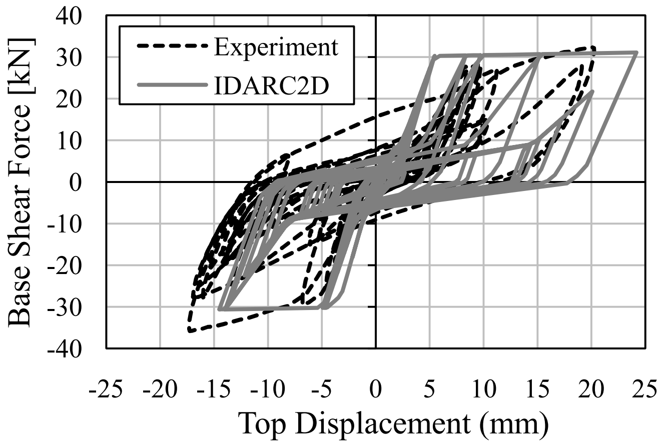

Figure A.2: Low mass 0.4 PGA

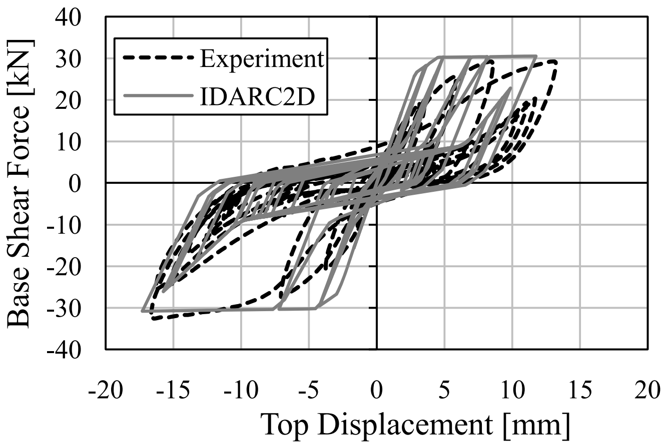

Figure A.3: High mass 0.2 PGA

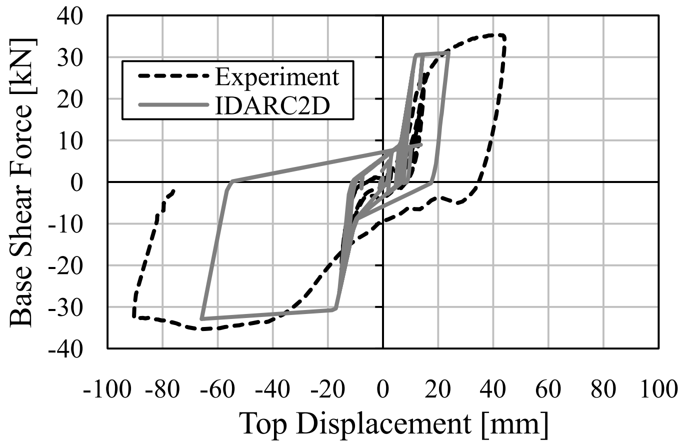

Figure A.4: High mass 0.4 PGA

APPENDIX A.2 : Infilled Frame Base shear force-top displacement relations

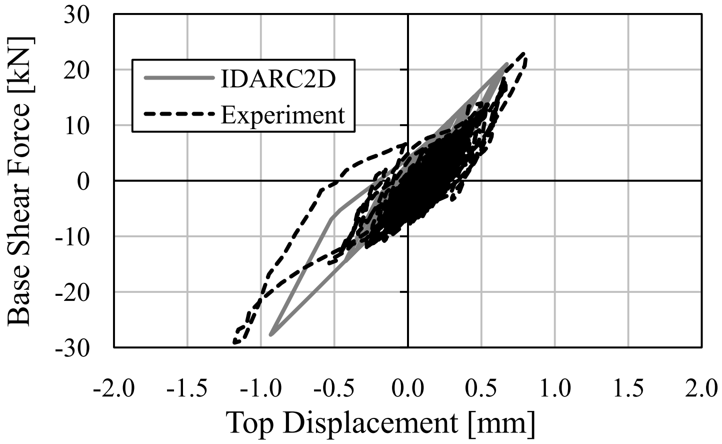

Figure A.5: Low mass 0.2 PGA

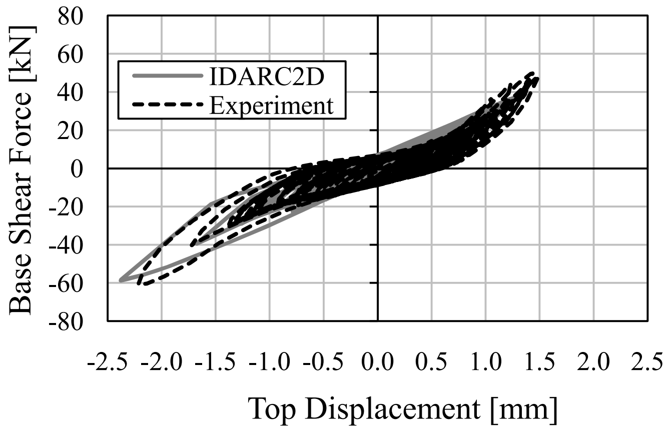

Figure A.6: Low mass 0.4 PGA

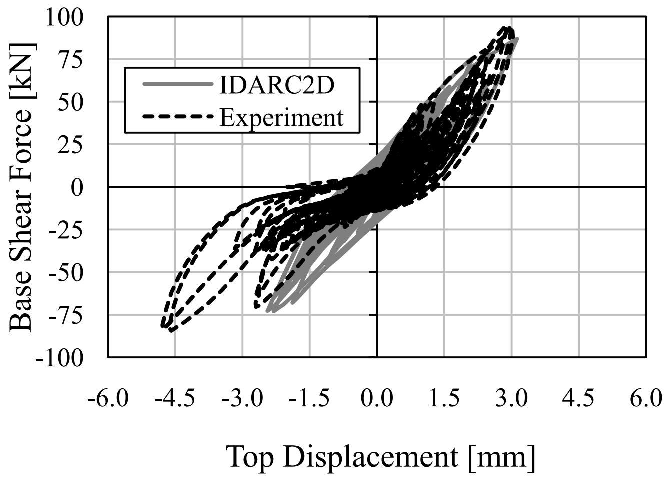

Figure A.7: High mass 0.2 PGA

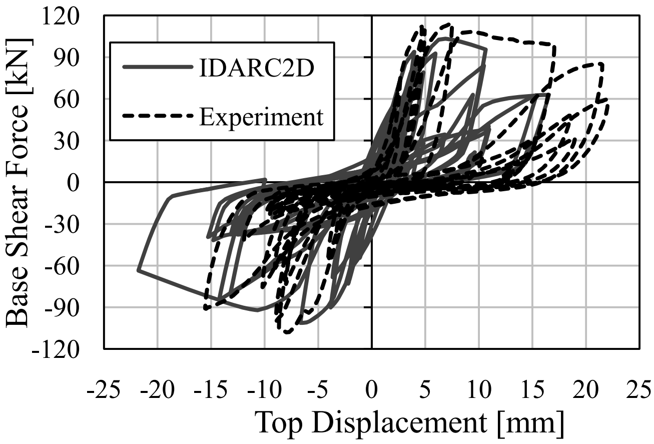

Figure A.8: High mass 0.4 PGA

APPENDIX A.3 : CFRP Retrofitted RC Frame Base Shear Force-Top Displacement Relations

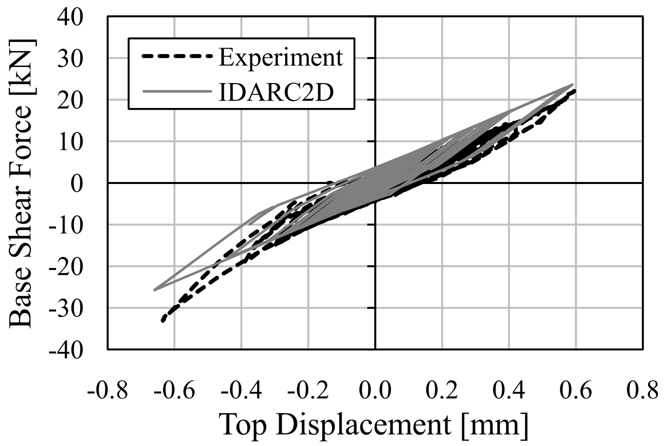

Figure A.9: Low mass 0.2 PGA

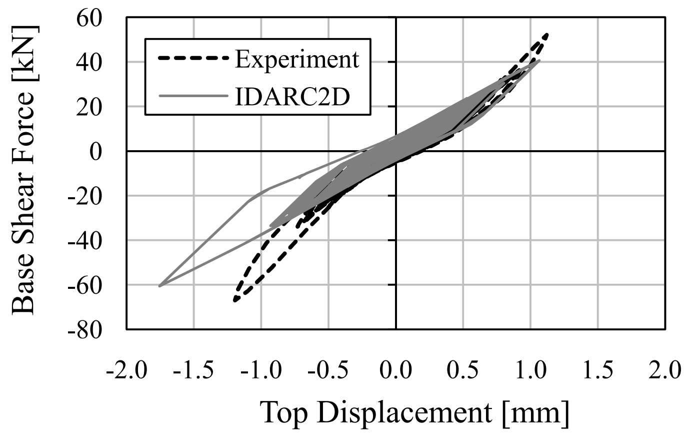

Figure A.10: Low mass 0.4 PGA

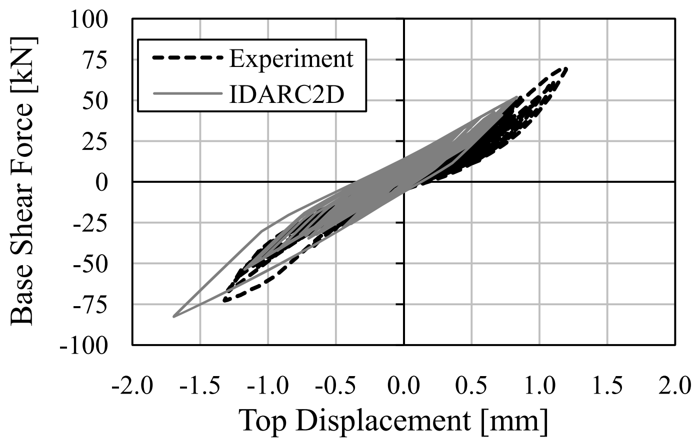

Figure A.11: High mass 0.2 PGA

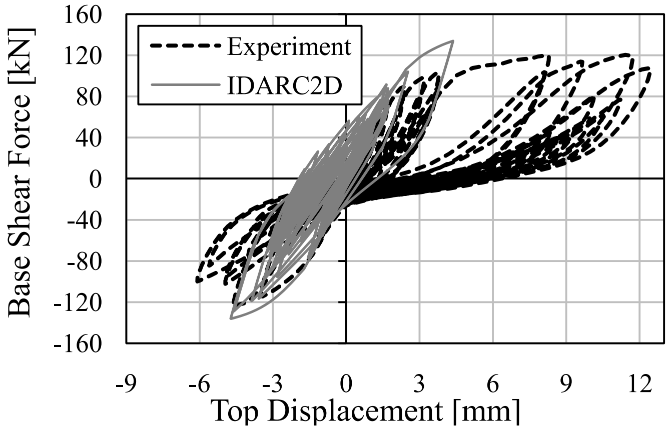

Figure A.12: High mass 0.4 PGA

APPENDIX A.4 : Bare Frame Lateral Top Displacement History

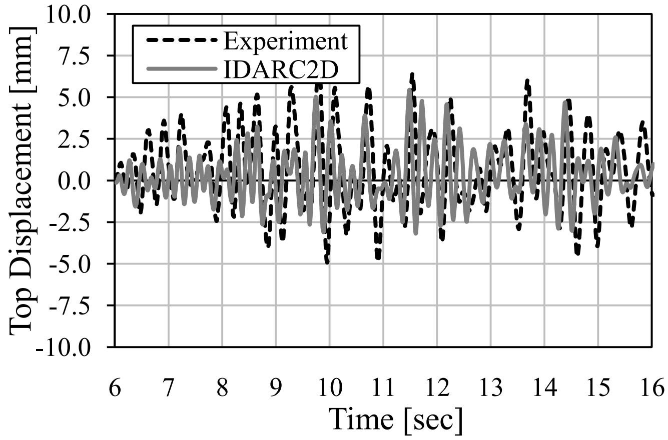

Figure A.13: Low mass 0.2 PGA

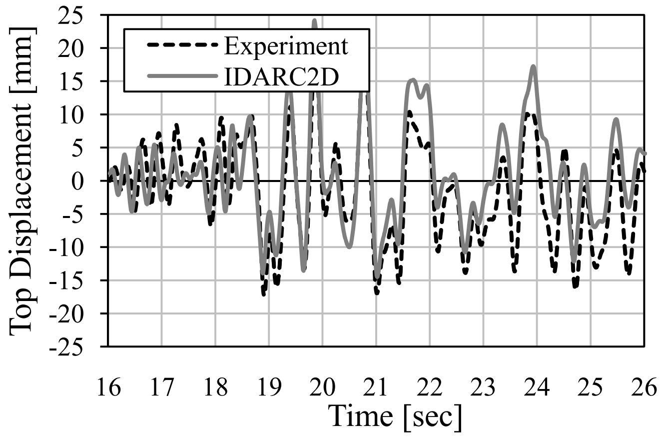

Figure A.14: Low mass 0.4 PGA

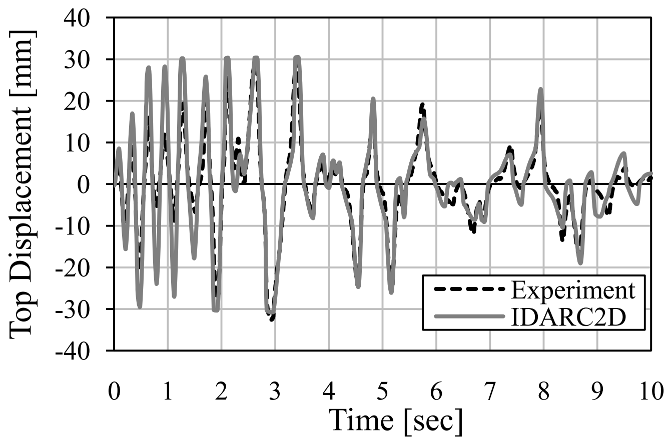

Figure A.15: High mass 0.2 PGA

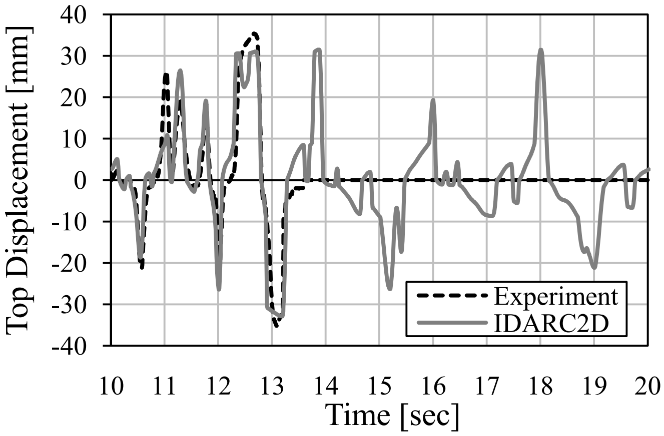

Figure A.16: High mass 0.4 PGA

APPENDIX A.5 : Infilled Frame Lateral Top Displacement History

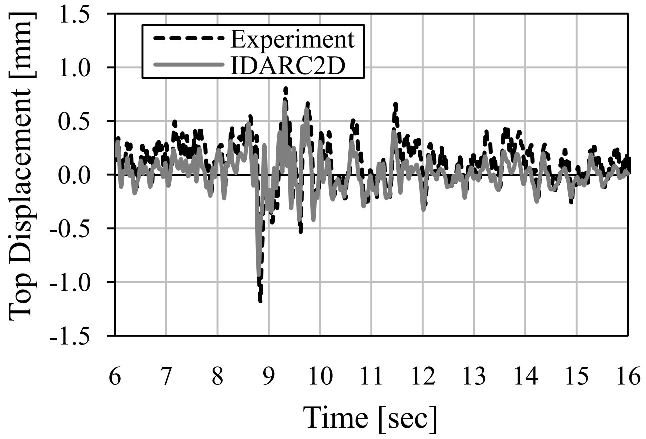

Figure A.17: Low mass 0.2 PGA

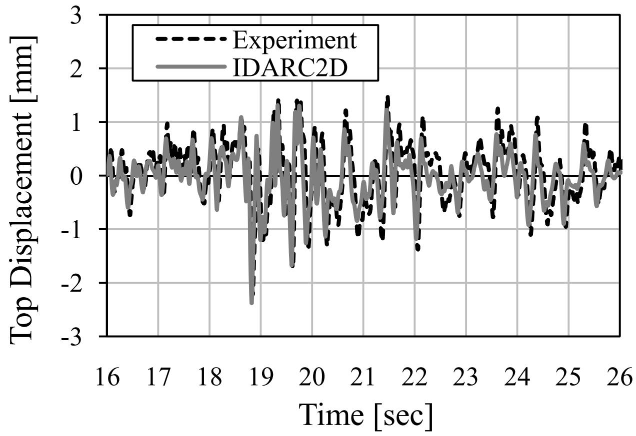

Figure A.18: Low mass 0.4 PGA

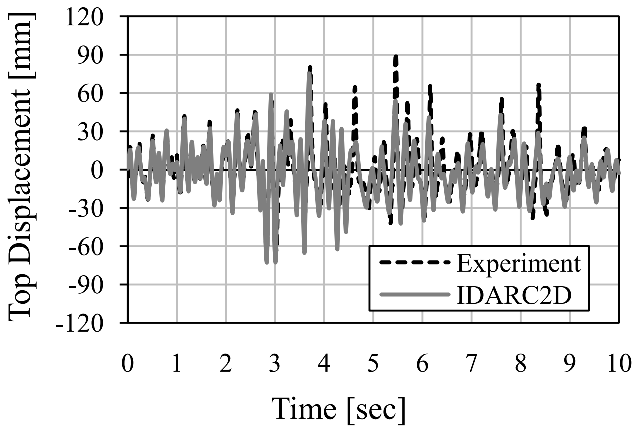

Figure A.19: High mass 0.2 PGA

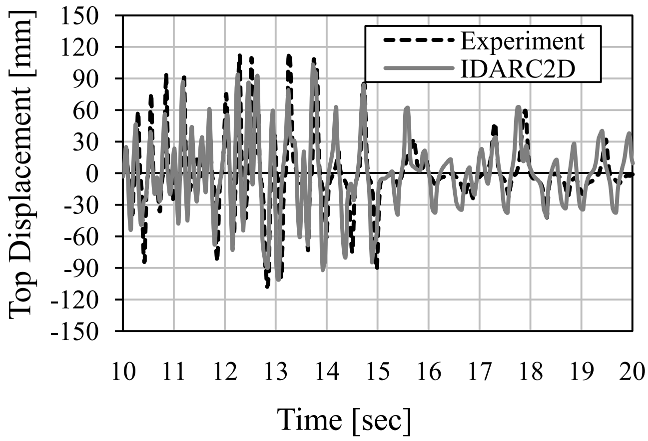

Figure A.20: High mass 0.4 PGA

APPENDIX A.6 : CFRP Retrofitted RC Frame Lateral Top Displacement History

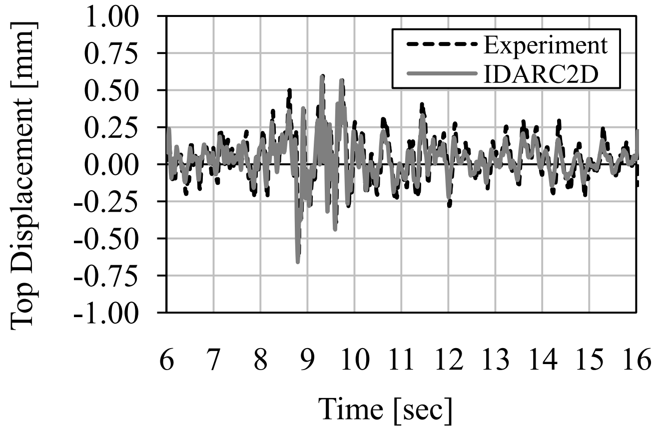

Figure A.21: Low mass 0.2 PGA

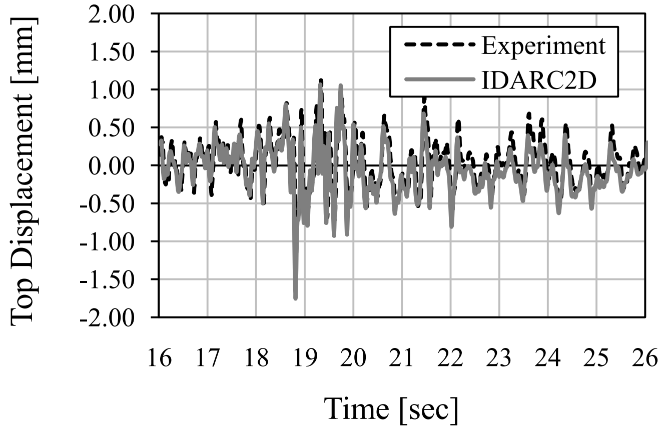

Figure A.22: Low mass 0.4 PGA

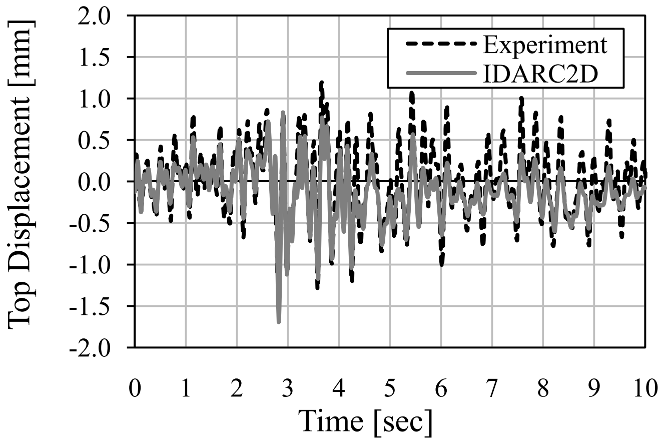

Figure A.23: High mass 0.2 PGA

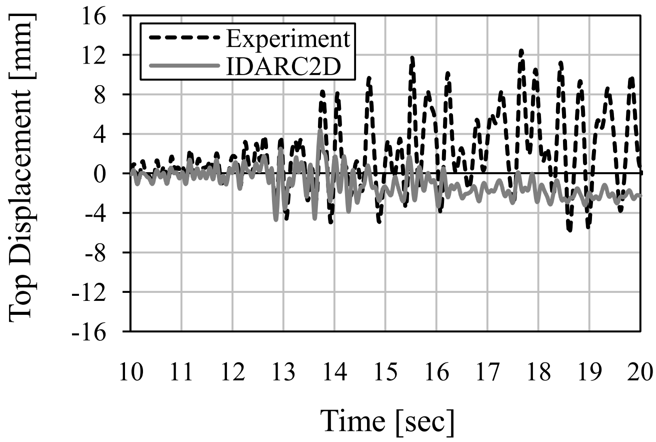

Figure A.24: High mass 0.4 PGA

APPENDIX A.7 : Bare Frame Base Shear Force History

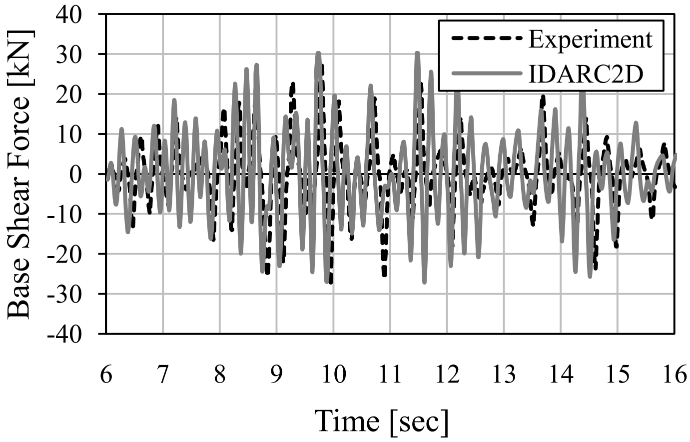

Figure A.25: Low mass 0.2 PGA

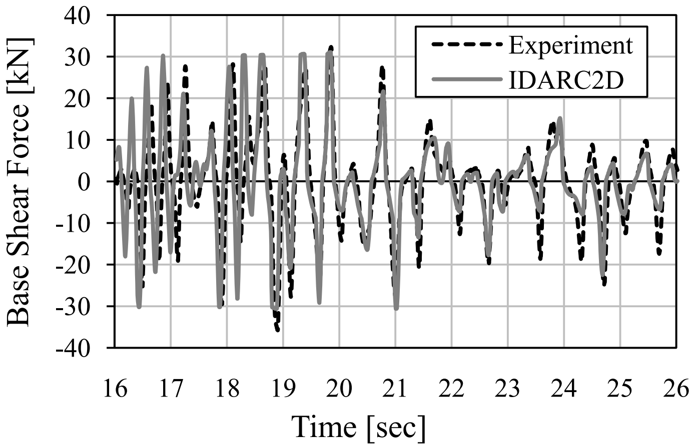

Figure A.26: Low mass 0.4 PGA

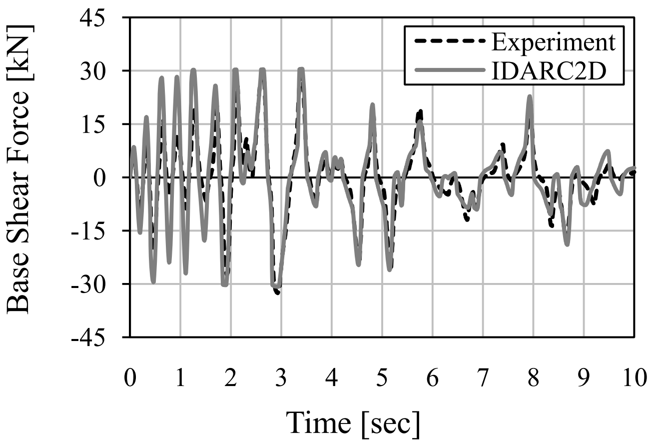

Figure A.27: High mass 0.2 PGA

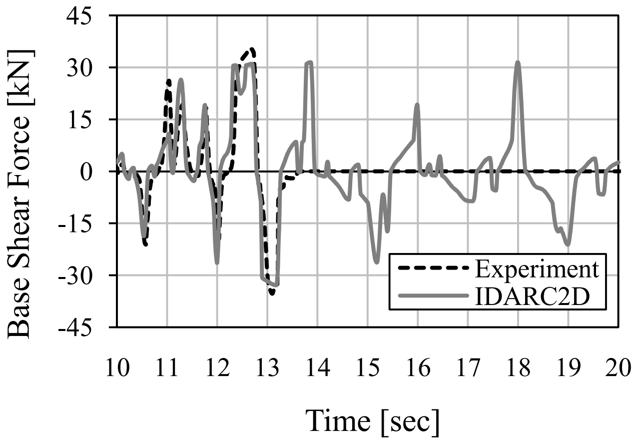

Figure A.28: High mass 0.4 PGA

APPENDIX A.8 : Infilled Frame Base Shear Force History

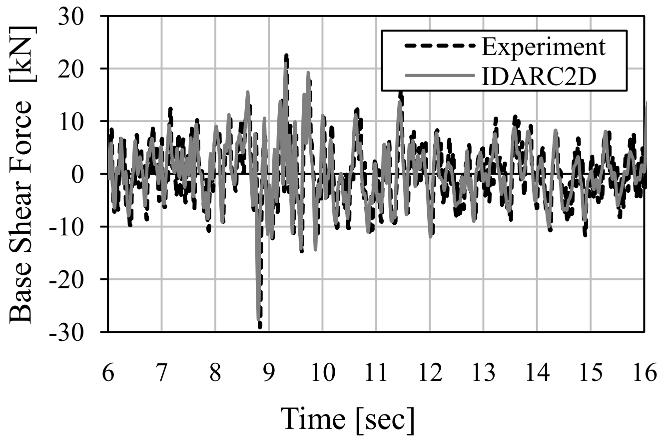

Figure A.29: Low mass 0.2 PGA

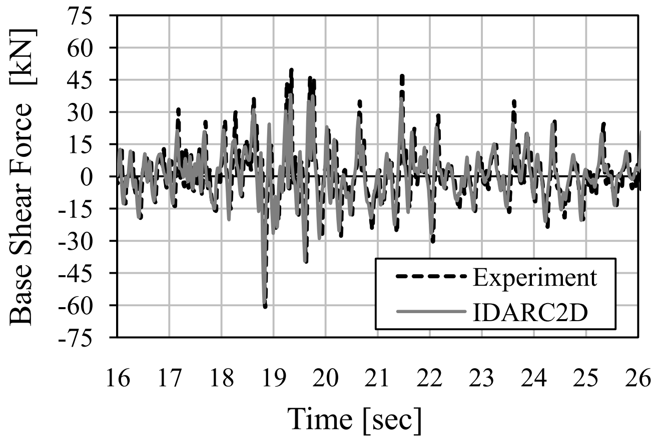

Figure A.30: Low mass 0.4 PGA

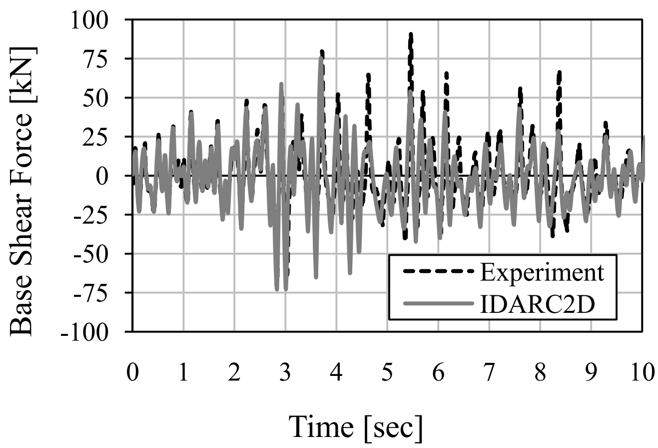

Figure A.31: High mass 0.2 PGA

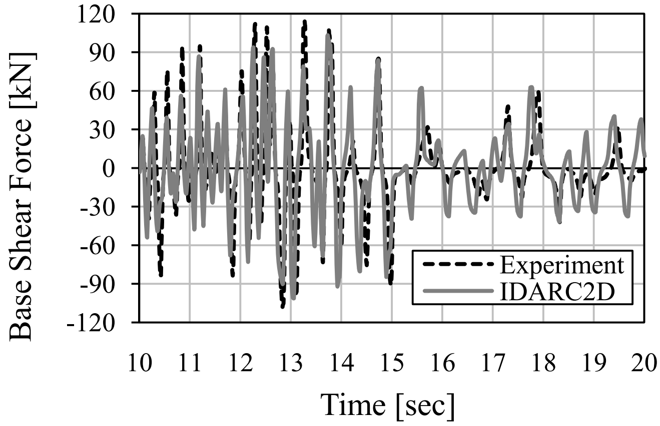

Figure A.32: High mass 0.4 PGA

APPENDIX A.9 : CFRP Retrofitted RC Frame Base Shear Force History

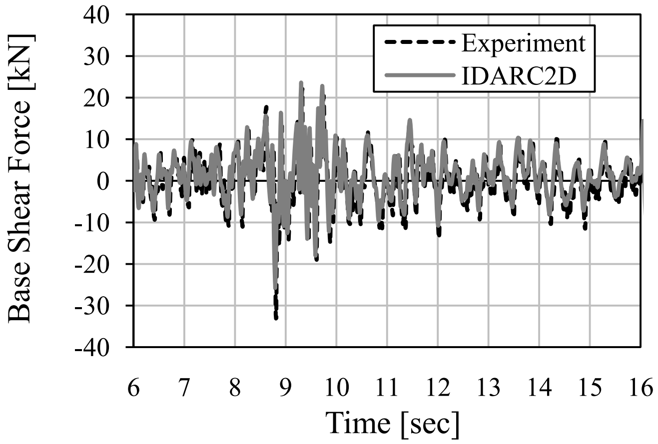

Figure A.33: Low mass 0.2 PGA

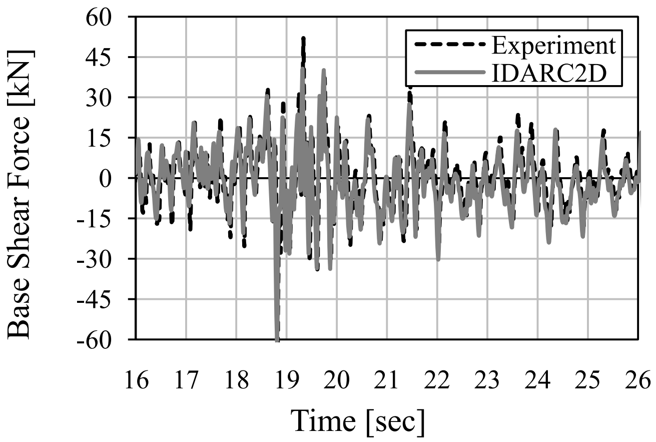

Figure A.34: Low mass 0.4 PGA

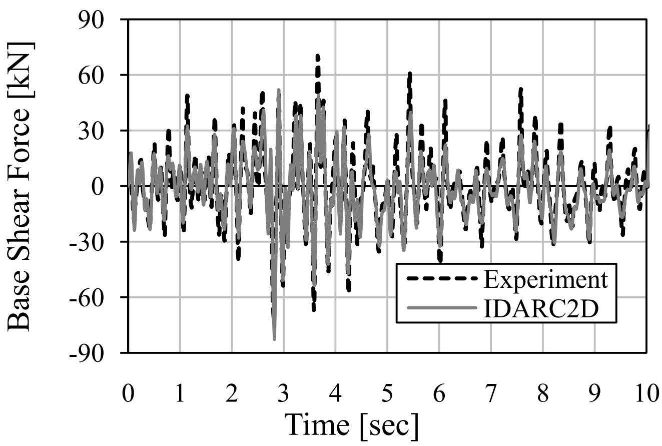

Figure A.35: High mass 0.2 PGA

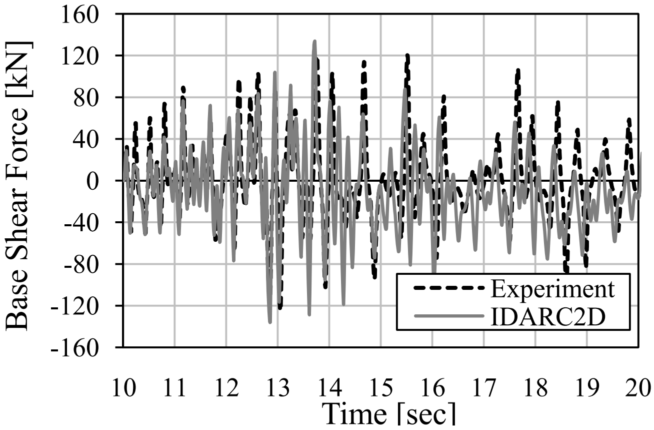

Figure A.36: High mass 0.4 PGA

CURRICULUM VITAE

Candidate's full name: Levent KILIC

Place and date of birth: Uzunkopru 5th Feb 1975

Permanent Address: Dikilitas Mah. Yeni Gelin Sk. 25/10 Besiktas Istanbul

Universities and Colleges attended: Ataturk University